

FEDERAL UNIVERSITY OF ITAJUBÁ
MECHANICAL ENGINEERING INSTITUTE

**Inverse problems applied to the experimental thermal and hygric analysis of
engineering materials**

Nícolas Pinheiro Ramos

Itajubá – Minas Gerais – Brazil
2024

**FEDERAL UNIVERSITY OF ITAJUBÁ
MECHANICAL ENGINEERING INSTITUTE**

Nícolas Pinheiro Ramos

**Inverse problems applied to the experimental thermal and hygric analysis of
engineering materials**

**A PhD thesis submitted to the Postgraduate
Program in Mechanical Engineering, as a requirement to
obtain the Doctorate degree in Mechanical Engineering.**

Area of Concentration: Energy, Fluids and Turbomachinery

Advisor: Prof. Dr. Sandro Metrevelle Marcondes de Lima e Silva

Co-advisor: Prof. Dr. Gilmar Guimarães

**Itajubá – Minas Gerais – Brazil
2024**

FEDERAL UNIVERSITY OF ITAJUBÁ
POSTGRADUATE PROGRAM IN MECHANICAL ENGINEERING

Nícolas Pinheiro Ramos

**Inverse problems applied to the experimental thermal and hygric analysis of
engineering materials**

This PhD thesis was approved by the following advisory committee:

Prof. Dr. Louis Gosselin – Université Laval (ULaval)

Prof. Dr. Roberto Lamberts – Federal University of Santa Catarina
(UFSC)

Prof. Dr. Antonio Augusto Araújo Pinto da Silva – Federal
University of Itajubá (UNIFEI)

Prof. Dr. Guilherme Ferreira Gomes – Federal University of Itajubá
(UNIFEI)

Prof. Dr. Gilmar Guimarães (Co-advisor) – Federal University of
Uberlândia (UFU)

Prof. Dr. Sandro Metrevelle Marcondes de Lima e Silva (Advisor) –
Federal University of Itajubá (UNIFEI)

Itajubá – Minas Gerais – Brazil
2024

In memory of my beloved
grandmothers Betilde and Benedita
for their love in every step of my
journey.

Acknowledgments

I thank so much my parents, Cecília and Denilson, my sisters, Núbia and Nádia, and my nephew, Benjamin. They have supported me unconditionally and allowed me to get to where I am. I will be always grateful for all the concern, patience, and encouragement dedicated to me.

I would like to especially thank my advisor Sandro, who has been sharing his life experience and scientific knowledge since 2015, and my lab mate Mariana, who has dedicated a lot of time and energy to the development of our studies.

I am also very grateful to my co-advisor Gilmar for the collaboration between LabTC-UNIFEI and LTCME-UFU.

Many thanks to Louis for the opportunity to do a research internship under his supervision at Université Laval. This is certainly a highlight in my academic journey. I could not fail to acknowledge Leonardo, whose collaboration made my stay in Canada much better.

I would also like to thank all my LabTC colleagues for helping me when I needed it. I must give a special thanks to Carollo, who guided my first steps into the world of experimental inverse heat transfer problems.

I am very grateful to CAPES for my doctoral scholarship.

It is important to highlight the financial support provided by CAPES and UNIFEI's Dean of Research and Postgraduate Studies for my sandwich doctorate.

FAPEMIG is also gratefully acknowledged for its grants and funding.

“Thermodynamically improbable, but here I am.”

Abstract

Ramos, N. P. (2024), *Inverse problems applied to the experimental thermal and hygric analysis of engineering materials*, PhD Thesis, Postgraduate Program in Mechanical Engineering, Mechanical Engineering Institute, Federal University of Itajubá.

Several relevant real-world applications rely on an inverse problem, which involves recovering unknown causes from observing their effects. This differs from the corresponding direct problem, whose solution involves predicting effects from a complete description of their causes. Naturally, inverse problems are more challenging than direct problems because, in general, they are ill-posed, i.e., the solution either does not exist, is not unique or it does not depend continuously on the input data. To soften this problematic aspect, applied inverse modeling requires detailed mathematical-physical modeling and well-designed experiments since the desired parameters are estimated by comparing calculated data with experimental measurements.

In this PhD thesis, inverse approach was applied to experimentally investigate three case studies:

- complementary experiments to simultaneously estimate the parameters describing the temperature-dependent thermal conductivity and specific heat of 304 austenitic stainless steel. Parameter estimation takes advantage of additional information provided by two heat-conducting solids with different geometries. It is an alternative approach to standard thermal characterization techniques, which are often beyond the reach of many laboratories.

- one-year on-site measurements to estimate various hygrothermal properties and thus calibrate the simulation model of a lightweight multilayer wall. A 2D fully coupled heat and moisture transfer model was used to investigate the in-use response of the panel junction region, which is critical in terms of airtightness. The results enable an accurate assessment of building operating conditions by reducing uncertainties in material input data.
- field data to determine the annual heat conduction flux through a wall assembly in an occupied house. Inverse modeling accounted for the physical interactions between outdoor environment and indoor occupancy. The methodology and the findings are useful to support decision-making on energy performance, as there is a lack of long-term field monitoring and information on dynamic heat flux related to prefabricated occupied dwellings.

All the above inverse analyzes were based on evaluating the match between data predicted by numerical simulations in COMSOL Multiphysics and measurements conveying the physical behavior of the component under study. Numerical and experimental data were processed and used for inverse estimation purposes in MATLAB environment. After careful analysis of sensitivity coefficients, different optimization approaches were used to solve the inverse problems. Bayesian statistical inference was applied to determine the estimates and corresponding uncertainties of the thermal properties of 304 stainless steel. The Broyden–Fletcher–Goldfarb–Shanno (BFGS) algorithm, which determines the descent direction by preconditioning the gradient with curvature information, was used in the second case study. The wall heat flux was estimated using the sequential function specification method (SFSM), which expresses temperature as function of heat flux by means of a first-order Taylor series. The results show that inverse modeling is a reliable tool for obtaining valuable information about the hygrothermal mechanisms and parameters involved in applied engineering problems.

Keywords: Inverse analysis, Hygrothermal characterization, Stainless steel, Complementary experiments; Multilayer wall assembly, Occupied prefabricated house, In situ performance.

Resumo

Ramos, N. P. (2024), *Problemas inversos aplicados à análise térmica e higrométrica experimental de materiais de engenharia*, Tese de Doutorado, Programa de Pós-Graduação em Engenharia Mecânica, Instituto de Engenharia Mecânica, Universidade Federal de Itajubá.

Várias aplicações importantes baseiam-se em um problema inverso, que envolve a recuperação de causas desconhecidas a partir da observação de seus efeitos. Já o problema direto correspondente envolve a previsão dos efeitos a partir de uma descrição completa de suas causas. Naturalmente, os problemas inversos são mais complicados do que os problemas diretos porque, em geral, eles são mal-postos, ou seja, a solução não existe, não é única ou não depende continuamente dos dados de entrada. Para amenizar esse aspecto problemático, a modelagem inversa aplicada requer uma modelagem matemática/física detalhada e experimentos bem planejados, já que os parâmetros desejados são estimados pela comparação dos dados calculados com as medições experimentais.

Nesta tese de doutorado, abordagem inversa foi aplicada para investigar experimentalmente três estudos de caso:

- experimentos complementares para estimar simultaneamente os parâmetros que descrevem a condutividade térmica e o calor específico dependentes da temperatura do aço inoxidável austenítico 304. A estimativa de parâmetros aproveita informações adicionais fornecidas por dois corpos condutores de calor com geometrias diferentes. Trata-se de uma abordagem alternativa às técnicas de caracterização térmica padrão, que geralmente estão fora do alcance de muitos laboratórios.

- medições de campo de um ano para estimar várias propriedades higrotérmicas e, assim, calibrar o modelo de simulação de uma parede leve multicamadas. Um modelo 2D de transferência de calor e umidade foi usado para investigar a resposta em uso da região de junção do painel, que é crítica em termos de estanqueidade. Os resultados permitem uma avaliação precisa das condições operacionais da edificação, reduzindo as incertezas nos dados de entrada do material.
- dados de campo para determinar o fluxo anual de condução de calor por meio de uma parede em uma casa ocupada. A modelagem inversa levou em conta as interações físicas entre o ambiente externo e a ocupação interna. Os resultados são úteis para apoiar a tomada de decisões sobre o desempenho energético, pois há uma falta de monitoramento de campo de longo prazo e de informações sobre o fluxo dinâmico de calor relacionado a residências pré-fabricadas ocupadas.

Todas as análises acima basearam-se na avaliação da correspondência entre dados calculados por simulações numéricas no COMSOL Multiphysics e medições que transmitem o comportamento físico do componente em estudo. Os dados numéricos e experimentais foram processados e usados para fins de estimação inversa em ambiente MATLAB. Após uma análise cuidadosa e minuciosa dos coeficientes de sensibilidade, diferentes abordagens de otimização foram usadas para resolver os problemas inversos. Inferência bayesiana foi aplicada para determinar as estimativas e as incertezas correspondentes das propriedades térmicas do aço inoxidável 304. O algoritmo Broyden-Fletcher-Goldfarb-Shanno (BFGS), que determina a direção de descida pré-condicionando o gradiente com informações de curvatura, foi usado no segundo estudo de caso. O fluxo de calor através da parede foi estimado usando o método sequencial da função especificada, que expressa a temperatura como função do fluxo de calor por meio de uma série de Taylor de primeira ordem. Os resultados mostram que a análise

inversa é uma ferramenta confiável para obter informações valiosas sobre os mecanismos e parâmetros higrotérmicos envolvidos em problemas de engenharia.

Palavras-chave: Análise inversa, Caracterização higrotérmica, Aço inoxidável, Experimentos complementares; Parede multicamadas, Casa pré-fabricada ocupada, Desempenho in situ.

List of figures

Figure 1. Schematic of the complementary heat conduction models: a) 1D thermal model; b) 3D thermal model.	31
Figure 2. D-optimality criterion for all sample surfaces. Unfolded view with the sensor location.	47
Figure 3. Scaled sensitivity coefficients of parameters describing the linear functions of $k(T)$ and $c_p(T)$	49
Figure 4. Schematic of the experimental arrangement used to simultaneously identify $k(T)$ and $c_p(T)$	50
Figure 5. Evolution of the PPDF versus the number of states of the Markov chain.	53
Figure 6. Temperature-dependent thermal conductivity of 304 austenitic stainless steel. Comparison of the lines determined in this study with curves reported in Valencia and Quested [24] and Graves et al. [61].	55
Figure 7. Temperature-dependent specific heat of 304 austenitic stainless steel. Comparison of the lines determined in this study with curves reported in Valencia and Quested [24] and Graves et al. [61].	56
Figure 8. PPDFs of the estimated parameters for the first experimental set.	57
Figure 9. Temperature histories for the 1D and 3D thermal models. Comparison of measurements with numerically computed temperatures.	58
Figure 10. Comparison between the retrieved heat flux histories.	59
Figure 11. Picture taken during the installation of the studied wall.	67
Figure 12. Two-dimensional cross-sectional view of the wall junction showing the different components and sensor locations.	68

Figure 13. Experimental ten-minute measurements of (a) temperature and (b) relative humidity.	69
Figure 14. Sensitivity coefficients for: (a) T_2 , (b) T_3 , and (c) ϕ_2	79
Figure 15. Evolution of the objective function over the number of iterations for the estimation of the hygrothermal properties of the wall.	80
Figure 16. Sensitivity coefficients of h_{ext} and h_{int} for: (a) T_2 , (b) T_3 , and (c) ϕ_2	84
Figure 17. Evolution of the objective function over the number of iterations for the estimation of h_{int} and h_{ext}	85
Figure 18. Heat (a) and moisture (b) fluxes through the interior wall surface. Comparison of the results for the effective hygrothermal properties estimated in this study with the results for reference parameters.	90
Figure 19. One-dimensional cross-sectional view depicting the wall layers and measurement locations (exterior and interior claddings not shown for clarity).	98
Figure 20. Field temperature measurements.	99
Figure 21. Annual heat flux through the internal wall surface.	108
Figure 22. Data used to evaluate the effective in situ thermal resistance of the wall assembly.	110

List of tables

Table 1. Simultaneous estimation of k and c_p parameters for 304 austenitic stainless steel. ...	55
Table 2. Reference information on the investigated hygrothermal properties.	76
Table 3. Estimated effective hygrothermal properties.....	81
Table 4. Estimated effective external and internal heat and moisture transfer coefficients.	86

Contents

1. Introduction	16
1.1 Fundamentals of inverse problems.....	16
1.2 Parameter estimation versus function estimation.....	17
1.3 Inverse problem solution.....	18
1.4 Application of inverse problems	20
1.5 Research objectives	21
2. Case Study 1: Complementary Experiments to Estimate the Thermal Properties of 304 Austenitic Stainless Steel.....	22
2.1 Austenitic stainless steel	22
2.2 Thermal characterization of metallic materials.....	23
2.3 Complementary data	27
2.4 Thermal problem modeling.....	29
2.4.1 One-dimensional thermal model	29
2.4.2 Three-dimensional thermal model.....	33
2.5 Bayesian inference for inverse solution	34
2.6 Sensitivity analysis.....	43
2.7 Experimental aspects.....	45
2.8 Heat conduction experiments	49
2.9 Results and discussion.....	51

2.10	Summary.....	59
3.	Case Study 2: One-year On-site Monitoring to Estimate Hygrothermal Properties of Wall Materials	61
3.1	Hygrothermal performance of building envelopes	61
3.2	One-year on-site monitoring	66
3.3	Simultaneous estimation of specific heat, thermal conductivity, and vapor resistance factor	70
3.3.1	Inverse problem approach for hygrothermal characterization.....	70
3.3.2	Hygrothermal problem with Dirichlet boundary conditions	71
3.3.3	Sensitivity analysis	75
3.3.4	Results and discussion	79
3.4	Simultaneous estimation of convective heat and moisture transfer coefficients	81
3.4.1	Hygrothermal problem with Robin boundary conditions.....	81
3.4.2	Sensitivity analysis	83
3.4.3	Results and discussion	84
3.5	Impact of model calibration on hygrothermal performance assessment.....	87
3.6	Summary	90
4.	Case Study 3: Estimating the Annual Heat Flux through a Prefabricated Wall Assembly from Field Data.....	92
4.1	Dynamic thermal analysis of envelope walls.....	92
4.2	Field thermal monitoring.....	97
4.3	Direct thermal problem	99

4.4 Inverse heat flux estimation	101
4.4.1 Sequential function specification method.....	101
4.4.2 Regularization parameter.....	104
4.4.3 Uncertainty analysis	105
4.5 Results and discussion.....	106
4.6 Summary	111
5. General conclusions	112
6. Appendix	114
6.1 Publications	114
6.2 Ongoing papers	115
6.3 Thermal property measurements.....	115
6.4 Sandwich PhD.....	116
7. References	117

1. Introduction

1.1 Fundamentals of inverse problems

The French mathematician Jacques-Salomon Hadamard studied the nature of mathematical models to accurately represent physical phenomena and defined the concept of well-posed and ill-posed problems[1].

These are the conditions for a problem to be considered well-posed according to Hadamard:

- There must exist a solution.
- The solution must be unique.
- The solution must depend continuously on the input data or the initial and boundary conditions.

A physical problem that does not satisfy all the criteria mentioned above is considered an ill-posed problem. All physical interactions between a body with its surroundings can be related to cause-and-effect problems [2]. For instance, in a heat transfer model, the causes are the initial and boundary conditions, thermal properties, heat generation sources, and geometrical characteristics. The effect, in turn, is the time evolution of the temperature distribution throughout the studied body. For a direct problem, the causes are known, and the effects are unknown and need to be determined. Most engineering studies are conducted in a direct (forward) manner, usually focusing on determining the effects. Direct problems are well-posed problems and remain stable for small changes in input data. On the other hand, an inverse

problem is a problem where the effects are measured and then used to determine one or more causes. In other words, inverse problems occur in a backward manner, i.e., they are governed in the opposite direction to nature. Since it is impossible to reverse time, the causality of nature prevents inverse problem solutions from being experimentally reproduced. This would imply a violation of the cause-and-effect relationship [3]. Inverse problems are naturally ill-posed. Most often, Hadamard's third criterion is not satisfied for this type of problem, and the second criterion is not satisfied sometimes either.

1.2 Parameter estimation versus function estimation

Inverse problems can be categorized into two classes [4]: parameter estimation and function estimation. In parameter estimation, a small number of parameters are to be estimated. By contrast, the number of unknown elements is generally high for function estimation, since a profile is estimated rather than strict values. Parameter estimation is usually concerned with the characterization of physical properties, which are not exposed to human influence or adjustments. Results of parameter estimations are usually given with confidence intervals and are only valid in the range covered by the experiments performed. This is not the case with a function estimation, where the estimates are inherent to the problem at hand. Unlike function estimations, parameter estimations deal with sought-after quantities that behave differently according to measurement variations. This implies that much more caution is required when designing and conducting experiments for parameter estimation purposes [4]. It is therefore crucial to perform a careful sensitivity analysis to increase estimation accuracy [5].

Although solving inverse problems is very useful, their ill-posedness makes the governing sensitivity matrices ill-conditioned and sometimes rank deficient. Ill-posedness means that the

existence of a unique solution cannot be guaranteed for small changes in the measurements, and there may be a long, narrow valley of solutions. Also on this matter, inverse analyzes of practical interest are constructed based on physical measurements, and measurements always contain errors. The same measurements taken under the same conditions but at different times are very likely to be different. Thus, real-world inverse problems are naturally noisy, and the results may not correspond fairly to the system being studied due to inaccuracies in data collection. To soften the difficulties related to this ill-posed character, a good awareness of model imperfections and measurement uncertainties is required [6] .

1.3 Inverse problem solution

Methods for solving inverse problems have been extensively researched and discussed [4], [7]. However, none are absolute and universally applicable [8] . This is because the correct choice of the optimization technique mainly depends on the kind of the problem at hand, with an approach being expected to be efficient for a given problem and work poorly for another [9]. In general, optimization techniques for computing inverse solutions can be roughly categorized into gradient-based and stochastic (probabilistic) methods.

The gradient-based approaches are exact mathematical methods and are more frequently used. These classical methods have fast convergence speed, high accuracy, and effectiveness as advantages. Nevertheless, as they use information about the slope of the objective function to define the search direction, calculating surface gradients and sensitivity coefficients is mandatory. Computing sensitivity derivatives is laborious when multidimensional, nonlinear, multimodal, discontinuous, and transient cases are considered. Gradient methods are not free from the “local minima trap” problem, which means to search for a local optimum solution

instead of a global optimum one [10]. They can exploit a limited search region around a given starting value, but they tend to fail when the starting value is far from the global solution [11]. Thus, these methods can be very inefficient to find good solutions when they are employed to minimize functions that have flat valleys, as is the case for the one at hand. The valley is easily found, but the converge to the global minimum lying inside the valley is difficult or even impossible. Along the valley, the function is very insensitive to changes in the desired parameters. This means that the bottom surface of the objective function is not strongly convex in the optima neighborhoods. Gradient-based methods are stable only if the Hessian matrix is positive definite, and they can even diverge if the initial guess is too far from the optimum [12].

The term stochastic may refer to random processes that can represent a system which evolution over time is described by combing available data (current and past knowledge) and predicted successive changes (future knowledge) [9]. Stochastic methods are approximation methods that do not depend on gradient fields for optimization. They generate and analyze random variables to find sufficiently adequate solutions to optimization problems. Since they search in a random way, derivative-free optimization methods have no perfect repeatability and can be more computationally efficient compared with gradient-based methods. However, they can be time-consuming when handling very simple problems, given the computational costs for iteratively achieving convergence [13], [14]. Additionally, stochastic methods are less susceptible to the “local minima trap”, obtaining the best solution that can be possibly found after a given number of iterations. Such techniques have been successfully used to solve inverse problems [15], [16], [17] and are very relevant in assessing engineering problems with complicated relationships between design variables [13]. Probabilistic methods can be helpful when dealing with ill-posed problems since they provide proper solutions from a population of good individuals (optimal points) or from a probability density (mean and standard deviation values).

1.4 Application of inverse problems

Inverse problems are a robust and effective tool to indirectly estimate quantities appearing in the mathematical formulation of physical phenomena [4]. Inverse analyzes are found in multi-scale physical processes, and applications range from the identification of constant parameters to the tracking spatial- and time-dependent functions [7]. Inverse methodologies are also constantly involved in everyday activities, such as medical imaging and dynamic aircraft position prediction [7]. A typical example is related to inferring information about the interior of a sample subjected to a scanning process from measured data on its surface [18].

The background needed to properly apply inverse approach to evaluate real engineering problems consists of the following functional milestones [18]:

- Mathematical modeling (inverse problem formulation, including governing equations, geometry, sources, coefficients, and initial and boundary conditions).
- Mathematical analysis (existence, uniqueness, stability).
- Numerical modeling (physics-based simulations or computational codes).
- Design of experiments (optimal placement of sensors, duration of measurements, configuration of experimental parameters).
- Experimental analysis (performing experiments to measure data that will serve as information for inverse problem solution).
- Computational analysis (implementation of programming codes to integrate the previous analyzes and process the raw data and results).

Therefore, different knowledge and tools are required to thoroughly accomplish the above tasks, which makes inverse approach highly interdisciplinary.

1.5 Research objectives

Thermal and hygric characterization of materials and structures are critical to obtain knowledge of their operational behavior. However, direct measurement or access to standard thermal characterization methods are often complicated due to experimental and financial issues. In this context, this research work seeks to employ inverse methodologies to the thermal and hygric analysis of different engineering materials. Three case studies are experimentally investigated in this PhD thesis:

In chapter 2, two complementary transient experiments are carried out to provide robust information to simultaneously estimate the parameters describing the temperature-dependent thermal conductivity and specific heat of 304 austenitic stainless steel.

In chapter 3, one-year on-site measurements are used to estimate various hygrothermal properties and thus calibrate the simulation model of a lightweight multilayer wall.

In chapter 4, the annual dynamic heat conduction flux through a wall assembly is estimated from field data measured in an occupied house.

Chapter 5 presents a general conclusion to this research work, providing an overview on the main aspects addressed.

Finally, an outlook on the activities carried out during the doctorate is presented in the Appendix.

2. Case Study 1: Complementary Experiments to Estimate the Thermal Properties of 304 Austenitic Stainless Steel

2.1 Austenitic stainless steel

The capacity of handling metallic materials has changed human history since Metal Ages. With the industrial revolution, the use of metals and their alloys in human activities increased rapidly owing to their distinct characteristics [19]. In today's highly energy-dependent society, technological progress and innovation depend on using metals, which are widely employed in numerous engineering applications. Metals offer quality, efficiency, and safety for human activities. They are necessary inputs used in providing essential services and products worldwide, like in the transportation, construction, telecommunications, and energy production and distribution sectors [19].

Stainless steels (SSs) are a very relevant group of metal alloys, since they are used in a large variety of applications, varying from everyday use in kitchen utensils and furnishings, to very advanced uses in the oil & gas, chemical, and aerospace industries. They are valued for their corrosion resistance, durability, strength, and aesthetic appeal. Stainless steels can be basically categorized into three groups according to their microstructure: ferritic, austenitic, and martensitic. These different metallurgical structures are obtained by modifying steel chemistry. To achieve specific properties, SSs contain substantial amounts of alloying elements, mainly chromium and nickel, but also molybdenum, silicon, carbon, nitrogen, and manganese [20].

There are over 150 grades of stainless steel, each with its particular properties. 300 series is a grade of austenitic stainless steel (ASS) and is the most used grade worldwide. 300-series

ASSs are used in mandatory heat-resistant structural applications given their properties regarding corrosion resistance, mechanical strength, metallurgical stability, fracture toughness, and ductility at high temperatures [20]. There are two important types of 300 austenitic stainless steels: 304 and 316. 304 ASS is used in about 60% of all applications. As they are austenitic, 304 ASS and 316 ASS are non-magnetic and have a low carbon content. This makes them highly weldable and formable. These two heat-resisting alloys are comparable in terms of mechanical properties and differ moderately in chemical composition. Generally, 304 ASS has more chromium and less nickel compared with 316 ASS. 316 ASS also incorporates approximately 2% molybdenum, which increases strength and chemical corrosion resistance [21]. Concerning their thermal behavior, it is known that chemical composition most considerably controls the thermal conductivity (k) and specific heat (c_p) of alloy steels [22]. Alloying elements also impact both thermal properties, which usually decrease with increasing the alloying degree [23]. Thus, 304 ASS has moderately higher c_p and k in comparison with 316 ASS [24].

2.2 Thermal characterization of metallic materials

Materials characterization is essential for evaluating the thermal behavior of a particular domain, since the robustness of thermal analyzes depends on how reliable the properties of the system being studied are. Reliable thermal property data lead to better results when designing, optimizing, and implementing heat transfer processes [12]. Additionally, temperature dependence is a key condition for metals because they are widely employed in temperature-varying applications. Considering thermal properties as constants can mislead to unrealistic numerical simulations when predicting materials' response to changes in the working

temperature [25]. Thus, methods for determining accurate temperature-dependent thermal properties of metallic materials are fundamental to thermal sciences.

Thermal properties of conducting materials, like metals, cannot generally be obtained via direct measurements. As a result, experiments can be designed and performed for measuring temperature and/or heat flux data which are further used in combination with mathematical expressions to determine the desired thermal parameter(s) [12]. Standardly, there are three different approaches for obtaining the thermal properties of a material. The first one consists of steady-state measurements of heat flux and temperature gradients, as in the guarded hot plate method [26]. Despite the high accuracy, this group of techniques is very time-consuming and can hardly ever be applied to high conducting materials. Also, they require specialized equipment and can furnish only thermal conductivity. The calorimetric approach, on the other hand, is very well suitable when the target is to obtain c_p . Differential scanning calorimetry (DSC), for example, has been extensively applied for this purpose. Nevertheless, these methods do not furnish thermal conductivity and manage to provide thermal properties only for high-temperature levels. Moreover, they also require specific and expensive equipment, and difficulties arise when dealing with inhomogeneous materials, due to the mandatory small sample size [27]. Lastly, the third approach introduces transient techniques, such as the transient hot wire method [28] and the laser flash method [29]. For both techniques, thermal conductivity and thermal diffusivity can be obtained (not simultaneously) within a much smaller period than that needed in steady-state experiments. Anyhow, the experimental assemblies also demand considerable financial and time resources for obtaining each thermal property. All these classical techniques have already been improved, yet, none of them is unrestricted, which means that methods for obtaining thermal properties are usually defined for specific materials and temperature ranges [12], [26].

Apart from the classical techniques, several novel methods for thermal characterization have been developed for engineering material applications [30]. These techniques should seek a trade-off between reliable outcomes and reasonable computational and experimental costs. Transient experimental methods for estimating the thermal properties of high-conducting materials are scarce. This is because it is difficult and expensive to design and carry out transient experiments for thermally characterizing metals, due to contact resistance effects and thermal sensitivity deficiencies when dealing with these materials [31]. Additionally, considerable efforts and expertise are needed to obtain well-planned and well-conducted experiments for thermal characterization. For these reasons, thermal characterization approaches for analyzing metallic materials are somewhat limited; there are not many approaches that can be used in these materials [32], [33], [34]. Some of these novel methods disregard temperature dependence [31], [35]. Several techniques cannot perform simultaneous estimations, assessing only one property, or requiring more than one process to achieve others [36]. Also, they generally do not consider data from the entire temperature domain. Naturally, techniques that seek to simultaneously estimate temperature-dependent thermal properties have also been studied and presented. Most evaluate temperature dependence using data regressions within small temperature ranges and do not consider data corresponding to the entire temperature domain [37], [38]. These approaches require several experiments or numerical simulations where the sample is subjected to different initial conditions. Finally, many approaches have not been experimentally validated, and have focused on only numerical or analytical analyzes [38], [39], [40].

Here, a linear variation of $k(T)$ and $c_p(T)$ in temperature is assumed and the constant and slope defining these functions are estimated. Previous studies, as per Mohebbi et al. [39], [41], [42], have shown that it is feasible to determine parameters for a linear form describing the temperature dependence of the thermal properties. However, it turns out that these papers cover

theoretical background on inverse heat conduction, since they perform analyzes from numerically simulated temperature data. In addition to not presenting experimental validation, their techniques were applied to a generic solid medium [39] or to insulation materials [41], [42] which does not lead to great difficulties concerning rank deficiency and valley bottom landscape.

Thermal conductivity and specific heat of the metallic material used are needed to obtain knowledge of the thermal behavior of metal parts present in engineering structures. However, access to standard thermal characterization methods is often complicated due to financial issues. In this context, this study seeks to present a simple experimental approach for simultaneously identifying the linearly temperature-dependent k and c_p of 304 austenitic stainless steel. Parameter estimation takes advantage of a relevant sensitivity increase, provided by two complementary transient experiments. Bayesian inference is used to analyze the accordance between experimentally measured and numerically calculated temperatures. Inverse thermal analysis is based on two heat-conducting solids with different geometries. In estimation problems, one seeks to obtain as much data as possible using as few sensors as possible. So, single thermocouple data are collected for each thermal model. The proposed technique provides a cost-effective and robust thermal property estimation from tests conducted at room temperature. Single-step estimation incorporates data from the whole temperature domain and infers a set of four parameters for linear functions representing the temperature dependence of k and c_p . This means that the linear relationship between thermal property and temperature is directly determined, with no need for fitting a regression line. Since the inverse methodology provides k and c_p at once, two or more different procedures are not required for obtaining both thermal properties, unlike most standard tests for measuring the thermal properties of metallic materials. The contact resistance effect at the heater-metal interface is evaluated at microscopic level and set as a reducing factor in the heat flux load supplied to the samples.

2.3 Complementary data

Complementary data are important because they can furnish additional information that can help to support or refute a hypothesis. Complementary data can also be used to generate new hypotheses or to help understand complex phenomena [43]. It is important to ensure that the collected data are as high quality as possible and that they come from a variety of sources [43]. The supplementary information provided by complementary experiments can improve the robustness of estimation procedures [43].

Parameter estimation is the process of using observations to estimate the values of parameters for a model. In many scientific disciplines, parameter estimation is an important task that allows researchers to make predictions and understand the behavior of a system [4]. The quality of the estimates depends on both the quality of the data and the chosen model. In parameter estimations, we need as much data as possible to give a solid basis to the optimization algorithm to find a solution that can reliably represent the studied physical phenomenon, in an acceptable error sense. Complementary data can be used to improve parameter estimation by providing more robust information that can help to constrain or identify the values of parameters. This is especially relevant when there are few observations or when they are noisy, as complementary data can help to reduce uncertainty and improve reliability. Additional information from complementary thermal models can enable simultaneous estimations with multiple objectives, since they decrease or even avoid rank deficiency [44]. Rank deficiency in this context basically means the lack of sufficient information in the available data to estimate the desired parameters. As the quantity of parameters to be found raises, data from complementary events enhances the robustness of inverse analyzes.

There are several reasons why complementary experiments contribute to obtaining better parameter estimation. First, different experiments may be sensitive to different aspects of the

system under study. This can enable for more complete coverage of the parameter space and reduce the uncertainty in the estimates. Second, different experiments may have different levels of precision. Complementary experiments can help to average out errors and improve the overall accuracy of the estimates. Finally, some types of experiments may be more expensive or difficult to carry out than others. By using a combination of experiment types, researchers can minimize costs while still obtaining reliable results [43].

Complementary data have been used in inverse problems of different fields of study. For instance, Boyd and Little [45] analyzed the application of complementary data to limited-angle computed tomography. Weichman et al. [46] used complementary information in an inverse problem to infer subsurface water distribution from Nuclear Magnetic Resonance (NMR) voltage measurements. Led and Gesmar [47] showed the importance of complementary experiments to determine chemical exchange rates using magnetization-transfer NMR technique. Cao et al. [48] used complementary data to boost the image quality of low-resolution sensors using super-resolution technique.

Complementary experiments have not been explored much to estimate thermal properties and have never been applied to metallic materials. McMasters et al. [44] studied the increase in sensitivity when using complementary one-dimensional heat conduction experiments to estimate constant thermal properties. Mehta et al. [49] inferred the temperature-dependent thermal conductivity and volumetric heat capacity of sweet potato puree using sequential parameter estimation. Benyathiar et al. [50] studied the optimal design of complementary experiments to simultaneously estimate the temperature-dependent thermal properties of sweet potato puree.

The combination of complementary data can reduce the correlation between desired parameters, improving the confidence region of estimates [44]. Further, the use of complementary experiments can improve the sensitivity coefficients of the parameters of

interest [50]. The target is to maximize the information that can be obtained from such experiments [44]. This is particularly significant for k , which usually has low sensitivity coefficients for transient models. Low sensitivity coefficients lead to significant difficulties when using mathematical programming techniques, since sensitivity and information matrices must be calculated in these methods. If there are insufficient suitable initial guesses, and large and uncorrelated sensitivity coefficients, the inverse solution diverges and fails when using classical gradient-based methods. This greatly restricts the search space and is not desirable when investigating materials that have not yet been thermally characterized.

2.4 Thermal problem modeling

2.4.1 One-dimensional thermal model

The first thermal model, shown in Figure 1a, considers transient nonlinear one-dimensional heat conduction over an isotropic plate, where phase change, convection, radiation, and heat generation are neglected. Thermal properties are considered to vary linearly with temperature, as per: $k = A + B \times T$, and $c_p = C + D \times T$; with parameters A , B , C and D being simultaneously estimated. The metal plate is uniformly heated on the top surface using a constant heat flux load. Thermal insulation condition is maintained on the bottom surface, where temperature information is measured from a single sensor. Thus, the thermal problem is governed by the heat diffusion equation expressed as follows:

$$\frac{\partial}{\partial x} \left(k \frac{\partial T}{\partial x} \right) = \rho c_p \frac{\partial T}{\partial t}, \quad 0 \leq x \leq L, t > 0 \quad (1)$$

where x is the direction of heat transfer; ρ is the constant density; t is the time; and T is the temperature, which is a function of x and t , i.e., $T = T(x, t)$.

Equation (2) and Equations (3)-(4) describe, respectively, the initial and boundary conditions to which the 1D model is subjected.

$$T(x, 0) = T_{in}, \quad 0 \leq x \leq L, t = 0 \quad (2)$$

$$-k \frac{\partial T}{\partial x} \Big|_{x=0} = \frac{T_h - T_p}{R_c}, \quad \text{at } x = 0, t > 0 \quad (3)$$

$$\frac{\partial T}{\partial x} \Big|_{x=L} = 0, \quad \text{at } x = L, t > 0 \quad (4)$$

where T_{in} is the initial temperature; T_h and T_p are the temperatures of the heater and plate at the contact point, respectively; L is the plate thickness; and R_c is the contact resistance, i.e., the reciprocal of the contact conductance h_c . R_c causes a decrease in the amount of heat conducted to the metallic sample, i.e., it represents a reducing factor in the heat flux load (q), supplied by the resistive heater.

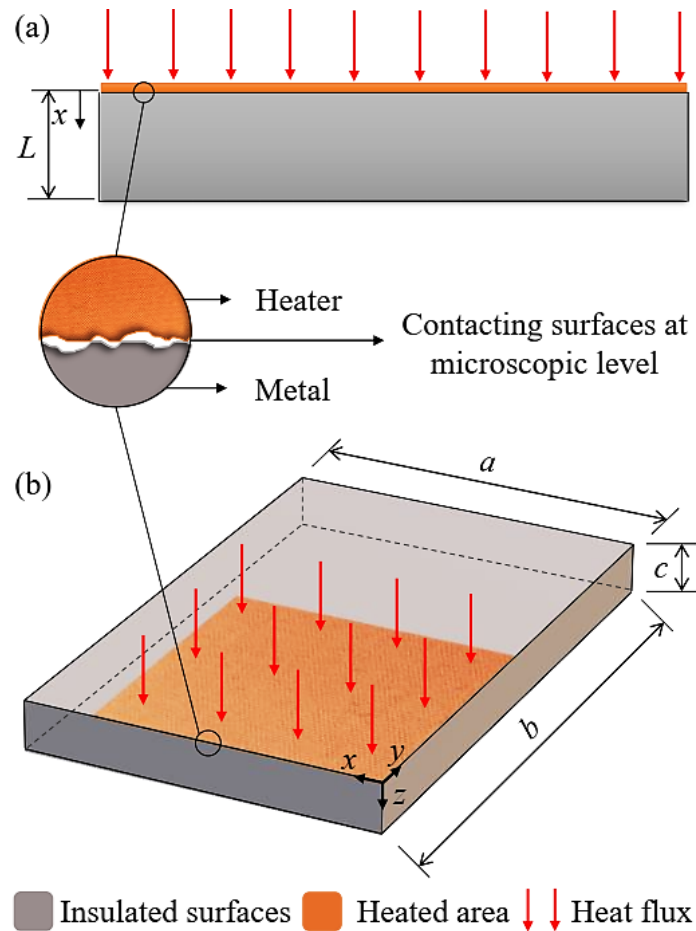


Figure 1. Schematic of the complementary heat conduction models: a) 1D thermal model; b) 3D thermal model.

The contact conductance existing at the heater-plate interface is due to two factors: i) the presence of air, causing interstitial conductance ($h_{interstitial}$), which is evaluated using the parallel-plate gap gas correlation and basically corresponds to the convection coefficient of the interstitial fluid; ii) and the contact spots, responsible for the constriction conductance ($h_{constriction}$). Radiation effects can be neglected because the experimental setup is kept below 400 °C [51]. Convection effects can also be disregarded since the interface gap thickness is too small to allow convection current [52].

The Cooper-Mikic-Yovanovich (CMY) correlation is used to calculate $h_{constriction}$. CMY correlation associates the constriction conductance with microscopical characteristics and compression load at the contacting interface, as follows [53]:

$$h_{constriction} = 1.25k_{contact} \frac{s_{asp}}{r_{asp}} \left(\frac{p}{H_c} \right)^{0.95} \quad (5)$$

where $k_{contact}$ is the thermal conductivity harmonic mean of the two materials in contact; H_c is the hardness of the softer material; p is the contact pressure; and s_{asp} and r_{asp} are, respectively, the average slope and roughness of the contact asperities.

The interstitial conductance is computed by the correlation shown below:

$$h_{interstitial} = \frac{k_{if}}{\gamma + M_g} \quad (6)$$

where k_{if} is the thermal conductivity of the interstitial fluid; γ is the mean separation thickness between the surfaces; and M_g is the gas parameter.

The contact resistance methodology used here is more completely presented in Ramos et al. [31], where the joint conductance at two contacting surfaces is assessed at microscopic level.

2.4.2 Three-dimensional thermal model

Consider a three-dimensional transient nonlinear heat conducting body. In the 3D thermal model (Figure 1b), the top surface is partially heated with a constant heat flux intensity. The isotropic metal plate is thermally insulated on all other surfaces. The thermal properties depend only on temperature, following the same linear relationship as the 1D formulation. Again, convection, heat generation, phase change, and radiation effects are neglected. Thus, this 3D direct problem can be described mathematically by Equation (7). The initial condition is given in Equation (8) and the boundary conditions in Equations (9)-(11). Two different thermal boundary conditions are applied to the upper surface (S). The boundary condition at the heated region (S_1) considers the thermal contact between the heater and the metallic plate. The rest of the upper surface (S_2) has a thermal insulation boundary condition.

$$\frac{\partial}{\partial x} \left(k \frac{\partial T}{\partial x} \right) + \frac{\partial}{\partial y} \left(k \frac{\partial T}{\partial y} \right) + \frac{\partial}{\partial z} \left(k \frac{\partial T}{\partial z} \right) = \rho c_p \frac{\partial T}{\partial t}, \quad 0 \leq x \leq a, 0 \leq y \leq b, 0 \leq z \leq c, t > 0 \quad (7)$$

$$T = T_{in}, \quad 0 \leq x \leq a, 0 \leq y \leq b, 0 \leq z \leq c, t = 0 \quad (8)$$

$$-k \frac{\partial T}{\partial z} \Big|_{z=0} = \frac{T_h - T_m}{R_c}, \quad \text{at } S_1, t > 0 \quad (9)$$

$$\frac{\partial T}{\partial z} \Big|_{z=0} = 0, \quad \text{at } S_2, t > 0 \quad (10)$$

$$\frac{\partial T}{\partial x}\Big|_{x=0} = \frac{\partial T}{\partial x}\Big|_{x=a} = \frac{\partial T}{\partial y}\Big|_{y=0} = \frac{\partial T}{\partial y}\Big|_{y=b} = \frac{\partial T}{\partial z}\Big|_{z=c} = 0, \quad t > 0 \quad (11)$$

where T depends on Cartesian coordinates (x, y, z) and time t , i.e., $T = T(x, y, z, t)$; a , b and c are the sample linear dimensions; S_1 is the region at the top surface where the heat flux is imposed, and is limited to $(0 \leq x \leq l_H, 0 \leq y \leq l_H, z = 0)$; l_H is the square section heater length, which is the boundary of the heated region S_1 ; and S_2 is the other portion of the top surface, which is subjected to thermal insulation. Thermal insulation is applied to all other domain boundary surfaces.

2.5 Bayesian inference for inverse solution

For the two heat conduction problems described above, one can formulate direct problems in which geometry, thermal properties, and initial and boundary conditions are known. These direct problems are solved to determine the transient temperature distribution in the metallic samples. On the other hand, it is also possible to deal with an inverse problem for which the thermal conductivity and specific heat are taken as unknown. The solution to this inverse problem, which seeks to estimate the quantities of interest (k and c_p), is feasible using transient temperature measurements. In the inverse thermal problem assessment, parameters for the thermal properties as linear functions of temperature are unknown quantities. Complementary transient temperature histories are measured at discrete time steps and then used to retrieve the vector containing the desired parameters $\mathbf{P} = [A, B, C, D]$. Thus, the inverse problem under consideration is defined and evaluated as an optimization problem, where the temperature distributions of both thermal models are numerically calculated, and then compared to

experimentally measured temperatures. The simultaneous inverse estimation of the linearly temperature-dependent thermal conductivity and specific heat of 304 ASS is performed considering data from the whole temperature domain.

The Bayesian inference is a stochastic manner of optimization. The Bayesian approach to statistics considers the inverse problem solution as a statistical inference based on analyzing the posterior probability distribution [54], [55]. The objective is to explore the posterior distribution related to the probability of a range of values for the unknown parameters, given temperature measurements. This condition makes statistical approaches considerably different from traditional deterministic techniques. Deterministic methods obtain single estimates of the unknown parameters whereas statistical methods do not generate only single estimates. Rather, the framework of Bayesian statistics produces a distribution that is employed to determine estimates that have different probabilities. Bayesian inference can assess not only knowledge regarding the uncertainties associated with the estimates, but also intrinsic regularization is provided to the inverse problem so that it can be turned into a well-posed problem [56]. As inserting subjective prior information is a fundamental principle of the Bayes' theorem, this statistical-based method is affected by initial guesses [56].

The Bayesian approach employs measurements as a foundation for establishing a "Gaussian tent" over these measured data, provided that the results can be well represented by a Gaussian distribution. This probabilistic regularization smooths the ill-posedness of the inverse problem and attempts to statistically account for unavoidable variations in the measurements [56]. In Bayesian estimation, the prime target is to infer the probability distribution of unknown quantities from available data (current and previous information), also named the posterior probability density function (PPDF). The Bayesian inference is based on the Bayes' theorem, which is stated as follows according to Kaipio and Fox [57]:

$$\pi_{\text{posterior}}(Z) = \pi(Z|Y) = \frac{\pi(Y|Z)\pi(Z)}{\pi(Y)} \quad (12)$$

where Z denotes the hypothesis (missing parameters, vector or scalar); Y represents the observations/ measurements (vector), i.e., the observed data related to the hypothesis; $\pi(Z|Y)$ is the PPDF, i.e., the conditional probability of Z given the observations Y ; $\pi(Y|Z)$ is the likelihood function, which is the conditional probability density function of the observations Y considering missing the unknown parameters Z ; $\pi(Z)$ is the prior density function (PDF), i.e., a statistical representation for the knowledge about the unknown parameters prior to the observations; $\pi(Y)$ is the marginal likelihood, which assesses the model fit and acts as a normalizing constant of Bayes' theorem. Therefore, after having observed Y , Bayes' formula is employed to obtain the distribution of Z conditional on Y , i.e., the posterior probability of the hypothesis considering some observations is achieved by multiplying its likelihood and prior probability.

An outlook on Bayesian inference on estimating thermal parameters is addressed here. Generally, the thermal properties of conducting materials cannot be directly measured. As a result, one can design experiments to obtain temperature measurements to solve an inverse problem to estimate the related and unknown quantities. In this sense, the thermal properties can be assumed as random variables and Bayesian inference can be employed to reconstruct the probability density functions of \mathbf{P} given the transient temperature measurements and thermal model.

Techniques based on Bayesian inference have proved their applicability to this kind of inverse problem since the temperature response is known to be a sufficient statistic of k and c_p [56]. Bayes' theorem is the mathematical method used to integrate new available data with previously obtained information. Markov chain Monte Carlo (MCMC) sampling was used to solve the inverse problem and then to evaluate the posterior distribution. MCMC sampling

methods are feasible approaches for computing estimates in cases where the quantity of unknown parameters is not very large [55]. These methods usually lead to computationally demanding solutions, which is a practical disadvantage. The inverse problem is solved by sampling candidate values from the PDF and evaluating them through the thermal model that generates results that are compared with the measured data through the likelihood function. All available knowledge is used to reduce the uncertainty present in a primary assumption related to inferential statistics. As new knowledge is achieved, there is a combination of previous and current information to devise the base for statistical processes. A candidate value that is consistent with the data receives a higher probability than a candidate value that is not. The evaluation of the thermal model and the update process from PDF to PPDF occurs simultaneously.

Let \mathbf{Y} denote the vector containing the experimentally measured temperatures, as follows:

$$\mathbf{Y}^T = [\mathbf{Y}_1, \mathbf{Y}_2, \dots, \mathbf{Y}_N] \quad (13a)$$

with

$$\mathbf{Y}_i = [Y_{1D_i}, Y_{3D_i}] \quad \text{for } i = 1, \dots, N \quad (13b)$$

where N are the number of measurements; and Y_{1D} and Y_{3D} are the components of \mathbf{Y}_{1D} and \mathbf{Y}_{3D} , the vectors of temperature measurements from the 1D and 3D experiments, respectively.

The vector \mathbf{P} is introduced into Bayes' theorem as the hypothesis Z , associating the inverse problem of interest here with the Bayesian inference. The Bayesian formulation for the simultaneous estimation is described in detail next:

$$\pi_{posterior}(\mathbf{P}) = \pi(\mathbf{P}|\mathbf{Y}) = \frac{\pi(\mathbf{Y}|\mathbf{P})\pi(\mathbf{P})}{\pi(\mathbf{Y})} \quad (14)$$

The calculation of the marginal probability density of the measurements $\pi(\mathbf{Y})$ can usually be ignored for a functional application of Bayes' formula since $\pi(\mathbf{P}|\mathbf{Y})$ must be a proper probability distribution. The PPDF can be thus rewritten as the product of $\pi(\mathbf{Y}|\mathbf{P})$ and $\pi(\mathbf{P})$, as follows:

$$\pi_{posterior}(\mathbf{P}) = \pi(\mathbf{P}|\mathbf{Y}) \propto \pi(\mathbf{Y}|\mathbf{P})\pi(\mathbf{P}) \quad (15)$$

The posterior distribution was estimated by the Metropolis-Hastings algorithm (MH-MCMC), the most popular Markov chain algorithm [55]. The implementation of the Metropolis-Hastings algorithm is performed by initially choosing a jumping distribution $p(\mathbf{P}^*, \mathbf{P}^{n-1})$, which is a probability density employed to obtain a new state \mathbf{P}^* given the current state \mathbf{P}^{n-1} of the Markov chain. After selecting this proposal distribution, the following steps must be repeated until achieving the total number of states G :

1. Take the state n of the Markov chain and draw a sample \mathbf{P}^* from a jumping distribution $p(\mathbf{P}^*, \mathbf{P}^{n-1})$;
2. Solve the direct problem using \mathbf{P}^* ;

3. Compute the posterior $\pi(\mathbf{P}^*|\mathbf{Y})$;
4. Compute the acceptance function:

$$\alpha = \min \left[1, \frac{\pi(\mathbf{P}^*|\mathbf{Y})p(\mathbf{P}^{n-1}, \mathbf{P}^*)}{\pi(\mathbf{P}^{n-1}|\mathbf{Y})p(\mathbf{P}^*, \mathbf{P}^{n-1})} \right]; \quad (16)$$

5. Generate a random value U which is uniformly distributed on $(0,1)$;
6. If $U \leq \alpha$, define $\mathbf{P}^n = \mathbf{P}^*$; otherwise, define $\mathbf{P}^n = \mathbf{P}^{n-1}$;
7. Set $n = n + 1$ and return to step 1.

In such a way, the sequence $\{\mathbf{P}^1, \mathbf{P}^2, \mathbf{P}^G\}$ representing the posterior distribution is generated. The inference on this distribution is determined from analyzing the samples \mathbf{P}^n . It is important to notice that \mathbf{P}^n values must only be considered after the chain has reached convergence to equilibrium. More theoretical details on MH-MCMC can be found in Kaipio and Fox [57].

Normal distributions are suitable to statistically characterize thermocouple measurements because of the central limit theorem. Measurement errors are usually the result of many other errors, and the combination of these errors leads to normality. Therefore, the measurement errors are taken as Gaussian random variables, additive and independent of the sought parameters \mathbf{P} . Thus, the likelihood function can be given as follow according to Wang and Zabararas [56]:

$$\pi(\mathbf{Y}|\mathbf{P}) = \frac{1}{(2\pi)^{N/2} |\mathbf{W}|^{1/2}} \exp \left\{ -\frac{1}{2} [\mathbf{Y} - \mathbf{T}(\mathbf{P})]^T \mathbf{W}^{-1} [\mathbf{Y} - \mathbf{T}(\mathbf{P})] \right\} \quad (17)$$

where $\mathbf{T}(\mathbf{P})$ is the numerical solution of the direct problems with a given \mathbf{P} at specific sensing locations. \mathbf{T} is given in function of the components of \mathbf{T}_{1D} and \mathbf{T}_{3D} , the vectors containing the numerical temperatures from the direct 1D and 3D thermal problems, respectively.

$$\mathbf{T}^T = [\mathbf{T}_1, \mathbf{T}_2, \dots, \mathbf{T}_N] \quad (18a)$$

with

$$\mathbf{T}_i = [T_{1D_i}, T_{3D_i}] \quad \text{for } i = 1, \dots, N \quad (18b)$$

\mathbf{W} is the covariance matrix of the measurement errors, which, for uncorrelated measurements, is given in the following form:

$$\mathbf{W} = \begin{bmatrix} \sigma_{Y_1}^2 & \cdots & 0 \\ \vdots & \ddots & \vdots \\ 0 & \cdots & \sigma_{Y_N}^2 \end{bmatrix} \quad (19)$$

The uncertainty σ_Y is due to the experimental temperature errors, which are assumed to be Gaussian with zero mean and standard deviation of 1 °C. This assumption is based on the procedure used to calibrate the thermocouple [55], which is addressed in the experimental section.

A critical issue in Bayesian statistics is its inherent subjectivity to prior data. Whether previous information about \mathbf{P} is available, it should be introduced into the PDF. In this context,

whether a Gaussian distribution is considered, the prior density function can be expressed as follows:

$$\pi(\mathbf{P}) = \frac{1}{(2\pi)^{M/2} |\mathbf{V}|^{1/2}} \exp \left\{ -\frac{1}{2} [\mathbf{P} - \boldsymbol{\mu}]^T \mathbf{V}^{-1} [\mathbf{P} - \boldsymbol{\mu}] \right\} \quad (20)$$

where M is the number of parameters to be estimated; $\boldsymbol{\mu}$ and \mathbf{V} are the mean and covariance matrices for \mathbf{P} , respectively. Matrix \mathbf{V} is computed as:

$$\mathbf{V} = \begin{bmatrix} \sigma_A^2 & 0 & 0 & 0 \\ 0 & \sigma_B^2 & 0 & 0 \\ 0 & 0 & \sigma_C^2 & 0 \\ 0 & 0 & 0 & \sigma_D^2 \end{bmatrix} \quad (21)$$

By contrast, if \mathbf{P} is unknown and there is no previous knowledge about it in advance, Bayes' postulate states that $\pi(\mathbf{P})$ should be a uniform distribution. Uniform prior distributions are improper, and sometimes noninformative. Proper posteriors can often be found from improper priors. Nevertheless, improper priors can lead to problems when dealing with a continuous parameter space. Thus, Jeffreys' priors, which are constructed to be "minimally acceptable" noninformative priors, can be used as reference priors [57]. For a uniform prior density function as reference assumption, $\pi(\mathbf{P}) \propto 1$ and the PPDF is then summarized as $\pi(\mathbf{Y}|\mathbf{P})$. This means that the posterior probability density becomes equal to the likelihood function, i.e., $\pi(\mathbf{P}|\mathbf{Y}) \propto \pi(\mathbf{Y}|\mathbf{P})$.

Finally, by replacing Equations (17) and (20) into Bayes' theorem, one can obtain this general formulation:

$$\ln [\pi(\mathbf{P}|\mathbf{Y})] \propto -\frac{1}{2}[(M + D) \ln 2\pi + \ln|\mathbf{W}| + \ln|\mathbf{V}| + S_{MAP}(\mathbf{P})] \quad (22)$$

where:

$$S_{MAP}(\mathbf{P}) = [\mathbf{Y} - \mathbf{T}(\mathbf{P})]^T \mathbf{W}^{-1} [\mathbf{Y} - \mathbf{T}(\mathbf{P})] + [\mathbf{P} - \boldsymbol{\mu}]^T \mathbf{V}^{-1} [\mathbf{P} - \boldsymbol{\mu}] \quad (23)$$

It can be noted from Equation (23) that the estimation procedure develops into an optimization problem, in which the point estimates for \mathbf{P} are achieved at the maximum of the posterior probability density (MAP – the maximum *a posteriori*). Therefore, despite using MH-MCMC to solve the inverse problem being studied, the estimation procedure could be performed by maximizing the posterior distribution, based on minimizing the maximum *a posteriori* objective function S_{MAP} . The first and second terms expressed on the right side of Equation (23) denote the trade-off between the likelihood and prior distributions, respectively, when estimating parameters by Bayesian inference. As stated earlier, all terms related to the prior distribution are set to 1 when a uniform prior model is injected into the estimation formulation. For smooth nonlinear but differentiable problems, like the one at hand, the MAP estimation problem can be solved using gradient-based optimization. MAP estimates were not used here because although they are generally fast and simple to compute, they do not provide statistical information about the estimates. For this purpose, MCMC sampling methods are usually recommended since they can easily make available information to calculate the uncertainty inherent to the posterior distribution.

2.6 Sensitivity analysis

An analysis of the sensitivity coefficients before carrying out experiments leads to a better experimental design when estimating unknown parameters. It provides guidance on how well-designed the experimental arrangement is and assesses the influence of each design variable on the mathematical model response [49]. Sensitivity analysis can also help to reduce ill-posedness and decrease experimental uncertainties. Sensitivity coefficients may seem more significant in classical gradient-based methods since they directly influence the topology of the objective function to be minimized. They are also necessary when building the sensitivity matrix to compute the estimates. However, sensitive information is also essential and needs to be analyzed when using stochastic-based methods. This is due to the fact that the sensitivity coefficients provide knowledge of the function behavior, guiding search and coverage of metaheuristics and impacting the Bayesian posterior distribution equilibrium. Thus, overall, a temperature response that is sensitive to the unknown parameter being estimated is always physically essential for understanding, formulating, and solving inverse problems [7].

Sensitivity coefficients assess the sensitivity of the temperature in relation to a change in the thermal parameter analyzed. A small sensitivity magnitude value denotes that large changes in the parameter result in small changes in the temperature field [4]. Estimating this parameter from temperature measurements is consequently difficult in such a case because the inverse problem is ill-conditioned. There is also ill-conditioning if the sensitivity coefficients are linearly dependent, or in other words, if one of the sensitivities is some combination of the others. Scaled sensitivity coefficients with large magnitudes that are linearly independent (uncorrelated) are needed for a reliable and accurate simultaneous parameter estimation [7]. The scaled sensitivity coefficient (J), which presents units of temperature, is the first partial derivative of the temperature T in relation to the parameter of interest P (i.e., A , B , C and D)

multiplied by the parameter itself: $J_P = P \times \partial T / \partial P$. For the 1D formulation, comparing different sensitivity plots using scaled sensitivity coefficients is more convenient because it provides sensitivities on the same basis. Nevertheless, sometimes even with modified sensitivity coefficients, it may be difficult to draw conclusions about the optimal conditions to evaluate the desired parameters. It is still more difficult when dealing with various parameters and several locations since lot of data must be examined graphically. This condition, which is the case of the 3D formulation, requires a straightforward criterion to assess the sensitivity.

The D-optimality concept has been successfully employed as an experimental design method to investigate the optimal aspects in heat transfer [58]. This criterion is formulated on the maximization of the determinant Δ of the information matrix $\mathbf{X}^T\mathbf{X}$, which is constructed from the sensitivity matrix \mathbf{X} and its transpose, as follows:

$$\Delta \equiv |\mathbf{X}^T\mathbf{X}| \quad (24)$$

$$\mathbf{X} = \frac{\partial \mathbf{T}^T}{\partial \mathbf{P}} \quad (25)$$

$$J_P = P \frac{\partial T}{\partial P} \quad (26)$$

where $\mathbf{X} = \partial \mathbf{T}^T / \partial \mathbf{P}$ is the sensitivity matrix of \mathbf{T} with respect to \mathbf{P} . So, the solution of the direct problem is needed to evaluate matrix \mathbf{X} . The inputs of this matrix are the first partial derivatives of the dependent variable \mathbf{T} , which is taken for each time and sensor location, in relation to the independent variable \mathbf{P} , which contains the parameters that are the target of the estimation technique proposed here.

This computationally efficient criterion provides guidance for experimental designs when dealing with high-dimensional problems, which require that a small number of sensors be used to accomplish the inverse solution, for practical reasons. Moreover, it is already known that k and c_p have linearly independent sensitivity coefficients for metallic materials. Thus, the D-optimality criterion is suitable for use in this study. Therefore, from the preliminary sensitivity analysis, one can evaluate which locations in the thermal model can contribute to more sensitive temperature measurements, resulting in better conditions for the simultaneous estimation of the thermal conductivity and specific heat of the metal slab. The sensitivity computation is carried out from the properties at room temperature obtained from Valencia and Queded [24]. While temperature dependence conducts to slightly different sensitivity values when carrying out the simultaneous estimation, this analysis seeks to furnish prior knowledge regarding the feasibility of the procedure. Additionally, Bayesian computation can also be employed to investigate how the thermocouple location affects the reliability region of the inverse solution. It is rather difficult to analytically analyze the thermocouple location effect on the PPDF. Therefore, this alternative method explores and reveals the effect of the sensor location by performing numerical simulations with data from different locations and comparing the posterior estimates (both point estimates and probability limits) from MCMC samples. This is another option to guide optimal experiment design in data-driven inverse heat conduction problems to obtain accurate solutions [56].

2.7 Experimental aspects

The location of temperature sensors is essential to evaluate an inverse thermal problem since it is necessary to convey a sufficiently complete information about the transient behavior

of the thermal model. Additionally, in data-driven inverse problems, it is important to achieve an accurate inverse solution using a minimum number of sensors, from a practical sense.

For high-conductivity materials, sensitivity coefficients are normally higher near heated regions. This means that better sensitivity would be obtained at the surface points under the heater. However, it is often not feasible to measure temperature at these locations using thermocouples, since the sensor strongly impacts the heater placement, leading to losses in heat transfer between the heater and metal. Embedded thermocouple wires need that some filler material to be introduced into a milled hole, which causes a discontinuity effect [59]. In this context, only the bottom surface can be explored to collect temperature data with wire thermocouples in the 1D thermal model [60]. Being the bottom surface the only point that can be explored to collect temperature, data from the 1D experiment was measured at $x = L$. Researchers have already shown that this location can transmit information that is sensitive enough to carry out the estimation process, given appropriate initial values [31], [60].

For the 3D formulation, a D-optimality-based sensitivity analysis was carried out to identify the most sensitive zones. Figure 2 shows a representation of the D-optimality criterion for all sample surfaces. The best regions for placing sensors are those that have greater values. An analysis of Figure 2 reveals that some zones of surfaces I, II, III and VI have D-criterion values with the same order of magnitude. However, as already said, when designing experiments for data-driven inverse heat conduction problems, it is of practical importance to make use of a minimum quantity of sensors to obtain a reliable, accurate inverse solution. Thus, taking into consideration the sensitivity analysis and experimental aspects (e.g., insulation deficiency), a single thermocouple was placed on the bottom surface (VI, $z = c$) at position (2.00, 2.00, $c = 8.90$) mm and welded with the aid of a capacitive discharge. Furthermore, from a practical aspect, it is worth mentioning that measuring temperature by a thermocouple at the heated surface (I, $z = 0$) is not feasible for metallic materials.

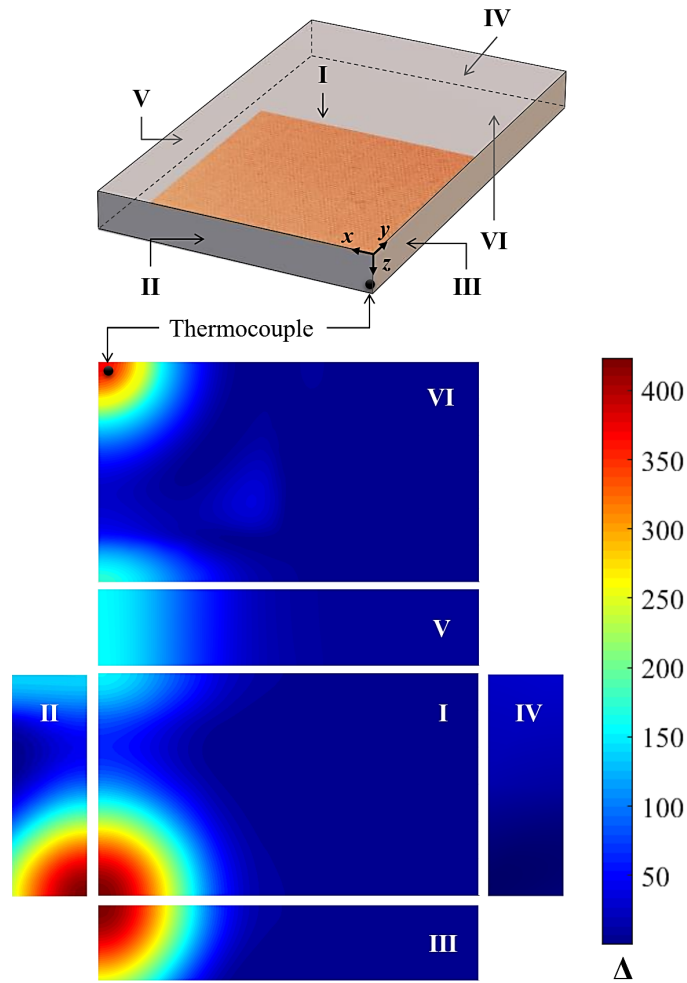


Figure 2. D-optimality criterion for all sample surfaces. Unfolded view with the sensor location.

Since the location of a single sensor in each experiment is a sensitive issue for the estimation procedure, the scaled sensitivity coefficients obtained by combining complementary thermal models must be examined. Figure 3 shows the scaled sensitivity coefficients for the 1D (J_{1D}) and 3D (J_{3D}) thermal models, and for their combination (J_{1D+3D}). One can note in this figure that complementary data increases the sensitivity coefficients of parameters C and D , corresponding to c_p , over the entire experiment. It is hard to obtain temperature data that is sufficiently sensitive to thermal conductivity when studying metals in transient state. This is because k has its sensitivity proportional to the imposed heat load, and substantially high heat

flux intensities are difficult to achieve experimentally. Due to its lower sensitivity, thermal conductivity is usually more affected by measurement errors, i.e., k is more imprecisely estimated compared to c_p . Thus, more importantly, complementary experiments increase the sensitivity coefficients of parameters related to k , i.e., A and B , at the beginning of the experiments. Although low sensitivity at initial stages is generally overcome later for well-designed whole domain estimations, its effects cannot be completely neglected, since regions with sensitivity deficiency can bias or even disable the estimation procedure [4]. It is difficult to evaluate estimations using temperature data from these regions, since they are very susceptible to errors. One can conclude that it is impossible to simultaneously identify all sought-after parameters if one only considers temperature measurements during the initial moments. One can also observe that combining temperature data provides uncorrelated sensitivity coefficients with good magnitudes over time. When estimating two or more parameters, one should attempt to achieve the largest value of the determinant of the information matrix, i.e., $\Delta = \max|\mathbf{X}^T\mathbf{X}|$. These are, respectively, the optimality criterion Δ for the 1D and 3D thermal models, and the combination of the two: 2.378×10^8 , 5.838×10^9 , and 3.991×10^{12} . One can see that there is a significant increase of 3 orders of magnitude in Δ when using complementary data. Even though the determinants of $\mathbf{X}_{1D}^T\mathbf{X}_{1D}$ and $\mathbf{X}_{3D}^T\mathbf{X}_{3D}$ can be null, the determinant of the sum $\mathbf{X}_{1D}^T\mathbf{X}_{1D} + \mathbf{X}_{3D}^T\mathbf{X}_{3D}$ is unlikely to be equal to zero. In this sense, the minimum hypervolume obtained from Equation (24) is defined by the maximum of the determinant of $\mathbf{X}_{1D}^T\mathbf{X}_{1D} + \mathbf{X}_{3D}^T\mathbf{X}_{3D}$ [44]. Since the purpose of sensitivity evaluations is to obtain prior knowledge about the inverse procedure feasibility, one can be assured that combining the collected measurements will greatly improve sensitivity and enable a suitably accurate inverse solution.

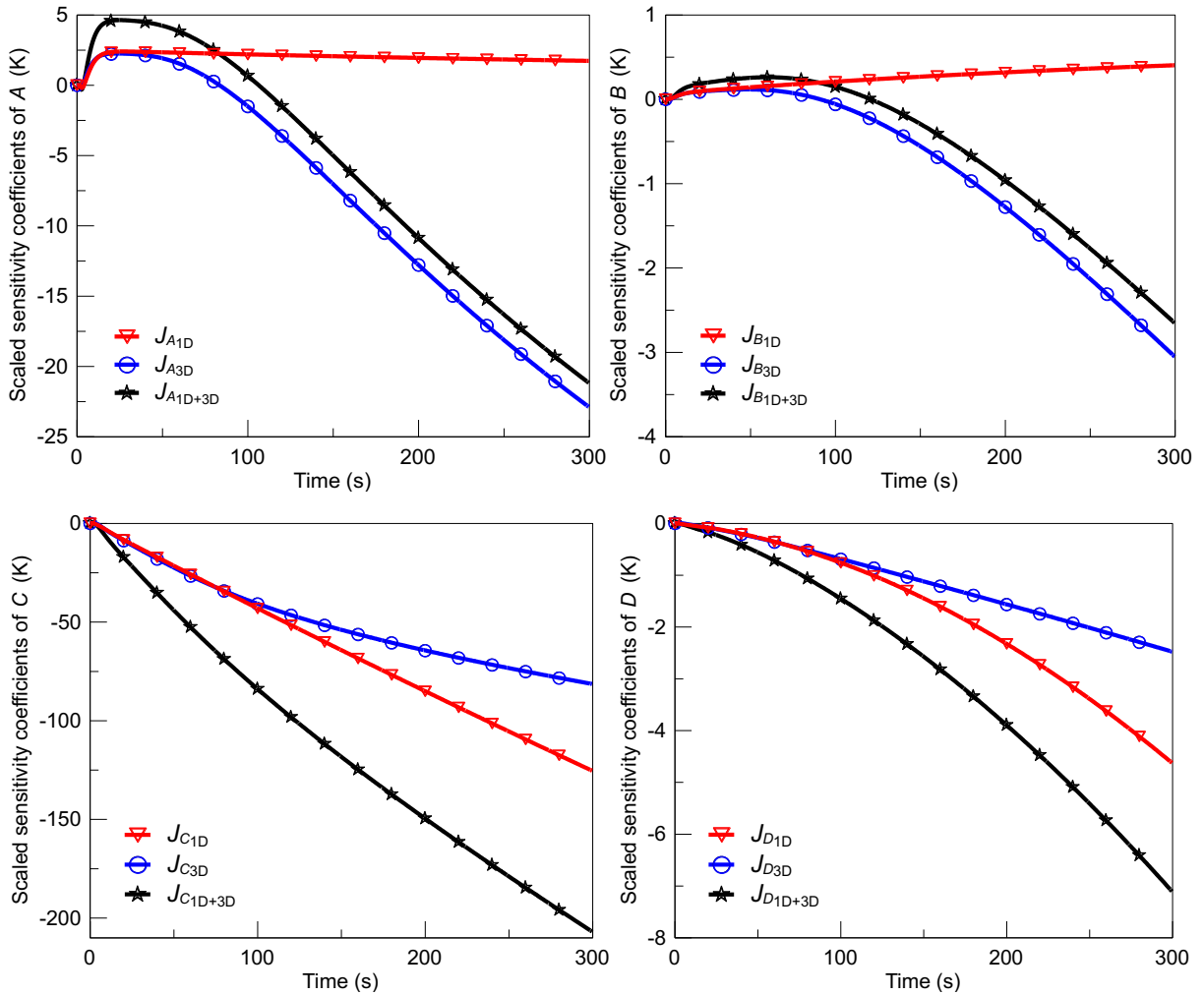


Figure 3. Scaled sensitivity coefficients of parameters describing the linear functions of $k(T)$ and $c_p(T)$.

2.8 Heat conduction experiments

Both experimental arrangements are somewhat similar and include: a metal plate with the top surface exposed to a constant heat flux, while the side and bottom surfaces were thermally insulated; a resistive heater (Omega SRFGA20210, 333.6 Ω); two insulation blocks made up of refractory ceramic fiber ($k = 0.05 \text{ W m}^{-1} \text{ K}^{-1}$ and $c_p = 865 \text{ J kg}^{-1} \text{ K}^{-1}$, at room temperature); a T-type thermocouple; a programmable digital DC power supply (IT6953A, least counts 1 mA,

1 mV); two digital multimeters (Minipa ET2042C, resolution $\pm 0.1 \Omega$, $\pm 0.01 \text{ A}$); a data acquisition system (DAS Keysight 34980A); and a computer. Figure 4 shows a representation of the experimental setups used to thermally characterize 304 austenitic stainless steel.

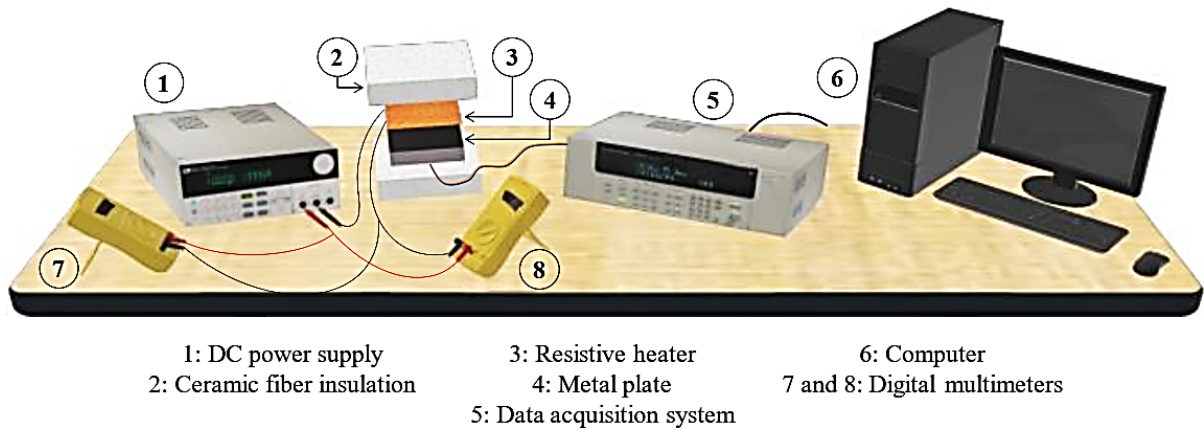


Figure 4. Schematic of the experimental arrangement used to simultaneously identify $k(T)$ and $c_p(T)$.

The test samples were milled and ground to the following dimensions (unit: mm): 49.95 width (a), 50.05 length (b), and 10.70 thickness (c), for the 1D experiment; and 60.30 width (a), 99.80 length (b), and 8.90 thickness (c), for the 3D experiment. These dimensions were assessed with a vernier caliper (Mitutoyo 530104BR, resolution $\pm 0.05 \text{ mm}$). The sample weights were taken by a precision balance (Bel S2202H, resolution $\pm 0.1 \text{ g}$) and divided by the volumes, determining the mean density at 8024 kg m^{-3} . The chemical composition of the 304 ASS specimens, which was determined using an XRF spectrometer (Niton XL3t-800), is as follows (in wt.%): 0.07C-18.5Cr-1.7Mn-9.3Ni-0.8Si-0.03P-0.03S-0.2Cu-Fe.

The specimens were placed in a pocket milled into the bottom insulation block, and initially kept at room temperature. They were heated for 300 s, reaching a temperature around $150 \text{ }^\circ\text{C}$ at the thermocouple location. Electric power was conducted to the heater by the digital

DC power supply, and both current and voltage were measured by the digital multimeters. Both experiments were performed using a heat flux input of 20000 W m^{-2} maintained constant during the entire duration of the tests, until power was switched off. Transient temperature measurements were collected at 0.1-sec intervals by the DAS, recorded, and then used as information to perform the simultaneous parameter estimation in the desktop computer. The thermocouples used (30AWG with resolution of $\pm 0.1 \text{ }^\circ\text{C}$, and diameter of 0.25 mm) were calibrated by comparing their readings with measurements from a PT-100 sensor in a thermostatic bath (Marconi MA184, resolution $\pm 0.01 \text{ }^\circ\text{C}$), and welded on the samples using capacitive discharge resistance welding.

One had to measure several physical quantities related to the experimental setups and introduce these into COMSOL Multiphysics to determine the contact resistance, which was $0.0010 \text{ K m}^2 \text{ W}^{-1}$ for the 1D experiment and $0.0012 \text{ K m}^2 \text{ W}^{-1}$ for the 3D experiment. A digital roughness meter (Mitutoyo SJ210, resolution $\pm 0.01 \text{ } \mu\text{m}$) measured surface roughness at $0.18 \text{ } \mu\text{m}$ for the 1D plate, $0.21 \text{ } \mu\text{m}$ for the 3D plate, and $0.83 \text{ } \mu\text{m}$ for the resistive heater. Contact pressure between the heater and the specimen was assessed by dividing the test setup weight by its cross-sectional area. Contact pressure was 1411.7 N m^{-2} and 1293.3 N m^{-2} for the 1D and 3D experiments, respectively. Hardness was determined with a hardness testing machine (Otto Wolpert-Werke Testor HT1, resolution of $\pm 0.5 \text{ HB}$), resulting in 125.5 HB for the 1D sample and 128.0 HB for the 3D sample.

2.9 Results and discussion

For any numerical simulation, the computed solution must be independent of the mesh size. Mesh independence assessments were performed for both thermal models by solving their

direct problems. For the 1D model, mesh geometries with 5, 8, 11, 14, and 17 elements were tested. Differences close to 0.003 °C were noted among the results using meshes with 11 and 14 elements. In the 3D model, temperature distribution was computed in COMSOL using five pre-defined mesh geometries, which were extremely-fine, extra-fine, fine, normal, and coarse. These were generated directly by the default meshing options and were adapted to the characteristics of the thermal problem. Differences no greater than 0.009 °C were noted between the results obtained with these meshes. Therefore, to obtain an accurate inverse solution at reasonable computational costs, when simultaneously identifying the sought thermal properties, the 11-element mesh was used to solve the 1D problem, and the “coarse” mesh was used to evaluate the 3D problem.

To assess the Bayesian estimation methodology, the total number of states (G) was set to 8000, which is enough to avoid the oscillation of the initial samples dealt with by the Markov chain with a reasonably fast computational rate. As the MCMC algorithm is not initialized at its stationary distribution, there may be some bias caused by its starting points. To compensate for this, the conception of burn-in period was introduced to reduce the effect of correlation between the initial MCMC samples on estimation results. This implies that some states (iterations) at the beginning of the MCMC run are eliminated, with the number of discarded states being chosen to be great enough for the MCMC chain to reach its invariant distribution by this time. Figure 5 shows the evolution of the natural logarithm of the PPDF $\ln[\pi(\mathbf{P}|\mathbf{Y})]$ as a function of the number of states of the Markov chain for the MCMC run using uniform prior and 8000 states. In this figure, it can be observed that the Markov chain converges reaching equilibrium in approximately 4000 states. Since the effect of the MCMC initial condition has suitably been dissipated, the first 4000 states of the MH-MCMC were disregarded for the statistical computation of the estimates.

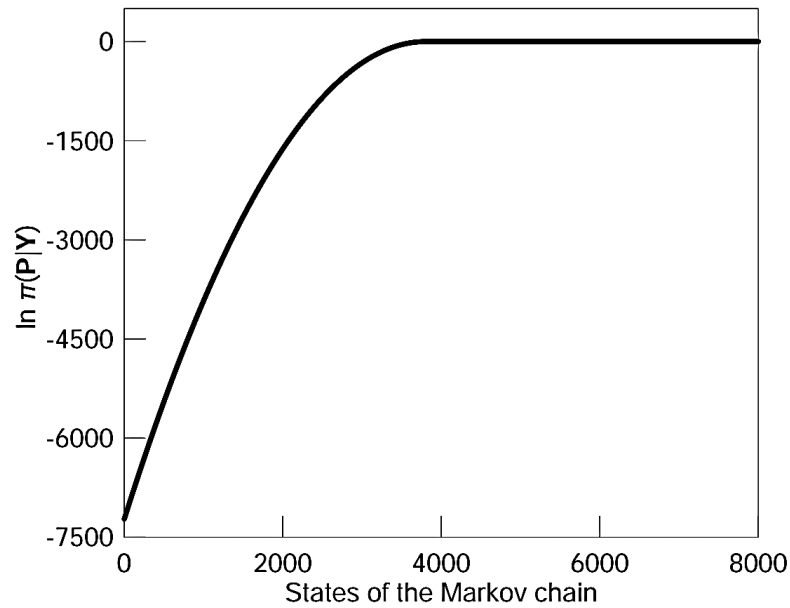


Figure 5. Evolution of the PPDF versus the number of states of the Markov chain.

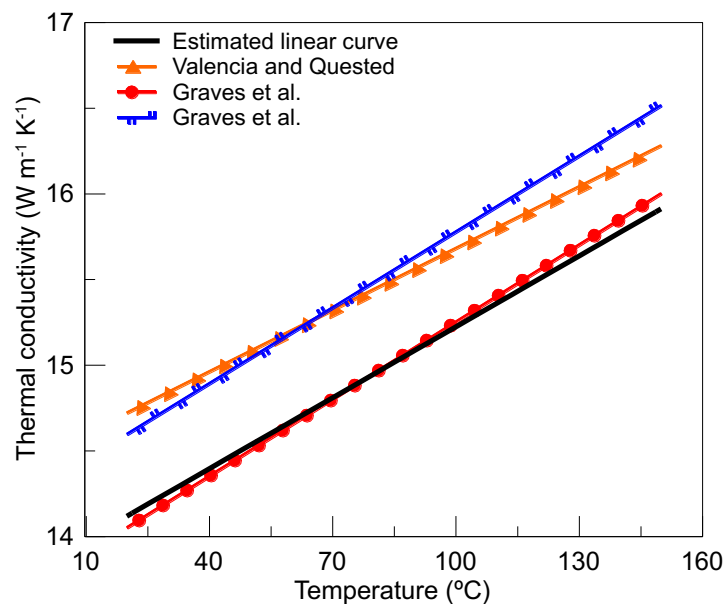
To solve the inverse problem here and guarantee convergence of the estimation process, a key point is that suitable prior knowledge about the sought-after parameters is needed. Generally, normally distributed models and uniformly distributed models are used as prior information. Inserting subjective prior information is a fundamental principle of the Bayesian framework that introduces bias in the estimation results, since this statistical-based method is easily affected by the initial guesses (prior distribution). The uniform distribution with probability density of $\pi(A) \sim U(0, 24) \text{ W m}^{-1} \text{ K}^{-1}$, $\pi(B) \sim U(0, 0.02) \text{ W m}^{-1} \text{ K}^{-2}$, $\pi(C) \sim U(0, 700) \text{ J kg}^{-1} \text{ K}^{-1}$, and $\pi(D) \sim U(0, 0.2) \text{ J kg}^{-1} \text{ K}^{-2}$ was assumed as prior and feasible search space. Analyzes were conducted to attempt to enlarge the search limits, but the outcomes were severely impacted when using wider search regions. Uniform priors enable accurate results with a reasonable computational cost, since some calculations are simplified when this kind of prior is used.

Table 1 shows the results of the simultaneous Bayesian estimation for five sets of complementary experiments. This means that measurements were replicated at least five times

for each specimen. The standard deviation values denote the probability uncertainty inherent to Bayesian statistics. The average of the Bayesian estimates was used to construct linear curves describing k and c_p versus temperature, as shown in Figures 6 and 7. These thermal property correlation equations, Equations (27)-(28), can be applied to temperatures ranging from 20 °C to 150 °C. Four significant digits were used to specify the parameters of interest, due to the number of significant figures of the less accurate quantity experimentally measured, namely the roughness measurement. Comparing the linear functions for $k(T)$ and $c_p(T)$ obtained in this study and literature data, it can be seen that the slopes of the k linear functions are very similar for all studies, which is not the case with c_p . In this sense, it is worthwhile to mention that variations may occur mainly due to differences in the thermal characterization methods used and in the chemical composition of the stainless steel investigated in this study and those studied elsewhere. For simplicity, since the behaviors are very similar, only the graphical results corresponding to the PPDFs of A , B , C , and D for the first experimental set are shown in Figure 8.

Table 1. Simultaneous estimation of k and c_p parameters for 304 austenitic stainless steel.

Set	Bayesian estimated values							
	A [$\text{W m}^{-1} \text{K}^{-1}$]		B [$\text{W m}^{-1} \text{K}^{-2}$]		C [$\text{J kg}^{-1} \text{K}^{-1}$]		D [$\text{J kg}^{-1} \text{K}^{-2}$]	
	Mean	SD	Mean	SD	Mean	SD	Mean	SD
1	13.91	0.30	0.01369	0.00039	493.5	11.7	0.1465	0.0028
2	13.28	0.27	0.01406	0.00045	489.3	12.8	0.1422	0.0032
3	14.01	0.35	0.01469	0.00040	494.0	12.4	0.1389	0.0026
4	14.33	0.31	0.01348	0.00042	490.9	12.0	0.1451	0.0029
5	13.80	0.29	0.01353	0.00037	489.8	12.5	0.1395	0.0029

**Figure 6.** Temperature-dependent thermal conductivity of 304 austenitic stainless steel.

Comparison of the lines determined in this study with curves reported in Valencia and Qusted [24] and Graves et al. [61].

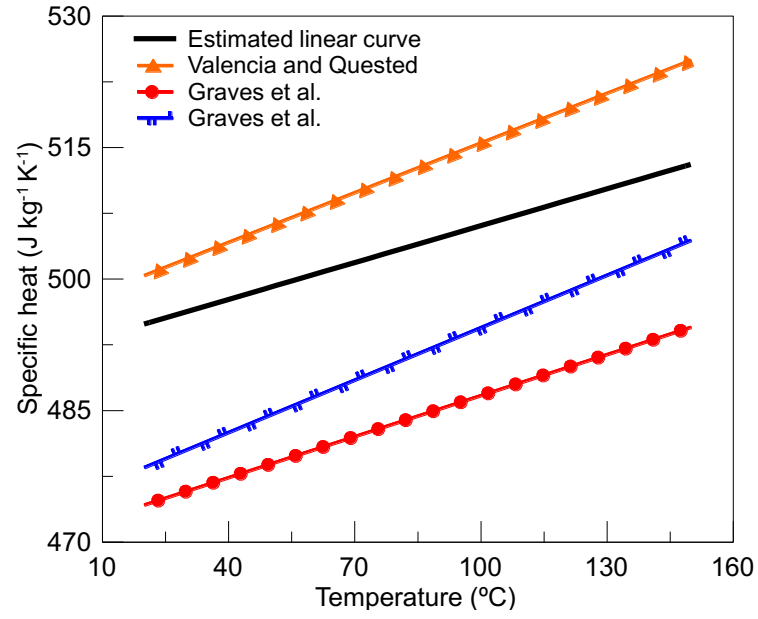


Figure 7. Temperature-dependent specific heat of 304 austenitic stainless steel. Comparison of the lines determined in this study with curves reported in Valencia and Qusted [24] and Graves et al. [61].

$$k(T) = 13.84 + 0.01380 \times T \text{ [W m}^{-1} \text{ K}^{-1}] \quad (27)$$

$$c_p(T) = 492.0 + 0.1402 \times T \text{ [J kg}^{-1} \text{ K}^{-1}] \quad (28)$$

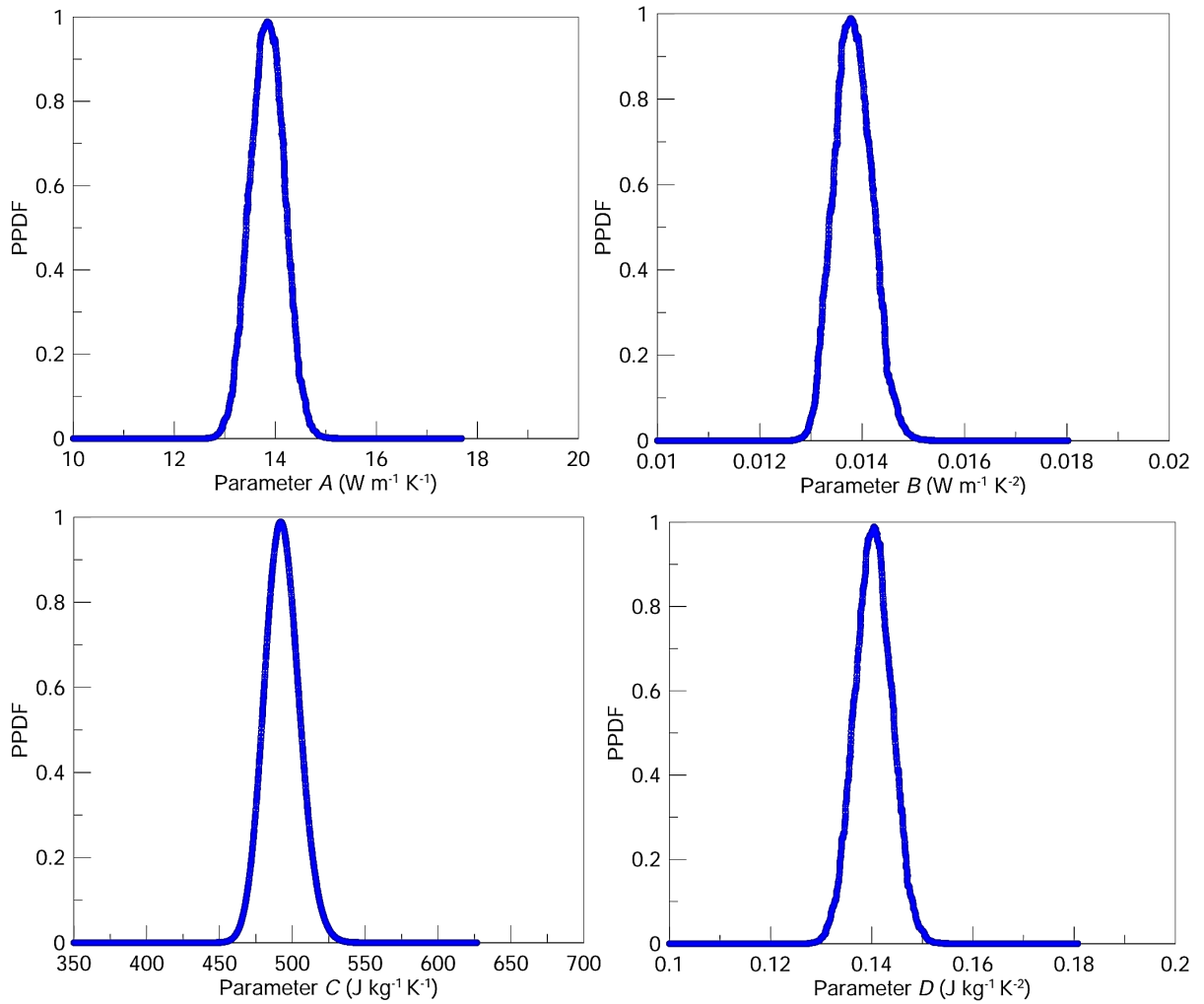


Figure 8. PPDFs of the estimated parameters for the first experimental set.

Ideally, the differences between the measured temperature and the corresponding calculated temperature are desirable to be close to zero, but that is impractical. Any object, warmer than its surroundings, naturally loses a portion of its thermal energy. Since the ceramic fiber insulation has non-null thermal properties, some heat loss is unavoidable, causing some variations in the heat flux. This means that the actual heat flux load is time-varying, rather than constant. As a result, the mathematical modeling of the physical problem is somewhat imperfect. Figure 9 shows a comparison between the measured temperatures of the first set of complementary experiments and the corresponding temperatures computed with the estimated curves. One can observe that the model-predicted temperature histories and the experimentally

measured temperatures match well for both thermal models. The largest residuals for the 1D and 3D formulation were 2.36 °C and 3.03 °C, in absolute values, respectively. These differences are acceptable because they represent approximately 1.8% and 2.5% of the maximum temperature variation, in a relative sense. This condition can be regarded as acceptable especially because one deals with a low-cost experimental setup in a transient state. Thus, unmodeled heat loss and inconsistencies involved in the inverse approach are proved to be minimal, indicating the adequacy of the thermal models used.

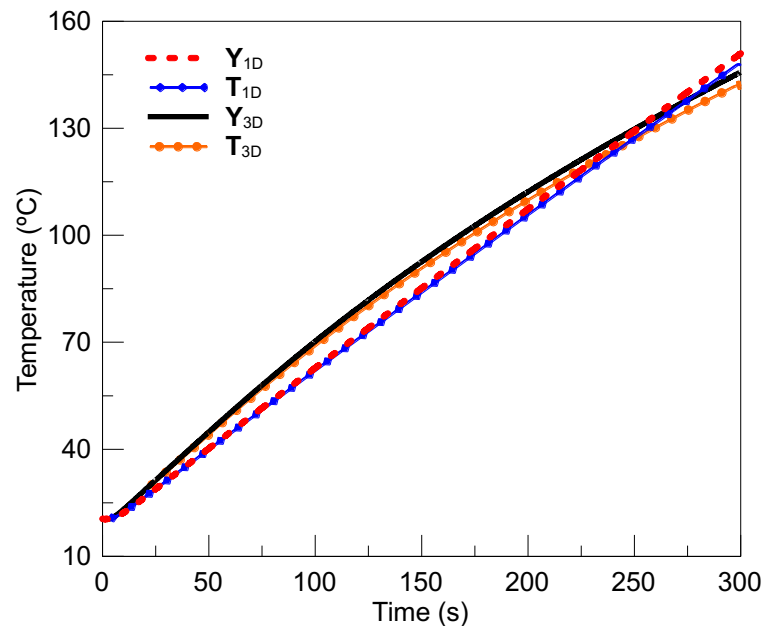


Figure 9. Temperature histories for the 1D and 3D thermal models. Comparison of measurements with numerically computed temperatures.

As part of the validation process, the repeatability of the estimation results is evaluated by performing the inverse retrieval of the heat flux intensity imposed, based on the estimated linear curves. The measured temperature data and lines estimated for the thermal properties are employed to retrieve the applied heat flux using Beck's nonlinear formulation with 10 future time steps [4]. Figure 10 shows a comparison between retrieved heat flux histories. An analysis

of this figure reveals that the heat fluxes agree well with the experimental heat load of 20000 W m^{-2} .

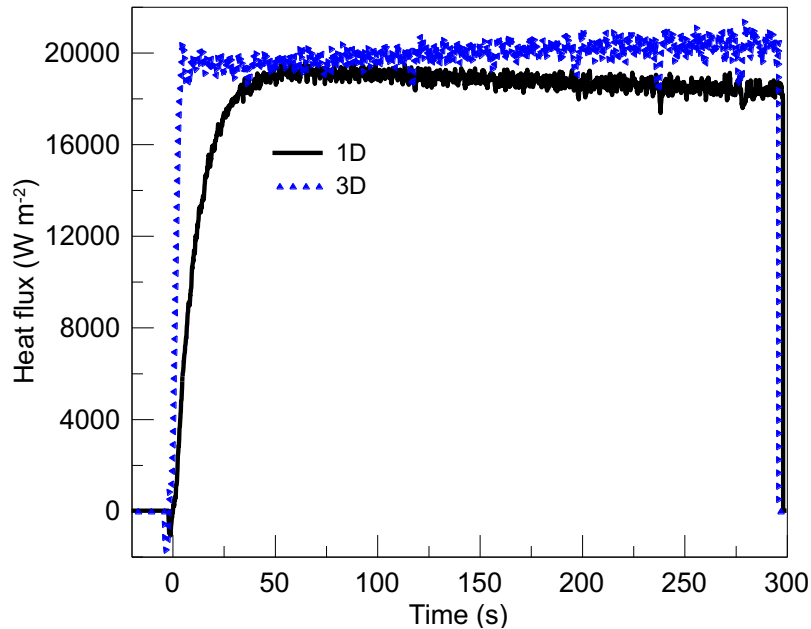


Figure 10. Comparison between the retrieved heat flux histories.

2.10 Summary

This first case study focused on using complementary experiments to simultaneously identify parameters describing the linearly temperature-dependent thermal conductivity and specific heat of 304 austenitic stainless steel. Inverse thermal analysis was based on combining measurements from two transient experiments conducted at room temperature, where each had a single sensor. Sensitivity analysis showed that complementary temperature measurements increased the sensitivity coefficients of parameters for c_p , and raised those for k at the initial stages, where lack of sensitivity is critical when handling metals. These more sensitive data produced a significant increase in the determinant of the information matrix, resulting in

improved estimates. Bayesian inference was used to take advantage of this additional sensitive information. Single-step estimation of temperature-dependent parameters was carried out considering measurement data corresponding to the entire temperature domain. As this study used a statistical optimization approach, probability distributions were obtained for the estimates instead of fixed values. Despite showing its well-known behavior of being sensitive to the prior information inserted into the statistical estimator, the Bayesian uncertainties had relatively small values, indicating the reliability of the results.

Future research work should focus on applying the proposed technique to different metallic materials, subjected to heat treatments. Additionally, as the current experimental setup provides reliable k and c_p estimates up to 150 °C, obtaining an experimental setup capable of handling higher temperature ranges would be important.

3. Case Study 2: One-year On-site Monitoring to Estimate Hygrothermal Properties of Wall Materials

3.1 Hygrothermal performance of building envelopes

With increasing concerns related to the environmental footprint of the construction sector, improving energy efficiency of buildings is an urgent need in the fight against climate change [62]. In this context, prefabrication or off-site construction can be an option to achieve more sustainable construction [63]. Modular construction can provide several environmental, economic, and social benefits, e.g. [62]: reduced environmental impacts, cost and time savings, increased on-site safety, high construction quality and efficiency, etc. In general, prefabrication offers a better life cycle performance compared to conventional (i.e., on-site) construction and can properly contribute to sustainable construction and extended durability [64].

However, there are still challenges when using prefabricated envelope modules [64]. A critical aspect is the air and water tightness at the junctions or interfaces between modular wall panels [65]. It is challenging to fully seal the joint regions due to their complex geometry [66]. In general, noticeable energy losses can directly be associated with air leakages due to poor airtightness [67], increasing the energy used for space heating and cooling. As indicated by Lozinsky and Touchie [68], air infiltration can represent up to 30 % of annual energy consumption for space heating in single-family homes located in a cold climate. A deficient airtightness can also cause moisture-related problems due to interstitial condensation (e.g., structural damage, mold growth, building materials decay, and compromising the indoor air quality), negatively impacting human health, building performance, and sustainability [69].

Building envelopes are composed of various porous materials in which heat and moisture (HAM) transport occurs, affecting the air quality, thermal comfort, and energy consumption of buildings, as well as the lifetime of building materials [70]. Condensation is possible when water vapor is cooled below the dew point, and it should be avoided at all costs to assure the durability of the assembly. Premature deterioration of building envelopes is also associated with pathologies related to moisture transport [66]. It is thus crucial to understand HAM transport in building components to reduce energy costs and optimize both the thermal performance and sustainability of building envelopes [71]. It is claimed that building energy consumption and thermal behavior could be more accurately predicted by accounting for moisture phenomena in numerical energy efficiency simulations [70], [72], [73]. HAM processes are physically coupled because the vapor saturation is temperature-dependent, and latent heat effects due to condensation or evaporation change the temperature field [74]. Moreover, simultaneous HAM transport in building materials and envelopes are associated with strongly nonlinear mechanisms [74]. Therefore, a coupled analysis of HAM phenomena helps to better investigate the hygrothermal performance of building envelopes.

The hygrothermal performance of buildings and their components has been extensively addressed in the literature [70], [72], [73], [75], [76]. Numerous numerical approaches have been developed over the years for modeling hygrothermal performance [71]. Nevertheless, it is well known that significant differences continue to exist between the actual operative behavior of a building envelope and numerical simulation results [70], [72], [77], [78]. For the performance of multilayered prefabricated wall panels, Palani and Karatas [79] showed recently that there are considerable disparities between experimental and computational results. This can be caused by numerous reasons, including potential differences between listed properties and on-site effective properties [80], [81]. For instance, compressed mineral wool batts inappropriately installed would not have the same thermal conductivity as the one

provided by the manufacturer. Moisture accumulation in building materials can also change their thermal and hygric properties. However, these variations are commonly omitted by material databases, meaning that applications of hygrothermal simulations are often subjected to doubts [82]. Although numerical model calibration is often performed using laboratory scale samples, building materials are subjected to dynamic and adverse weather conditions when placed into service, and their actual behavior can differ from that obtained in controlled experiments [70], [83]. Indeed, field research has proven that the hygrothermal performance of building assemblies is often worse than laboratory predictions [15]. Wall defects, like cracks and delamination, as well as meteorological variations are hard to avoid and predict, so a method to estimate the effective hygrothermal in situ properties would therefore be convenient [80]. A reliable approach to reduce the gap between simulations and on-site performance is to use simulation models calibrated with hygrothermal properties estimated from field hygric and thermal measurements [72], [84]. This reduces the uncertainties of the input quantities of the model, resulting in realistic numerical simulations that accurately predict the final performance of building envelopes. Furthermore, moisture transport should not be neglected, as doing so is known to induce errors when predicting the properties of building materials [15], [85].

As HAM phenomena are decisive in building energy efficiency, several studies have been performed to investigate the hygrothermal behavior of wall assemblies. For this purpose, temperature and moisture data are generally measured at various positions within the wall assembly with different boundary conditions. For instance, Piggot-Navarrete et al. [86] investigated wood-framed walls; Alvarado-Alvarado et al. [87] studied green wall assemblies; Belloum et al. [88] considered bio-based concrete walls; Colinart et al. [89] and Wu et al. [90] analyzed different types of multilayered walls; Sawadogo et al. [91] studied phase change material hemp concrete walls; and Zhan et al. [92] investigated steel-framed wall assemblies.

The temperature and moisture data measured in these studies might be used in mathematical formulations to identify the properties of the building materials that constitute the walls and provide calibrated models. In this sense, most researchers evaluated wall properties using temperature data in heat transfer models, disregarding moisture transport [15]. This is because experimental hygrothermal analyzes are much more challenging than pure thermal studies [70]. Even so, some recent studies have performed the calibration of hygrothermal models using field measurements of temperature and moisture content. For instance, Sadłowska-Sałęga and Radoń [93] investigated a historic wooden church; Gomes et al. [94] conducted studies on typical concrete assemblies; Ibrahim et al. [95] studied silica-aerogel-based insulating composite walls; Costa-Carrapiço et al. [96] evaluated the hygrothermal behavior of vernacular dwellings; Ren et al. [97] studied a solar greenhouse with straw walls; and Sabapathy and Gedupudi [98] investigated rice straw envelope assemblies.

As shown above, much effort has been put in to experimentally analyze hygrothermal phenomena in different types of envelopes. However, no previous work has been dedicated to estimating several properties of various components of a lightweight wall assembly based on long-term field measurements in particular for prefabricated envelopes. The on-site estimation of hygrothermal properties of multilayered walls is a topic in building engineering that deserves further research [99]. Such characterization is relevant as the properties of two specimens of the same building component might differ due to manufacturing, assembly, and installation procedures [86]. Moreover, longer experiments under real climatic conditions and human occupancy loads result in more accurate properties [100]. There is still a need for information about the field hygrothermal behavior of building envelopes to enhance their performance assessment [82], [101]. The lack of both field data and accurate monitoring of environmental actions and effects is more pronounced on a detached-house scale [84]. Thus, it is critical to

employ calibrated material properties to better assess the actual energy interaction of the building envelope with its environment and occupants.

This study seeks to fill the research gap in identifying the effective hygrothermal properties of a lightweight prefabricated wall in operation in a cold climate. We address the concern raised by Piggot-Navarrete et al. [86] about further field research into the impact of prefabricated envelope panel-junctions on the hygrothermal performance of the envelope and the energy efficiency of buildings. This is because of the complex hygrothermal response of the building envelope near a wall-to-wall junction, which is a critical region in terms of airtightness, heat loss, and moisture transport. We are also in line with what was stated by Panico et al. [70] and Panico et al. [72] by using long-term field monitoring data to estimate the most influential input material properties and consequently obtain a well-calibrated model for realistic and accurate hygrothermal simulations. This is because the use of input parameter measurements, such as those relating to materials and climate conditions, is in any case the best way to significantly reduce uncertainties in numerical assessments [70]. Moreover, according to Costa-Carrapiço et al. [96] and Panico et al. [70], only very few studies in the literature calibrate hygrothermal models using long-term data collection in actual dwellings and data measured inside wall components.

Inverse HAM analysis is used to estimate the effective hygrothermal properties of various building materials in a prefabricated lightweight building envelope. The inverse problem method is a robust tool in science and engineering, enabling the indirect identification of desired unknown quantities from available measurements [102]. Parameter estimation seeks to infer related properties or attributes that are responsible for the measured response of a system. Although useful, evaluating inverse problems is challenging because these are often ill-posed and ill-conditioned due to an information deficit. This implies that inverse solutions are usually not unique and are sensitive to perturbations in experimental and prior data [103]. In this study,

one-year on-site temperature and RH measurements in an envelope are used to solve inverse problems capable of estimating the specific heat (c), thermal conductivity (k), and vapor resistance factor (μ -value) of various building materials, as well as the convective heat (h) and moisture (h_m) transfer coefficients. Performance results obtained with the estimated effective properties are shown and compared with results yielded by reference values. The differences found highlight the importance of estimating effective material properties to calibrate simulation models and thus obtain more accurate insight into the actual hygrothermal behavior of wall assemblies.

3.2 One-year on-site monitoring

The residential detached house considered for the field assessment was constructed in Quebec City (Canada) in 2021 and was occupied just after its construction. The studied wall assembly, whose installation is shown in Figure 11, is located on the ground floor and is North oriented. This prefabricated wall has a newly developed joint sealing system, designed by an industrial partner (USPTO patent number 11447944) and studied by Julien et al. [104]. The wall has six main components (from exterior to interior): weather-barrier membrane, expanded polystyrene (EPS) insulation board, mineral wool batts parallel to 2×6 in wooden studs, laminated strand lumber (LSL) wooden studs at the junction, oriented strand board (OSB), and a polyethylene vapor-barrier. The properties of the LSL studs and OSB panels are considered as equal since both materials are made from strand and have similar densities.

Calibrated TE Connectivity NB-PTCO-011 RTD (Berwyn, PA, USA) temperature sensors and Honeywell HIH-4602-C (Golden Valley, MN, USA) RH sensors were used to monitor the wall, with respective accuracies of ± 0.45 °C and ± 3.5 %RH. As shown in

Figure 12, in which temperature and RH sensors are respectively labeled Y and H , they were installed at positions $x_1 = -A/2 = -0.095$ m, $x_2 = -0.040$ m, $x_3 = 0.070$ m, and $x_4 = A/2 = 0.095$ m. The sensors were attached to the wall using thermally conductive paste, and an insulating material was used to fill the holes to minimize heat losses and moisture transport. Great caution was taken when installing the sensors to affect the thermal behavior of the wall as little as possible. The sensing locations were selected near the wall-to-wall junction, where HAM transfer can be considered two-dimensional. Additionally, it can be difficult to achieve fully efficient sealing in this region, resulting in air leakage. The wall-to-wall junction is indicated by the red dashed line in Figure 12.



Figure 11. Picture taken during the installation of the studied wall.

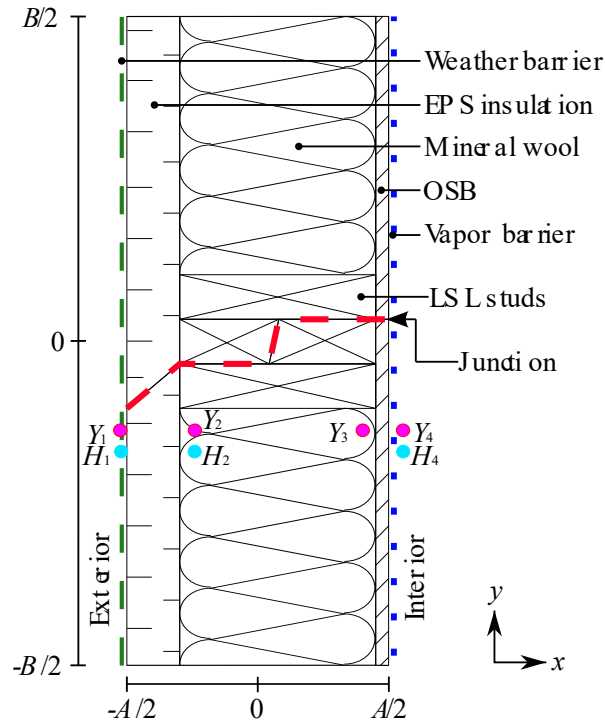


Figure 12. Two-dimensional cross-sectional view of the wall junction showing the different components and sensor locations.

The hygrothermal response of the wall assembly was monitored from September 2021 to August 2022, and transient measurements were collected at a sampling period of 10 min. Measured temperature and RH data are shown in Figure 13. The house became occupied around mid-September, when an increase in temperature profiles can be noted. It can be seen that Y_1 and Y_2 are noisier due to sudden and severe changes in external climate conditions, with more intense HAM mechanisms and loads. These temperatures decrease between the end of September and December, and remain low from January to March. Differently, these same temperatures increase in spring and almost all summer (i.e., between April and July), reaching stable behavior during August. Temperatures Y_3 and Y_4 , in turn, have a stable evolution over the year, being rather uniform in late autumn and throughout winter, due to the use of the heating system. Similar to Y_1 , H_1 also has an unstable behavior since the sensors at the exterior surface are directly subjected to weather seasonality and variation. The RH on the outdoor surface

decreases and reaches its minimal values in winter. This is expected as the outdoor air loses its ability to hold onto water when the temperature decreases. Measurement H_2 suffers considerable variations throughout the year since this location is close to the external surface, where weather events have a stronger impact. As expected, the lower temperatures of autumn and winter yield higher RH values at this location, as the temperatures approach the dew point. H_4 has a much more stable behavior compared to H_2 and is noisier during autumn and winter. Measurement H_4 strongly depends on the behavior and activity of the occupants as well as on the heating system, due to the closeness of this sensor to the indoor air conditions. Also concerning the RH at the indoor surface, it becomes drier from the beginning of the monitoring, matching the period when the house was occupied, and the heating system turned on due to cold weather. Note that no RH measurement was available at the point where Y_3 is located. After being collected, data were recorded on a computer. This dataset was later used to perform the inverse estimations with COMSOL Multiphysics with LiveLink for MATLAB, as described below.

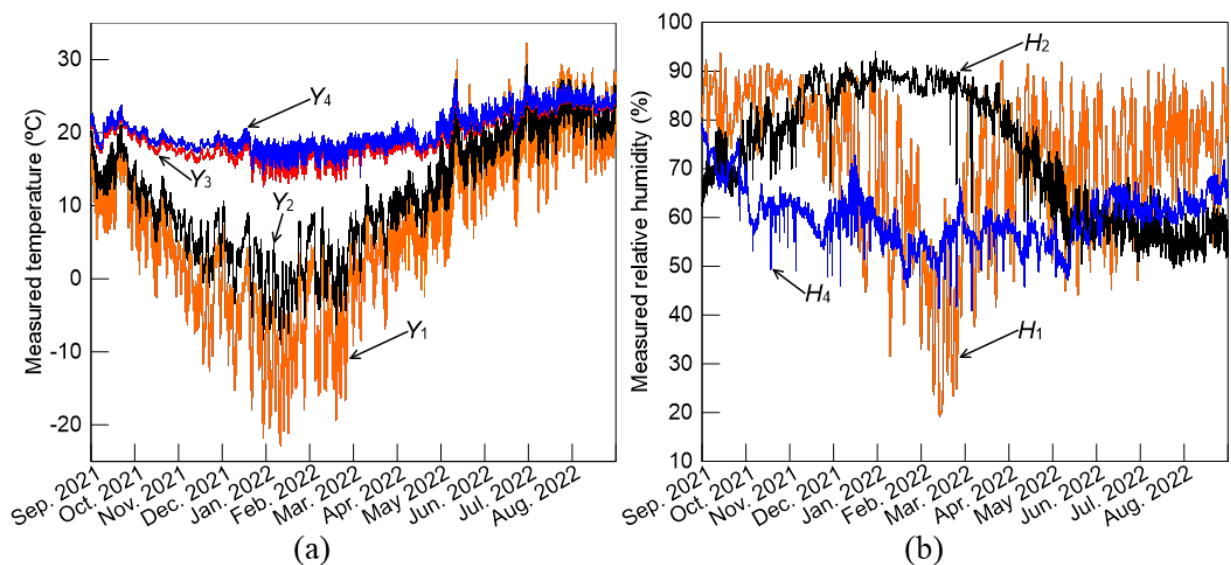


Figure 13. Experimental ten-minute measurements of (a) temperature and (b) relative humidity.

3.3 Simultaneous estimation of specific heat, thermal conductivity, and vapor resistance factor

3.3.1 Inverse problem approach for hygrothermal characterization

Inverse methodologies have been used to study engineering problems involving HAM phenomena, as well as to calibrate building energy models [15], [77], [99], [100], [102]. In this context, temperature and RH measurements can be used for solving inverse problems and then estimating related hygrothermal properties. Therefore, the desired properties are taken as unknown variables, and an optimization technique is used to retrieve their values, given mathematical-physical modeling and field measurements.

The inverse problem, in which both temperature and relative humidity are influential, is based on minimizing the following dimensionless normalized residual sum of squares:

$$F(\mathbf{P}) = \frac{1}{N} \sum_{i=1}^N \left\{ w_{Y_i}^{-1} [Y_{2_i} - T_{2_i}(\mathbf{P})]^2 + w_{Y_i}^{-1} [Y_{3_i} - T_{3_i}(\mathbf{P})]^2 + w_{H_i}^{-1} [H_{2_i} - \phi_{2_i}(\mathbf{P})]^2 \right\} \quad (29)$$

where $\mathbf{P} = [P_1, P_2, \dots, P_L]$ incorporates L unknown properties to be simultaneously estimated, T and ϕ are the numerically calculated temperature and RH data at the measurement points, respectively. They are coupled and obtained by numerically solving the direct problem with a given \mathbf{P} at the sensing locations. w_Y and w_H are weighting coefficients associated with the variances of temperature and RH measurements, respectively. N is the number of discrete measurements taken during the monitoring period.

From Equation (29), it can be seen that the parameter estimation at hand relies on a least squares problem that minimizes the sum of the squared differences between model predictions and measurements. Convexity is a key property of least squares functions since it enables derivative-based algorithms to efficiently converge and find solutions to optimization problems [102]. In this study, the Broyden-Fletcher-Goldfarb-Shanno interior-point (BFGS-IP) method is used to evaluate the inverse problem and thus estimate \mathbf{P} . This nonlinear gradient-based technique has been efficiently used as a robust tool for solving optimization problems in a variety of applications [105].

3.3.2 Hygrothermal problem with Dirichlet boundary conditions

The target here is to simultaneously estimate the effective hygrothermal properties of materials of the on-site monitored wall. For this purpose, an inverse problem based on the transient two-dimensional simultaneous HAM transfer within the wall is considered. The wall assembly is composed of several layers of different materials. The hygrothermal properties of the building materials are taken as unknown, and the contact at the interface of neighboring layers is considered perfect. All wall layers are initially subjected to known temperature and relative humidity fields. External and internal boundary conditions are prescribed temperature and prescribed RH, which are provided by the sensors placed on the wall surfaces (i.e., Y_1, H_1, Y_4, H_4). Thermal modeling considers energy storage, heat conduction, and latent heat effect due to vapor condensation. Hygric modeling considers moisture storage, capillary forces, and water vapor diffusion due to differential pressure. Thus, the physical problem involving fully coupled HAM transport is governed by the following equations:

$$\rho c \frac{\partial T}{\partial t} - \nabla \cdot \left[k \nabla T + L_V \frac{\delta_{air}}{\mu} \nabla(\phi p_{sat}) \right] = 0, \quad (30)$$

$$\forall x \in [-A/2, A/2], \forall y \in [-B/2, B/2], \text{ for } t > 0$$

$$\frac{\partial w}{\partial \phi} \frac{\partial \phi}{\partial t} - \nabla \cdot \left[D \frac{\partial w}{\partial \phi} \nabla \phi + \frac{\delta_{air}}{\mu} \nabla(\phi p_{sat}) \right] = 0, \quad (31)$$

$$\forall x \in [-A/2, A/2], \forall y \in [-B/2, B/2], \text{ for } t > 0$$

subjected to the boundary conditions:

$$T(x, y, t) = Y_1(t), \quad \forall x = -A/2, \forall y \in [-B/2, B/2], \quad \text{for } t > 0 \quad (32)$$

$$\phi(x, y, t) = H_1(t), \quad \forall x = -A/2, \forall y \in [-B/2, B/2], \quad \text{for } t > 0 \quad (33)$$

$$T(x, y, t) = Y_4(t), \quad \forall x = A/2, \forall y \in [-B/2, B/2], \quad \text{for } t > 0 \quad (34)$$

$$\phi(x, y, t) = H_4(t), \quad \forall x = A/2, \forall y \in [-B/2, B/2], \quad \text{for } t > 0 \quad (35)$$

$$-\left[k \nabla T + L_V \frac{\delta_{air}}{\mu} \nabla(\phi p_{sat}) \right] \cdot \mathbf{n} = 0, \quad \forall x \in [-A/2, A/2], y = -B/2, \quad (36)$$

$$\text{for } t > 0$$

$$-\left[D\frac{\partial w}{\partial \phi}\nabla\phi + \frac{\delta_{air}}{\mu}\nabla(\phi p_{sat})\right] \cdot \mathbf{n} = 0, \quad \forall x \in [-A/2, A/2], y = -B/2, \quad (37)$$

for $t > 0$

$$-\left[k\nabla T + L_V\frac{\delta_{air}}{\mu}\nabla(\phi p_{sat})\right] \cdot \mathbf{n} = 0, \quad \forall x \in [-A/2, A/2], y = B/2, \quad (38)$$

for $t > 0$

$$-\left[D\frac{\partial w}{\partial \phi}\nabla\phi + \frac{\delta_{air}}{\mu}\nabla(\phi p_{sat})\right] \cdot \mathbf{n} = 0, \quad \forall x \in [-A/2, A/2], y = B/2, \quad (39)$$

for $t > 0$

with the initial conditions:

$$T(x, y, t) = T_0(x, y), \quad \forall x \in [-A/2, A/2], \forall y \in [-B/2, B/2], \quad \text{for } t = 0 \quad (40)$$

$$\phi(x, y, t) = \phi_0(x, y), \quad \forall x \in [-A/2, A/2], \forall y \in [-B/2, B/2], \quad \text{for } t = 0 \quad (41)$$

where t is the time; T is the temperature; ϕ is the relative humidity; ρ is the density; c is the specific heat; k is the thermal conductivity; μ is the vapor resistance factor; L_V is the latent heat of evaporation; δ_{air} is the vapor permeability of still air; D is the moisture diffusivity; p_{sat} is the vapor saturation pressure; w is the water content (moisture storage function); and \mathbf{n} is a generic unit normal vector.

Although calibration is of key importance for accurate building energy modeling, nonlinear transient studies of coupled HAM transport using on-site measurements are challenging [72], [78], [106]. This is mainly due to the complex nature of these dynamic phenomena and the large abrupt variations in weather conditions which severely affect measurements [107]. The outdoor RH is especially impacted, showing abrupt changes and several peaks close to 100 %, which are detrimental to convergence when calculating the hygrothermal response of the wall. To reduce numerical instabilities, the measurements used as boundary conditions were subjected to hybrid algebraic-trigonometric polynomial filtering before being introduced into COMSOL. Although it introduces some bias into the problem modeling, experimental data with smooth transition enable better numerical performance of finite-element-based HAM simulations [108] and provide regularization to estimation procedures [58]. The initial condition is also a concern in simulation models using measurements taken on building walls [15]. On this matter, data measured at $t = 0$ were used to perform a steady-state study and thus obtain well-established temperature and humidity profiles throughout the 2D geometry, that were then used as initial conditions of the transient simulation. This improves numerical convergence since the wall components are insulating materials with significant hygrothermal inertia.

The problem described above is said to be a direct problem when the hygrothermal properties, geometry, and initial and boundary conditions are known. Transient temperature and RH fields within the building wall can be obtained by solving the direct problem. COMSOL Multiphysics was used to solve the direct problem because this software has in its presets a specific module to study coupled HAM transport in building materials. COMSOL uses a mathematical formulation based on the European standard CSN EN 15026-2007, which introduces a validated simulation model for assessing the hygrothermal performance of building materials.

As already seen, the solution to an inverse problem is initiated by evaluating the direct problem at differing parameters and then comparing the outcomes obtained with experimental data. In this context, the independence of results from mesh refinement and time stepping is fundamental to ensure the validity of model-predicted data. The influence of spatial and temporal discretization was investigated by assessing the variation of direct problem solutions when varying the number of mesh elements and time-step tolerance. Mesh and time-step independences were said to be reached when ϕ_2 , the most sensitive variable, showed relative deviations below 3 % for every time-step [107]. Simulations were conducted in COMSOL Multiphysics using meshes with 8816 triangular elements and a time stepping tolerance of 10^{-2} .

3.3.3 Sensitivity analysis

By examining Eqs. (30) and (31), it can be seen that the hygrothermal properties involved in the physical problem are ρ , c , k , μ , and D . It is important to mention that L_V and δ_{air} are not properties of the wall materials; they are related to water vapor and air, respectively. Density and specific heat are linearly dependent on each other and thus cannot be estimated together. In this case, one must choose between specific heat and volumetric heat capacity (ρc) to be targeted in the estimation process. It is instructive to perform a sensitivity analysis to obtain information on how temperature and RH at the sensing locations are impacted by changes in specific heat, thermal conductivity, vapor resistance factor, and moisture diffusivity. All sensitivity-related computations are performed using forward difference approximation to the derivatives and considering property values from a validated building materials database. This database is available within WUFI 2D simulation program. Table 2 gives reference information on the investigated hygrothermal properties.

Table 2. Reference information on the investigated hygrothermal properties.

Material/Component	Reference hygrothermal properties			
	c [J kg ⁻¹ K ⁻¹]	k [W m ⁻¹ K ⁻¹]	μ [-]	D [m ² s ⁻¹]
1) Weather-barrier membrane	$c_1 = 2300$	$k_1 = 2.3$	$\mu_1 = 300$	$D_1 = 1 \times 10^{-14}$
2) EPS board	$c_2 = 1450$	$k_2 = 0.03$	$\mu_2 = 73$	$D_2 = 1 \times 10^{-9}$
3) Mineral wool batt	$c_3 = 850$	$k_3 = 0.055$	$\mu_3 = 1.2$	$D_3 = 1 \times 10^{-14}$
4) OSB and LSL studs	$c_4 = 2100$	$k_4 = 0.1$	$\mu_4 = 144$	$D_4 = 5 \times 10^{-12}$
5) Vapor-barrier membrane	$c_5 = 2300$	$k_5 = 2.3$	$\mu_5 = 20054$	$D_5 = 1 \times 10^{-12}$

In this study, sensitivity analysis provides prior knowledge about which unknown properties can be estimated from available measured data. Sensitivity coefficients evaluate the sensitivity of the dependent variable (temperature and RH) with respect to a change in the analyzed hygrothermal property. The scaled sensitivity coefficients are calculated by multiplying the analyzed property by the first partial derivative of temperature or RH in relation to this property [4]. For example, $X_{T_2, k_1} = k_1 \times \partial T_2 / \partial k_1$ is the sensitivity coefficient of k_1 (the thermal conductivity of the weather barrier) for data T_2 . A small sensitivity implies that large changes in the property produce small changes in the temperature/RH measurements. This means that the information contained in the measurements is insufficient to estimate the property, making the inverse problem ill-conditioned [102], [109]. In general, the accuracy associated with the estimation of a parameter decreases as its scaled sensitivity coefficient approaches the measurement uncertainty. In this case, inverse analysis cannot properly evaluate the effects of such parameter on the measured data. Ill-conditioning is also present when the sensitivity coefficients of two properties are correlated (linearly dependent). This leads to the

unfeasibility of estimating these properties simultaneously. Thus, to obtain an optimal parameter estimation, it is desirable to have uncorrelated scaled sensitivity coefficients with large magnitudes for all hygrothermal properties being simultaneously inferred. This minimizes the generalized variance of the results, ensures good conditioning of the inverse problem solver, and provides realistic and accurate estimates [102], [109].

As measurements Y_1 , Y_4 , H_1 , and H_4 are boundary conditions, measurements Y_2 , Y_3 , and H_2 can be considered to estimate the desired hygrothermal properties. By calculating the corresponding numerical data of these sensing locations (i.e., T_2 , T_3 , and ϕ_2) and investigating their sensitivities, one can define which properties can effectively be found from the inverse approach, i.e., which properties will constitute \mathbf{P} . This vector will be composed of a set of properties to be simultaneously estimated using measured temperature and RH as information. Sensitivities associated with specific heat, thermal conductivity, vapor resistance factor, and moisture diffusivity of all wall components are analyzed.

Figure 14 shows how the sensitivity coefficients of the parameters of interest (i.e., c , k , μ , and D) concerning data T_2 , T_3 , and ϕ_2 evolve over time. The sensitivity coefficients not shown have much lower values than those shown and cannot be estimated. Since wall temperature and moisture gradients are mainly due to the outside conditions, it is understandable to observe lower sensitivities for T_3 compared to T_2 , whose sensor is closer to the external surface. T_2 is found to have three sensitivity coefficients of good magnitude: X_{T_2,k_2} , X_{T_2,k_3} , and X_{T_2,k_4} . However, their behavior is correlated, which prevents accurate estimation of more than one property from this temperature. Likewise, T_3 presents the same condition, but for two sensitivities: X_{T_3,k_2} and X_{T_3,k_4} . In other words, T_2 enables the identification of k_2 or k_3 or k_4 , and T_3 of k_2 or k_4 . In summary, combining temperatures T_2 and T_3 provides sufficient information to estimate two thermal conductivities. A different scenario is obtained when considering RH. It can be observed that c_4 , k_2 , k_3 , k_4 , μ_2 , μ_3 , and μ_4 have good uncorrelated sensitivities for ϕ_2 ,

which greatly enlarges the number of targets of the hygrothermal identification problem. Considering moisture transport not only enhances the problem physics and yields a more realistic case study, but also increases the capability and robustness of the simultaneous parameter estimation. Since a fully coupled hygrothermal analysis is performed, measurements Y_2 , Y_3 , and H_2 are therefore considered together in Eq. (29), all contributing to simultaneously estimating the following properties: c_4 , k_2 , k_3 , k_4 , μ_2 , μ_3 , and μ_4 . This is because, as shown above, the available experimental data were found to have good and linearly independent sensitivity coefficients in relation to these properties. It should be mentioned that the estimation is feasible even if some sensitivities have correlated behaviors in some periods throughout their evolution. This is because difficulties due to low sensitivity and linearly dependent relationship in localized regions are generally overcome when whole-domain data are considered [4].

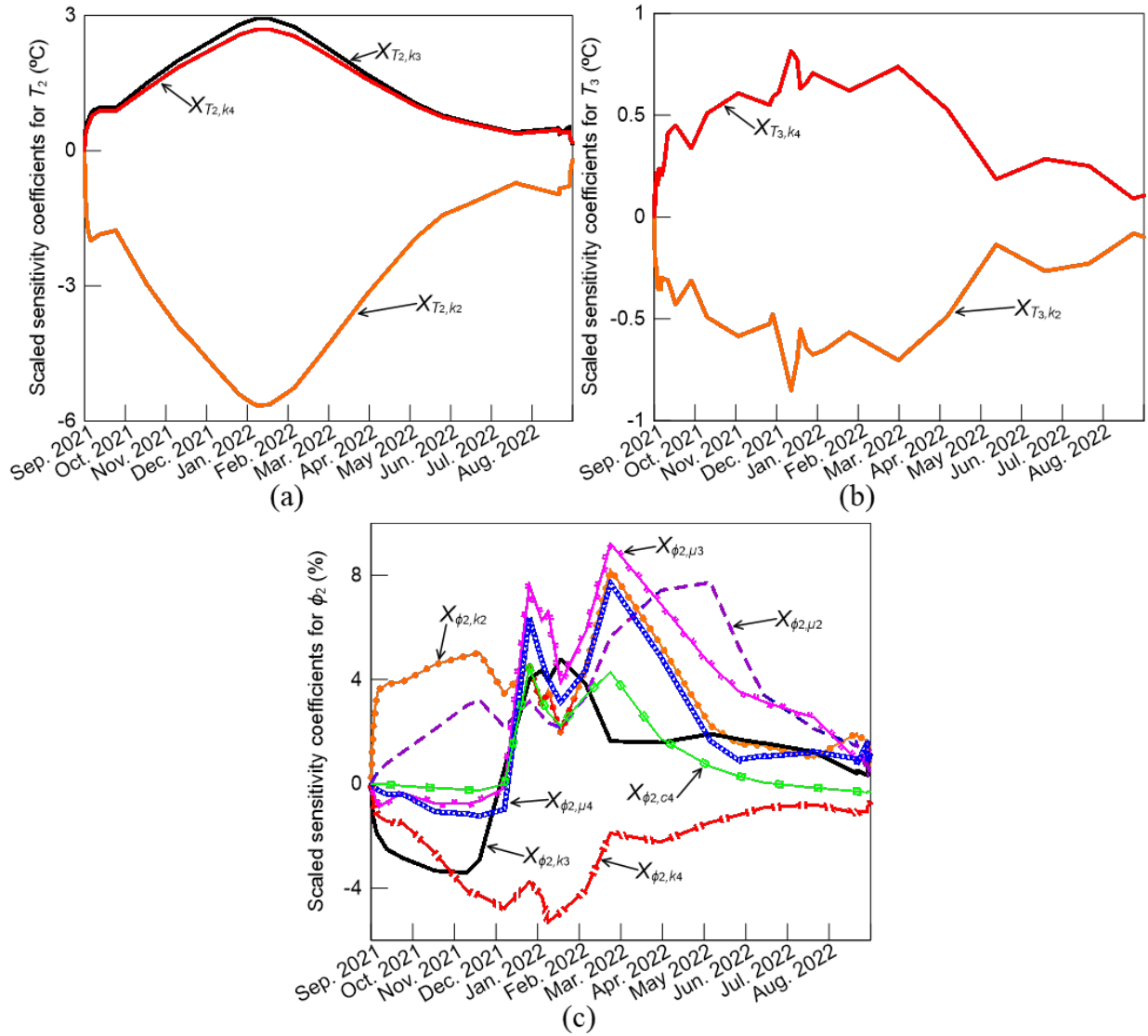


Figure 14. Sensitivity coefficients for: (a) T_2 , (b) T_3 , and (c) ϕ_2 .

3.3.4 Results and discussion

The literature values shown in Table 2 are taken as the initial guesses for the inverse hygrothermal identification problem. The search ranges are defined considering that each parameter of interest might vary by up to $\pm 25\%$ from its reference value. The evolution of the objective function when solving the hygrothermal characterization problem is shown in Figure 15. Convergence was considered to be achieved when the norm of the solution varied

by less than 1 % in subsequent iterations. The objective function has an initial value of 962039.1 (which is outside the plot limits) and decreases drastically at the first iteration. This indicates that there is a large deviation between the actual hygrothermal response of the wall and that obtained by numerical simulation based on reference properties.

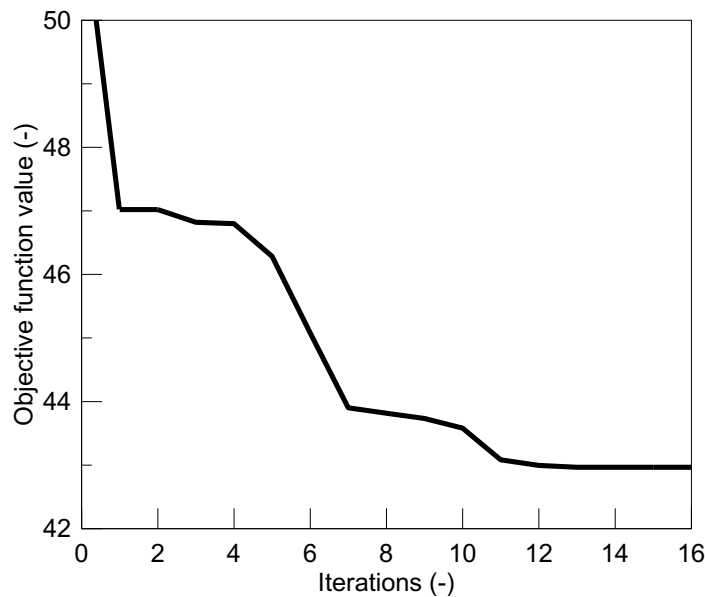


Figure 15. Evolution of the objective function over the number of iterations for the estimation of the hygrothermal properties of the wall.

The estimated effective values for the desired hygrothermal properties are given with four significant digits in Table 3. The Bonferroni method [4] is used to determine confidence intervals for the estimates, at 99 % probability. Expressing the estimated properties within bounds provides much more informative results. This is very important because inverse problems are ill-posed and carry uncertainties due to errors and approximations during experimental and modeling work. For instance, the numerical model approximates the real physical system, and the experimental data are obtained from intrusive sensors. With the exception of the thermal conductivity of mineral wool insulation, the effective estimates of this

study are lower than the reference values given by WUFI 2D. This implies that, in general, the database values tend to overestimate the real hygrothermal properties of the investigated wall materials.

Table 3. Estimated effective hygrothermal properties.

Material/Component	Property	Estimated effective value
2) EPS insulation	k_2 [W m ⁻¹ K ⁻¹]	0.02765 ± 0.00120
	μ_2 [-]	60.57 ± 2.78
3) mineral wool insulation	k_3 [W m ⁻¹ K ⁻¹]	0.05723 ± 0.00511
	μ_3 [-]	1.159 ± 0.037
4) OSB panel and LSL studs	c_4 [J kg ⁻¹ K ⁻¹]	2097 ± 154
	k_4 [W m ⁻¹ K ⁻¹]	0.08017 ± 0.00458
	μ_4 [-]	116.4 ± 7.6

3.4 Simultaneous estimation of convective heat and moisture transfer coefficients

3.4.1 Hygrothermal problem with Robin boundary conditions

Here, the focus is on determining the convective HAM transfer coefficients between the wall and the internal and external environments. With the exception of h and h_m , all other

properties and parameters as well as the indoor and outdoor environmental conditions are assumed to be known. It is worth mentioning that the previously optimized property values were used as input data. The same formulation detailed before is used, except for the boundary conditions. Now, convective HAM fluxes are considered instead of prescribed temperature and RH. This means that Robin boundary conditions are imposed on the inside and outside wall surfaces. Equations (42) and (43) shown below replace Eqs. (32) and (33), and Eqs. (44) and (45) replace Eqs. (34) and (35). External climate data (T_{ext} and ϕ_{ext}) were obtained from a weather station located near the monitored house. Indoor conditions (T_{int} and ϕ_{int}) were taken as functions of T_{ext} , according to DIN 4108-3. Therefore, the boundary conditions become:

$$-\left[k\nabla T + L_V \frac{\delta_{air}}{\mu} \nabla(\phi p_{sat})\right] \cdot \mathbf{n} = h_{ext}(T_1 - T_{ext}), \quad (42)$$

$$\forall x = -A/2, \forall y \in [-B/2, B/2], \quad \text{for } t > 0$$

$$-\left[D \frac{\partial w}{\partial \phi} \nabla \phi + \frac{\delta_{air}}{\mu} \nabla(\phi p_{sat})\right] \cdot \mathbf{n} = M h_{m_{ext}}(C_1 - C_{ext}), \quad (43)$$

$$\forall x = -A/2, \forall y \in [-B/2, B/2], \quad \text{for } t > 0$$

$$-\left[k\nabla T + L_V \frac{\delta_{air}}{\mu} \nabla(\phi p_{sat})\right] \cdot \mathbf{n} = h_{int}(T_4 - T_{int}), \quad (44)$$

$$\forall x = A/2, \forall y \in [-B/2, B/2], \quad \text{for } t > 0$$

$$-\left[D \frac{\partial w}{\partial \phi} \nabla \phi + \frac{\delta_{air}}{\mu} \nabla(\phi p_{sat})\right] \cdot \mathbf{n} = M h_{m_{int}}(C_4 - C_{int}), \quad (45)$$

$$\forall x = A/2, \forall y \in [-B/2, B/2], \quad \text{for } t > 0$$

where h is the convective heat transfer coefficient; M is the molar mass of water vapor; h_m is the convective moisture transfer coefficient; and C is the vapor concentration, which is a function of T and ϕ . In the problem formulation, the convective moisture transfer coefficient is expressed as a function of the convective heat transfer coefficient, as per Lewis's formula [110]:

$$h_m = \frac{h}{\rho_{air} c_{air}} \quad (46)$$

Using the new boundary conditions described above and the simultaneous HAM transfer governing equations, the coupled temperature and RH fields within the wall assembly can be dynamically simulated.

3.4.2 Sensitivity analysis

Since h and h_m are correlated, measurements Y_2 , Y_3 , and H_2 are considered in Eq. (29) to estimate h , which is then used to indirectly estimate h_m . The sensitivity coefficients are calculated using reference information from Xu et al. [110], as follows: $h_{ext} = 25 \text{ W m}^{-2} \text{ K}^{-1}$ and $h_{int} = 8 \text{ W m}^{-2} \text{ K}^{-1}$. Their evolution in time is shown in Figure 16. It can be seen that both temperatures are more sensitive to h_{int} , while RH has a higher sensitivity coefficient for h_{ext} . Since h_{ext} and h_{int} have sensitivities with good magnitudes and uncorrelated behaviors for different data, both convective heat transfer coefficients can be estimated simultaneously using the available measurements. As done before, the reference values for h are taken as initial guesses. Broader search limits considering a maximum deviation of $\pm 50 \%$ are used because convective HAM coefficients vary considerably in building wall applications [15].

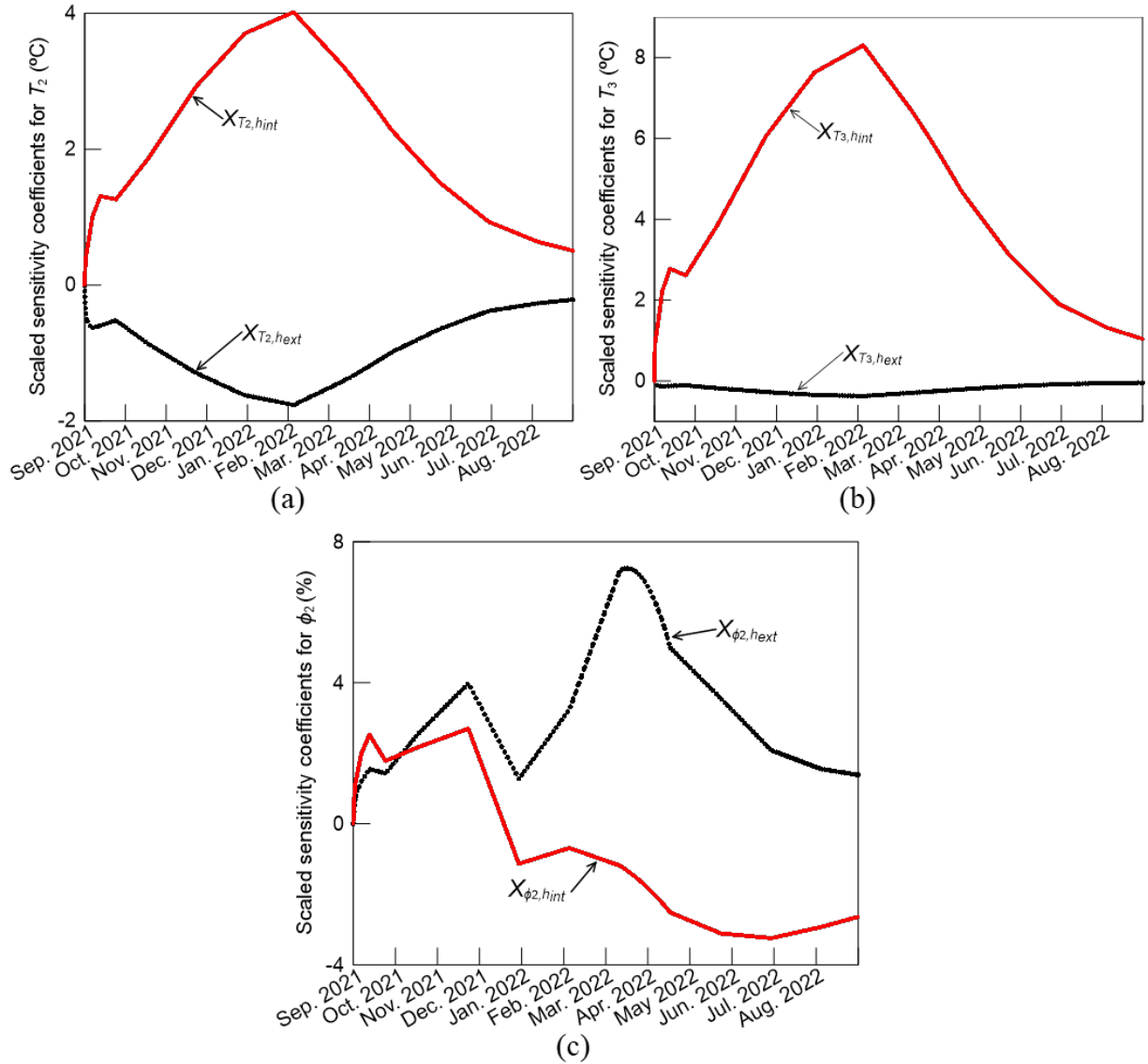


Figure 16. Sensitivity coefficients of h_{ext} and h_{int} for: (a) T_2 , (b) T_3 , and (c) ϕ_2 .

3.4.3 Results and discussion

Figure 17 shows the objective function behavior during the simultaneous estimation of h_{ext} and h_{int} . It can be seen that the final value of the objective function here is smaller than its correspondent value in Section 3.3. The lower error when convergence is achieved is due to the use of the previously estimated effective properties and Robin boundary conditions. Both

aspects enable the numerical simulation to more closely match the actual hygrothermal response of the wall.

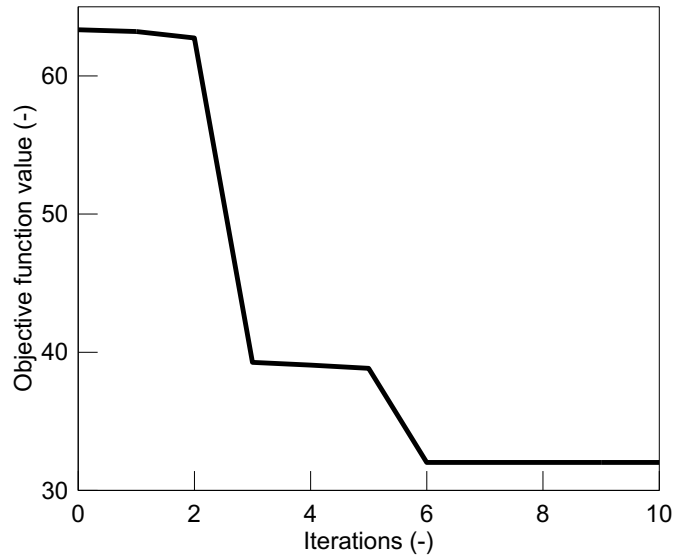


Figure 17. Evolution of the objective function over the number of iterations for the estimation of h_{int} and h_{ext} .

Table 4 gives the estimated external and internal convective heat transfer coefficients and their confidence limits. The external and internal convective moisture transfer coefficients, indirectly identified from h_{ext} and h_{int} , are also given in this table. The confidence bounds of $h_{m_{ext}}$ and $h_{m_{int}}$ were determined by error propagation from h_{ext} , h_{int} , ρ_{air} , and c_{air} . It can be seen that the literature benchmarks underestimate the convective phenomena on the external surface of the investigated building, while the convective response of the internal surface is overestimated.

Table 4. Estimated effective external and internal heat and moisture transfer coefficients.

Property	Estimated effective value
h_{ext} [W m ⁻² K ⁻¹]	30.12 ± 1.54
h_{int} [W m ⁻² K ⁻¹]	4.262 ± 0.201
$h_{m_{ext}}$ [m s ⁻¹]	0.02569 ± 0.00179
$h_{m_{int}}$ [m s ⁻¹]	0.003635 ± 0.000247

Root-mean-square error (RMSE) is a statistical measure that is often used to evaluate the deviations between model-predicted values and those observed experimentally. Its purpose is to combine the errors in predictions for various data points into a single metric representing the overall predictive capability. RMSE is always positive, and, in general, a smaller value is better than a higher one. Here, RMSE is used to measure and compare numerical prediction accuracy. It is calculated for temperature and RH considering two different datasets: the effective hygrothermal properties estimated by inverse problem and the initial properties obtained from WUFI 2D and Xu et al. [110]. RMSE is calculated as follows:

$$RMSE = \sqrt{\frac{\sum_{i=1}^N [Measurement_i - Prediction_i]^2}{N}} \quad (47)$$

When T_2 , T_3 , and ϕ_2 are calculated using all the estimated effective hygrothermal properties (i.e., c_4 , k_2 , k_3 , k_4 , μ_2 , μ_3 , μ_4 , h_{ext} , h_{int} , $h_{m_{ext}}$, and $h_{m_{int}}$), values of 2.50 °C, 1.14 °C, and 3.92 % are obtained for $RMSE_{T_2}$, $RMSE_{T_3}$, and $RMSE_{\phi_2}$. 3.68 °C, 2.01 °C, and 6.44 % are the

values for these three metrics when reference properties are used to predict T_2 , T_3 , and ϕ_2 . This confirms that the hygrothermal model fits the experimental data better when calibrated with the properties estimated in this study. Therefore, this work can be considered successful in using one-year on-site measurements to solve inverse problems and thus provide more accurate hygrothermal input simulation data.

3.5 Impact of model calibration on hygrothermal performance assessment

In practice, buildings are naturally subjected to thermal and moisture loads, and the wall assembly is the barrier offering thermal and moisture resistance. The hygrothermal behavior of walls controls to a good extent the amount of energy required to ensure optimal comfort conditions for occupants. Uncontrolled HAM fluxes within building walls can damage thermal insulation and cause mold growth, thus making buildings unhealthy and less energy efficient [9]. Adequate strategies for managing HAM phenomena can prevent such serious problems. Therefore, understanding HAM transport across wall components is paramount for building design since it contributes to more sustainable and healthier building enclosures [111].

Since the effective hygrothermal properties were estimated, it is possible to evaluate their influence on the hygrothermal performance of the wall assembly. For this purpose, the problem used in Section 4, which involves Robin boundary conditions, is considered. The problem is solved for two datasets of hygrothermal properties: i) the effective estimates determined in this study; ii) reference properties from WUFI 2D and Xu et al. [110]. Values given by WUFI 2D are used for the properties that are not estimated in the present work.

The vapor-barrier membrane is the wall component in direct contact with the indoor environment, where hygric and thermal conditions are critical for occupant comfort. Moreover, it is the main responsible for controlling moisture flux through the wall assembly. Thus, the hygrothermal performance of the wall is investigated by calculating the annual heat (Q_w) and moisture (G_w) fluxes through the interior surface. Q_w and G_w account for normal diffusive and convective heat fluxes.

Figure 18 shows the calculation results for Q_w and G_w as a function of time. Different hygric and thermal behaviors can be observed over the annual evolution of the HAM fluxes. Negative values indicate that the building enclosure loses heat/moisture. Positive values denote heat/moisture gain through the wall assembly. The physical behavior of buildings is derived from the continuous energy response of their components to outdoor climatic conditions and indoor comfort requirements. The heat flux profile is directly associated with the temperature gradient within the wall. Thus, since Y_4 remains above Y_1 almost during the entire monitored period, the wall practically only experiences outgoing heat flux. Heat loss is large in autumn and winter, and small in spring and summer. Since the investigated wall is in a cold climate region, greater heat losses occur in winter due to the cold weather which yields higher differences between outdoor and indoor temperatures. Q_w is lower when determined with the estimated effective properties. Heat fluxes for both configurations differ most significantly during winter. This implies that the reference hygrothermal properties can be misleading in predicting building energy demand in the most critical period. By integrating Q_w with respect to time over the year, the total annual thermal energy loss through the wall per unit of area can be calculated. A total heat loss of 34.2 kW h m^{-2} ($1.2 \times 10^8 \text{ J m}^{-2}$) is obtained using the property estimates, while reference properties lead to a value of 44.4 kW h m^{-2} ($1.6 \times 10^8 \text{ J m}^{-2}$). This means that the literature benchmarks overestimate the annual thermal losses of the wall by about 30 %.

The moisture flux G_w also varies according to the interaction between external and internal environments. Its behavior is dependent on the gradients of partial water vapor pressure and RH, which at the same time depend on temperature, so consequently its profile is different from that of the heat flux. The behavior of G_w is more heavily influenced by the exterior RH, since the studied building envelope is more permeable on the exterior side than on the interior one. Permeable external insulation and weather protection work together with an internal vapor control membrane to increase the durability of the envelope in relation to the potential for interstitial condensation and subsequent moisture-related damage. In this context, an accurate numerical prediction of the moisture flux in the wall is crucial for evaluating the inward wetting and outward drying processes. This is because, for an energy-efficient building design, the resilience and sustainability of envelope assemblies should rely directly on effective passive moisture management. For locations with cold climate like Quebec City, summer is the most humid season and therefore the most critical period in terms of absorption and storage of water in building enclosures. It is precisely during this critical season, when the hot, humid air causes a high level of inward moisture transport, that the results of both datasets show more significant deviations. The time integral of G_w is also calculated to determine the total mass of moisture per unit of wall surface area transported throughout the year. Using the estimated effective hygrothermal properties yields a value of $-7.86 \times 10^{-5} \text{ kg m}^{-2}$, while $-9.73 \times 10^{-5} \text{ kg m}^{-2}$ is obtained for the literature properties. This implies that the literature benchmarks overestimate the annual hygric behavior of the wall by about 24 %. Therefore, both Q_w and G_w calculations demonstrate the importance of the present work in providing accurate in situ input data to calibrate the wall simulation model, thus obtaining more realistic assessments of hygrothermal performance and energy efficiency.

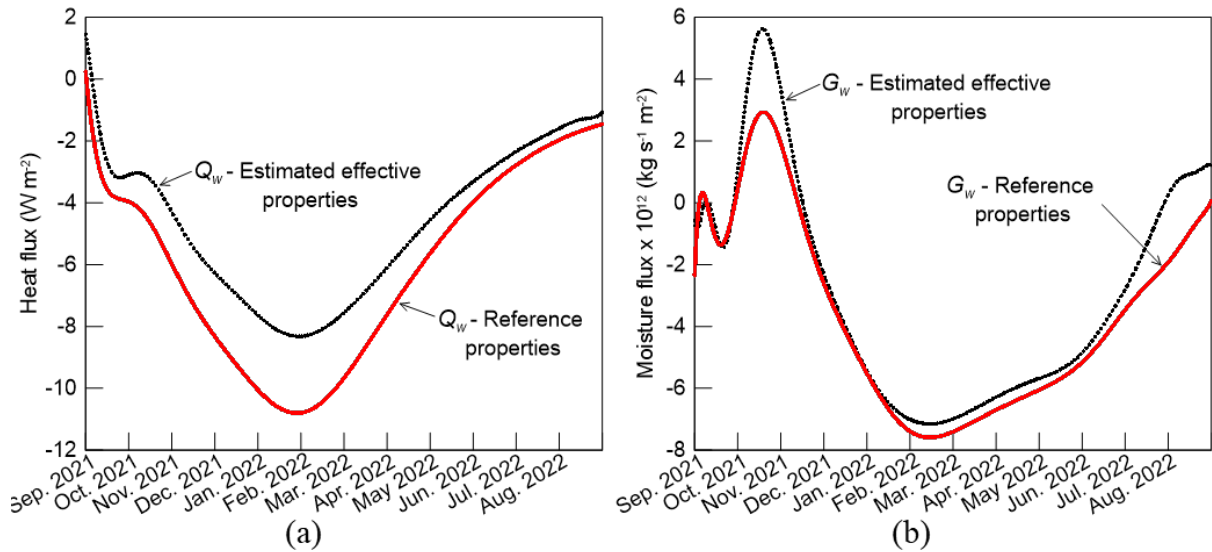


Figure 18. Heat (a) and moisture (b) fluxes through the interior wall surface. Comparison of the results for the effective hygrothermal properties estimated in this study with the results for reference parameters.

3.6 Summary

HAM analysis is a critical aspect of building science and engineering as it provides insight into energy efficiency, indoor comfort, sustainability, and safety. Hygrothermal characterization based on field measurements and subsequent model calibration enable simulations to better assess the behavior of building components and systems under actual environmental conditions. In this second case study, hygrothermal properties of different materials of a prefabricated wall assembly were estimated by inverse problems considering fully coupled HAM transfer. One-year on-site temperature and relative humidity data were used to estimate specific heat, thermal conductivity, vapor resistance factor, as well as convective heat and moisture transfer coefficients.

With the exception of the thermal conductivity of mineral wool and the external HAM transfer coefficients, all other properties were determined to be lower than literature benchmarks. This means that the literature references overestimated the effective values of the hygrothermal properties of the studied building envelope. The largest difference between the estimates and the reference properties reached almost 50 %.

The impact of model calibration on the assessment of the wall hygrothermal performance was addressed by calculating the heat and moisture fluxes through the interior surface throughout the year. These calculations considered two different datasets: one with the effective estimates determined in this work, and the other with literature benchmark properties. The greatest deviations in the thermal response were found during the cold season, which is the most critical period in terms of energy demand. As to the hygric response, the largest differences were found during the warm months. The total energy loss and total moisture transport per unit of wall surface area were determined by integrating the HAM fluxes throughout the year. Literature reference values were shown to overestimate the annual thermal response by about 30 % and the annual hygric response by about 24 %. All this demonstrates the importance of the present characterization approach to obtain a well-calibrated building simulation model capable of more accurately predicting the hygrothermal performance of the prefabricated wall assembly.

Future research work should investigate the dependence of the hygrothermal properties of the wall on temperature and moisture content. By performing similar studies in different assemblies, it would also be possible to improve building property databases to account for in situ performance.

4. Case Study 3: Estimating the Annual Heat Flux through a Prefabricated Wall Assembly from Field Data

4.1 Dynamic thermal analysis of envelope walls

With growing concern about climate change and global warming, much attention has been focused on building enclosures, as they are responsible for major energy consumption and greenhouse gas emissions [112]. Energy consumption in buildings is used in good part to maintain a thermally comfortable indoor environment [112], [113], [114]. According to the Canadian Wood Council [115], about 20% of total energy consumption in temperate regions is used for heating, cooling, and lighting in residential buildings. As the energy performance of residential housing plays a key role in the sustainability of the building sector [115], [116], outdoor-to-indoor heat exchanges need to be carefully analyzed, aiming to reduce heating/cooling needs without affecting the quality of life of residents [112]. The envelope is critical to protect the built environment from severe external climate conditions [112], and limit heat gains and losses, which in turn directly impact energy demand. As a result, improving walls offers great potential for energy savings, as they are responsible for around 50% of the total energy gain/loss in a building [90]. In this context, knowledge of the heat flux through the internal surfaces of building envelopes is essential to ensure occupant thermal comfort and energy efficiency [112], [117].

Despite its importance, the thermal performance of building walls is not often investigated after construction and during the operational phase [118]. Therefore, although it is one of the most accurate ways to evaluate the actual thermal behavior of building

components [100], [119], on-site assessment is rarely performed due to the complexity and cost of proper data collection and the difficulty of post-processing field measurements [119], [120]. Moreover, some field investigations found that the final thermal performance of building envelopes was worse than predicted by laboratory tests [15]. In real-field applications, building envelopes are subject to uncontrolled seasonal climate cycles and dynamic internal loads [72]. Thus, the hygrothermal conditions experienced during operation can greatly change between buildings located in different climate zones [15], [119]. This complicates the extrapolation of standard laboratory data for long-term predictions on field thermal performance [121]. Additionally, on-site investigations better assess the impact of construction specificities on the behavior of building components [78], [121]. For example, hidden defects in the envelope due to aging or manufacturing/installation faults (e.g., layer rupture, non-emerging cracks, and delamination) can compromise airtightness and impair effective thermal performance [116]. The impact of such quality flaws on the ability of building envelopes to meet their in-use energy efficiency target is more accurately evaluated by extensive field research [86], [122].

The in situ thermal analysis of building envelopes is typically based on steady-state thermal resistance (or its reciprocal, thermal transmittance), which is the common basis of most building energy codes around the world [112], [123], [124]. Among the most relevant steady-state techniques are the heat flux meter method, guarded hot plate method, hot box method, infrared thermography, natural convection and radiation method, and temperature based method [125]. However, the adaptability of these steady-state approaches is limited when applied to dynamic indoor environments and extreme weather conditions [123]. Likewise, there is a lack of extensive research on employing such methods in field assessments due to their tedious and costly nature, which limits the type of wall studied and the testing season [123]. Moreover, they are mainly suitable for homogeneous walls with low thermal inertia and have difficulty assessing the thermal performance of multilayer composite walls under different

climatic and heating/cooling conditions [113], [120], [126]. This is because these techniques employ relatively simple calculations that do not accurately capture the transient thermal response of envelope walls [125]. As most buildings are subject to highly dynamic thermal load [123], it is critical to investigate and understand the unsteady heat transfer behavior of inhomogeneous envelope walls to optimize building design [112], [120], [127], [128].

Among the most commonly used approaches for evaluating dynamic heat flux in building envelopes are the admittance method, the response factor method, the transfer function method, and numerical methods for differential equations [127], [129]. For instance, Fang and Chen [130] applied the transfer function method and periodic response factor method for coincident design weather data generation; Tariku and Hemmati [131] used the response factor method to perform a transient heat transfer analysis of multidimensional building envelopes; Bishara et al. [128] developed a robust numerical model to investigate and improve the dynamic thermal characteristics of a spruce wood wall; Zhou et al. [132] investigated the thermal behavior of a Trombe wall with PCM (phase change material) using numerical simulations; Zhou et al. [132] established a finite-difference numerical model to analyze the transient heat transfer in a heat recovery building envelope; Zhou et al. [132] employed machine learning and finite-element approach to predict heat fluxes through thermally anisotropic building assemblies; Zhang et al. [133] used the finite difference method to develop a climate-responsive design technique for dynamic heat transfer analysis of building envelopes; Martinez et al. [134] established a simulation approach for the disaggregation of dynamic and multidimensional heat transfer phenomena in envelopes.

Some recent studies have particularly investigated the annual transient heat flux through building walls based on long-term field data. Mazzeo et al. [135] developed a numerical calculation technique to determine the temperature and the heat flux fields in envelopes with PCM layers. Their thermal behavior evaluation method used characteristic days that were

periodically repeated throughout the considered month, and the method was applied to buildings located in continental and Mediterranean climates. Thomas et al. [112] presented an analytical method to calculate heat flux considering the wall orientation, the materials, and the location of the construction. Their approach, which is based on the admittance method and equivalent sol-air temperature, was applied to three types of building envelope walls in different locations in Argentina. Rathore et al. [136] analyzed peak temperature, thermal amplitude, time lag, and decrement factor of small-scale concrete envelopes with and without PCM capsules in tropical climates. Vox et al. [137] used energy balances to study heat flux reduction through the wall of a building prototype with hollow brick masonry and a green façade in the Mediterranean climate.

Despite the extensive research work by the above-mentioned studies, to the best of the authors' knowledge, no previous study has performed an inverse analysis of the annual field behavior of the heat flux through the internal surface of a multilayer lightweight wall of an occupied prefabricated house in a cold temperate zone. Such a gap is also apparent from the reviews of Yang et al. [120], who reviewed developments in theoretical and experimental methodologies for the field evaluation of the thermal performance of building structures, and Rouchier [138], who provided an overview of inverse tools and techniques applied to building physics. In fact, Piggot-Navarrete et al. [86] recently indicated the need to investigate the in situ thermal performance and energy efficiency of prefabricated building envelopes due to the current lack of data and knowledge on the topic. Despite the ecological and financial advantages and the expected growth in the market share of multilayer prefabricated wall assemblies [139], Palani and Karatas [140] showed in a recent study that their in-operation thermal performance can be uncertain, leading to overdesigning building envelope systems.

Numerical simulations can calculate the temperature field and heat flux in a building component given its geometry, initial temperature, boundary conditions, and thermal

properties [129]. Proper and detailed mathematical modeling of the thermal physics of building envelopes is critical for the reliability of numerical simulations [120]. Although current simulation tools are sophisticated, they are subject to uncertainties, especially those from boundary conditions [72]. Indeed, as shown by Panico et al. [70], integrating field data collection into these simulations for effective thermal assessment should not be neglected in order to obtain realistic simulations in building engineering. Although using in situ measurements to impose boundary conditions is the most suitable way to reduce uncertainties in building modeling [72], there is a notable absence of field research assessing the impact of external climate boundary and internal loads on building thermal performance [70]. Moreover, very few studies in the literature currently use long-term monitoring data in real dwellings and measurements in wall assemblies to obtain reliable simulation models [96].

In this case study, the in-operation thermal performance of a multilayer wall assembly is evaluated using an inverse approach, based on numerical modeling and in situ monitoring. The envelope wall investigated is part of an occupied prefabricated two-story house in Quebec City (Canada). One-year temperature sensor measurements were collected in the assembly and then used to solve a heat flux estimation problem. The main contribution of this paper is to show how the annual inner heat flux through a prefabricated lightweight wall evolves and how inverse analysis can be used for the accurate in situ dynamic assessment of building walls. Unlike most standardized methods, the present alternative approach deals only with temperature measurements taken under transient conditions, and does not require additional devices such as flux meters, heaters, infrared cameras, etc. This makes the proposed inverse methodology very practical since actual walls undergo considerable fluctuations in inside and outside conditions throughout the seasons, and temperature sensors are one of the most fundamental and widely used sensors for monitoring and controlling building enclosures. As evaluating the dynamic thermal characteristics of multilayer walls is a relevant ongoing research topic [86], [112],

[115], [118], the present inverse approach enables the continuous in situ monitoring of the effective thermal performance of building envelopes. Moreover, the results on heat flux are useful by providing reliable qualitative and quantitative information to support decision-making towards more energy-efficient prefabricated constructions.

4.2 Field thermal monitoring

The object of the present field research is the same prefabricated wall assembly presented in Section 3.2. For heat flux estimation, the 190 mm-thick wall was considered a 1D medium, consisting of five layers, as per Figure 19: ① high-density polyethylene foil (weather barrier), ② expanded polystyrene (EPS) board, ③ mineral wool batts parallel to wooden studs, ④ oriented strand board (OSB) panel, and ⑤ low-density polyethylene foil (vapor barrier). Interactions with the exterior cladding and interior thin finish coat were neglected, as these items have a minor thermal role; their main function is to serve as protection against water and fire, according to the National Energy Code of Canada for Buildings. Moreover, since the air layer behind the exterior cladding is ventilated, its temperature and RH levels are practically the same as those outside. As shown in Figure 19, thermocouples installed at $x_0 = 0$ mm, $x_1 = 55$ mm, $x_2 = 155$ mm, and $x_L = 190$ mm were considered for the inverse estimation of heat flux.

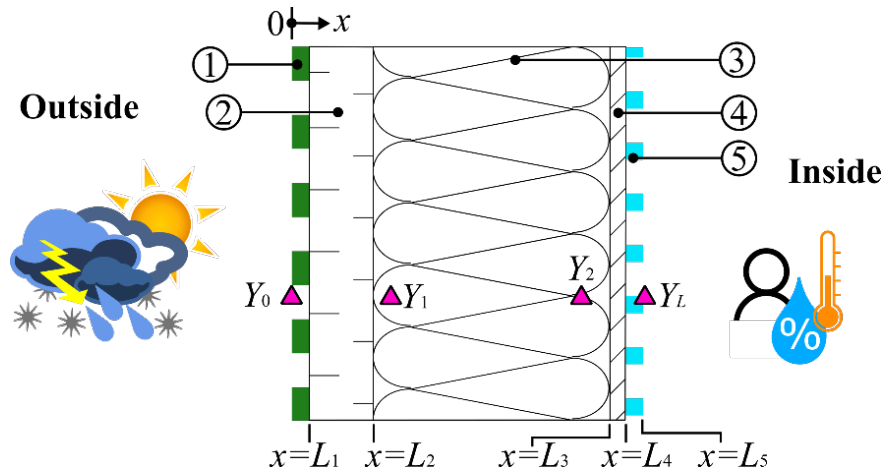


Figure 19. One-dimensional cross-sectional view depicting the wall layers and measurement locations (exterior and interior claddings not shown for clarity).

Figure 20 shows the field temperature data measured. The thermal response of the wall was monitored at a 10-min sampling period for one year, from September 2021 to August 2022. Long on-site data collection enables the impact of environmental (external) and occupation (internal) factors on heat flux to be taken into account during all seasons. A noticeable change in temperature profiles can be seen at the beginning of data collection, corresponding to the period when the residents moved in (around mid-September). Temperatures Y_0 and Y_1 are noisy due to intense external loads arising from changes in the weather conditions of a seasonal temperate climate. These readings remain reasonably cold over data collection, with a drop from September to December and low values until March, according to the cold periods (fall and winter). In a different way, Y_0 and Y_1 begin to get warmer from April (early spring) to the point where they seem to stabilize between July and August (late summer). Measurements Y_2 and Y_L have a stable evolution over data collection, remaining much steadier in late fall and winter, most likely due to the action of the heating system thermostat. This shows that these sensors are highly dependent on indoor conditions and occupant activities. Once measured and

recorded, the temperature dataset was then used to carry out the inverse heat flux estimation in COMSOL Multiphysics with LiveLink for MATLAB, as described below.

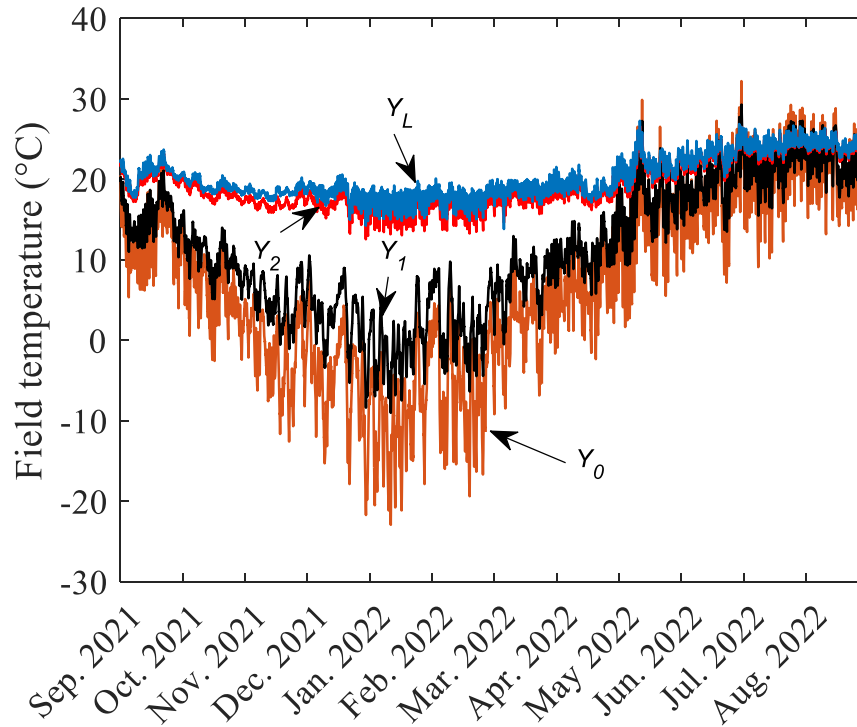


Figure 20. Field temperature measurements.

4.3 Direct thermal problem

As shown in Figure 19, the wall assembly under study is considered as a one-dimensional multilayer medium subject to transient heat transfer. Initially, all the wall materials are uniformly subject to temperature T_{in} . The thermal contact between adjacent layers is considered to be perfect. The exterior wall surface is subject to a specified temperature boundary condition based on measurement Y_0 . The interior surface is considered to be subject to a thermal flux boundary condition, i.e., the energy transferred via heat flux at $x = L_5$ is equal to the heat

transferred via conduction within the envelope. The transient heat flux through the inner surface, which is the target of this inverse analysis, is governed by the dynamic energy interactions of the occupants with the outdoor and indoor built environment. This means that the thermal energy entering or leaving the interior of the building envelope is considered an unknown boundary condition for the purposes of estimating it as a surface heat flux history. Thus, the direct thermal problem can be expressed as follows:

$$k_s \frac{\partial^2 T_s}{\partial x^2} = C_s \frac{\partial T_s}{\partial t}, \quad L_{s-1} < x < L_s, \quad s = 1, 2, 3, 4, 5 \quad (48)$$

with the initial condition:

$$T_s(x, 0) = T_{in}, \quad s = 1, 2, 3, 4, 5 \quad (49)$$

subject to the following boundary conditions at $x = 0$ and at $x = L_5$:

$$T|_{x=0} = Y_0 \quad (50)$$

$$-k_5 \left. \frac{\partial T_5}{\partial x} \right|_{x=L_5} = q \quad (51)$$

and subjected to perfect thermal contact conditions:

$$-k_s \left. \frac{\partial T_s}{\partial x} \right|_{x=L_s} = -k_{s+1} \left. \frac{\partial T_{s+1}}{\partial x} \right|_{x=L_s}, \quad s = 1, 2, 3, 4 \quad (52)$$

$$T_s|_{x=L_s} = T_{s+1}|_{x=L_s}, \quad s = 1, 2, 3, 4 \quad (53)$$

where x is the direction of heat flux [m]; t is the time [s]; $T = T(x, t)$ is the temperature [$^{\circ}\text{C}$]; k is the thermal conductivity [$\text{W m}^{-1} \text{K}^{-1}$]; C is the volumetric heat capacity [$\text{J m}^{-3} \text{K}^{-1}$]; L_s is the layer thickness [m]; h is the convective heat transfer coefficient [$\text{W m}^{-2} \text{K}^{-1}$]; q is the transient heat flux entering or leaving the indoor built space [W m^{-2}]; and s is an index to identify the wall layers. The material property data of the wall layers were obtained from WUFI, a simulation program developed by the Fraunhofer Institute for Building Physics to investigate heat and moisture transfer in building components.

4.4 Inverse heat flux estimation

4.4.1 Sequential function specification method

Inverse problems can determine, from a set of measurements, the factors that produced them. In engineering applications, inverse analysis identifies unknown parameters using an optimization algorithm to minimize the error between measured and calculated/simulated data [127]. By using inverse methodology, building engineering researchers have gathered experimental data and mined for information on material and component characterization,

building energy performance assessment, model predictive control, among others [120], [127], [138].

In the present inverse analysis, the time-dependent heat flux through the inner surface of the studied wall is estimated using the sequential function specification method (SFSM) with future times regularization. The SFSM is an effective tool for solving inverse problems and has been widely employed in several different applications in thermal sciences [141], [142], [143], [144]. Although the traditional SFSM is based on a Neumann-type boundary condition, it can also be formulated with other boundary conditions [142], [145].

In the SFSM, the heat flux history is discretized and components $q_1, q_2, q_3, \dots, q_{n-1}$ are assumed to be known previously in order to estimate q at current time n . This inverse approach uses additional temperature information from future times r , i.e., $Y_n, Y_{n+1}, Y_{n+2}, \dots, Y_{n+r-1}$, to improve the stability of the ill-posed inverse heat conduction problem. This implies that the conception of future time assumes that heat flux remains constant over r future time steps. Further technical details on the SFSM can be found in Woodbury [4] and Woodbury et al. [145].

Applying the SFSM, the solution to the present inverse problem is achieved by minimizing the following least-squares objective function:

$$S(q) = \sum_{i=1}^M \sum_{j=n}^{n+r-1} [Y_{i,j} - T_{i,j}(q)]^2 \quad (54)$$

where M is the number of thermocouples; r is the number of future time steps; Y is the experimentally measured temperatures; and T is the numerically calculated temperatures at the sensing locations obtained by solving the direct problem. The field measurements from the thermocouples at x_1 and x_2 (i.e., Y_1 and Y_2) are contained in Y and are used to estimate q . This

is relevant because using data from more than one sensor provides additional information and leads to more accurate estimates [145].

Equation (54) can be minimized by differentiating S in relation to q , as follows:

$$\frac{\partial S}{\partial q_j} = 2 \sum_{i=1}^M \sum_{j=n}^{n+r-1} \varphi_{i,j} [Y_{i,j} - T_{i,j}(q_j)] = 0 \quad (55)$$

where φ is the sensitivity coefficient, which is conveniently calculated using a finite difference scheme:

$$\varphi_{i,j} = \frac{\partial T_{i,j}(q)}{\partial q_j} \approx \frac{T_i(q_j + \delta q_j) - T_i(q_j)}{\delta q_j} \quad (56)$$

where δq is a small variation in q . Since T is a function of q , temperature can be expressed by a first-order Taylor series, as follows:

$$T_{i,j} \cong \hat{T}_{i,j} + \varphi_{i,j}(q_j - \hat{q}_j) \quad (57)$$

Substituting Equation (57) into Equation (55) gives:

$$q_j = \hat{q}_j + \frac{\sum_{i=1}^M \sum_{j=n}^{n+r-1} \varphi_{i,j} (Y_{i,j} - \hat{T}_{i,j})^2}{\sum_{i=1}^M \sum_{j=0}^{r-1} \varphi_{i,j}^2} \quad (58)$$

where \hat{T} and \hat{q} are the temperature and heat flux values at the previous time step and q is the heat flux at the current time. Equation (58) is used in a sequential algorithm to estimate all the components of the annual heat flux history. The SFMSM computational procedure for estimating q_j can be summarized as follows:

1. Load the field temperature measurements Y ;
2. Load the numerical model built in COMSOL into MATLAB;
3. Read the coordinates of the sensors located at x_1 and x_2 ;
4. Set the regularization parameter r ;
5. Consider constant heat flux over r future time steps, i.e., $\hat{q}_j = \hat{q}_{j+1} = \hat{q}_{j+2} = \dots = \hat{q}_{j+r-1}$;
6. Solve the direct problem to determine the temperature field of the wall assembly at x_1 and x_2 ;
7. Compute the sensitivity coefficient φ ;
8. Compute the current heat flux component q_j .
9. Repeat the previous steps throughout the domain of measured data.

4.4.2 Regularization parameter

The use of future time steps in the SFMSM has a regularizing effect on the heat flux estimation to overcome ill-posedness. This regularization technique provides stability to the inverse estimation procedure by using additional temperature data from future times. Although

it significantly stabilizes the inverse algorithm, the future times regularization unavoidably introduces bias into the estimation results. Thus, properly determining the degree of regularization is important in order to achieve a trade-off between the stability and bias of the estimation [145]. Although it has been addressed in some papers [146], [147], selecting optimal regularization is still a challenging issue in applying the SFSM [142].

In this study, the discrepancy principle is used to provide guidance to select the value of the regularizing parameter r . In this approach, r is selected as small as possible but large enough so that the temperature residual R_T is consistent with the error in the measured data, i.e., the accuracy of the temperature sensors σ_Y [4], [147]. In mathematical terms:

$$R_T = \sqrt{\frac{\sum_{i=1}^M \sum_{j=n}^{n+r-1} (Y_{i,j} - T_{i,j})^2}{Mr}} \approx \sigma_Y \quad (59)$$

4.4.3 Uncertainty analysis

Solving the inverse problem requires information on all parameters involved in the physical model except the heat flux, which is estimated by comparing numerical and measured temperature data. Thus, the inverse solution is sensitive to the accuracy of the modeling and input parameters [145]. Measured temperature is obtained from intrusive sensors and is subject to uncertainties inherent in experiments. In field assessments, experimental conditions are usually far from controlled laboratory conditions, which affects data collection. Moreover, numerical temperature is subject to uncertainties in the thermal properties introduced into the mathematical model, which in turn represents an approximation of the real physical system being studied.

The accuracy of the inverse heat flux estimation is assessed using an approach based on the uncertainty propagation technique by Blackwell and Dowding [148]. In this sensitivity-based approach, the output uncertainty is calculated by propagating the input uncertainties through the numerical model. Thus, the uncertainty of the retrieved heat flux (σ_q) is estimated by the sum of squares of uncorrelated errors associated with the initial temperature (T_{in}), the field temperature measurements (Y), and the thermal properties of the wall materials (k and C), as follows:

$$\sigma_{q_j} = \sqrt{\left(\frac{\partial q_j}{\partial T_{in}} \sigma_{T_{in}}\right)^2 + \sum_{s=1}^5 \left(\frac{\partial q_j}{\partial k_s} \sigma_{k_s}\right)^2 + \sum_{s=1}^5 \left(\frac{\partial q_j}{\partial C_s} \sigma_{C_s}\right)^2 + \sum_{i=1}^M \sum_{j=n}^{n+r-1} \left(\frac{\partial q_j}{\partial Y_{i,j}} \sigma_Y\right)^2} \quad (60)$$

The terms on the right-hand side of Equation (60) evaluate how much the heat flux (output) changes in relation to changes in T_{in} , Y , k , and C (inputs). The term related to Y is computed according to the technique of filter coefficients by Blackwell and Beck [149]. The terms associated with k and C are computed using finite difference approximation. The error in T_{in} becomes insignificant over time [149].

4.5 Results and discussion

The annual heat flux through the internal wall surface was determined using 6 future time steps based on the discrepancy principle described in Section 4.4.2. The resulting estimated heat flux (solid line) and its uncertainty (shaded area) are shown in Figure 21. It can be seen that q is noisier and has larger errors in colder periods due to abrupt and severe variations in the

experimental field temperature data. Negative values of q indicate heat loss, i.e., heat leaving the interior environment towards the outside. Positive values indicate heat gain, i.e., heat entering indoors. The transient thermal behavior of the building wall is derived from the continuous and dynamic energetic response of its layers/materials to external climatic conditions and internal comfort requirements. The surface heat flux is directly related to the temperature gradient within the wall assembly and indicates if external or internal loads are predominant. Thus, as Y_0 remains colder than Y_L for most of the monitored period, the indoor space practically only experiences outgoing heat flux, i.e., it loses heat. As the residential house is in a region with a temperate cold climate, there are greater heat losses in winter due to the very low temperatures outside. Peak heat losses of around 5.5 W m^{-2} are observed in the freezing months of January and February. The heat flux becomes positive in the transition period between late spring and early summer. Peak heat gains of around 1.0 W m^{-2} are observed in July and August, the warmest months of summer in Quebec City. The lower magnitude of heat gain is due to the greater proximity between the temperatures within the wall and the likely opening of doors and windows.

In terms of building energy assessment, in addition to information about heat flux, it is relevant to evaluate the overall thermal performance of the wall during the heating and cooling seasons. The total thermal energy leaving or entering the room per unit of area is calculated by integrating the q profile shown in Figure 21 with respect to time. For the heating period (i.e., from September to March), a value of $17.86 \text{ kW h m}^{-2}$ ($6.43 \times 10^7 \text{ J m}^{-2}$) is found for the total heat loss through the internal wall. For the free cooling period (i.e., from April to August), the total heat gain through the inner wall surface is calculated at 0.96 kW h m^{-2} ($3.45 \times 10^6 \text{ J m}^{-2}$).

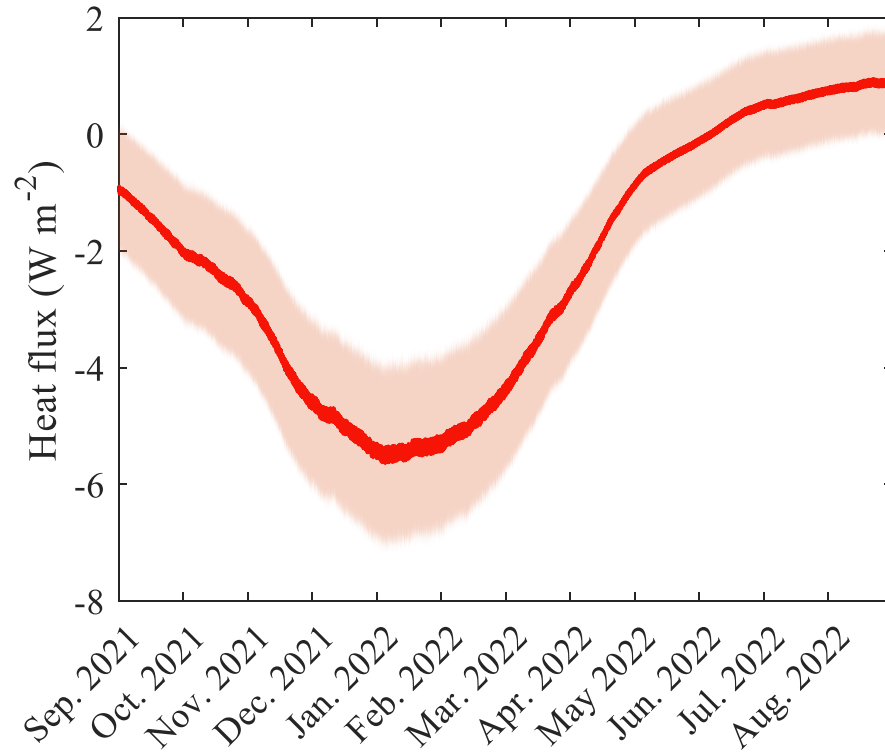


Figure 21. Annual heat flux through the internal wall surface.

The most critical thermal characteristic of a multilayer wall is its overall thermal resistance (R -value), which describes its steady-state behavior and can be assessed based on heat flux measurements, the outcomes of which can be processed with the average method [120], [124]. The average method is a direct calculation to estimate the R -value by assuming steady-state heat transfer and neglecting thermal mass [120], as shown in Eq. (61).

$$R\text{-value} = \frac{\sum \Delta T}{\sum q} \quad (61)$$

Therefore, this method requires two temperature sensors installed on the surfaces of the wall assembly to calculate ΔT and a heat flux meter to measure q on the wall surface with more stable conditions [120]. Differently, as a validation exercise, this study evaluates the effective

thermal resistance of the investigated assembly using the heat flux estimated in combination with the temperature measurements taken at the wall boundaries, i.e., Y_0 and Y_L .

The duration of the thermal monitoring, over which the sums are carried out for the average method, should last at least three days [120]. Very large fluctuations in indoor and outdoor conditions during and immediately before data collection can affect the measurement length. Changes in the direction of heat transfer violate the steady-state assumption and studies in periods when this condition is probable, such as the summer, should be avoided [120]. Field data are typically measured during periods with a difference between indoor and outdoor temperatures of at least 10 °C [120]. Thus, the average method is usually only employed in cool or cold periods, when the heating equipment is turned on [120].

Accurate in situ measurements that match the above requirements can be challenging and complicated in locations such as Quebec City, where the case study building is located. This is because the city has cold seasons with harsh weather conditions and many periods with snow or rain. In this context, the recordings of measurements Y_0 and Y_L were analyzed to determine the best 72-hour monitoring period to assess the effective thermal resistance of the assembly using the average method. Figure 22 shows the raw data selected to calculate the wall's R -value. These data correspond to three consecutive days in April, in early spring, when the outside temperature was somewhat stable but still relatively low. Temperature measurements were smoothed using a Savitzky-Golay filter and considered to be in quasi-steadiness. Based on the average method, the in situ thermal resistance of the studied wall assembly was determined to be 4.96 m² K W⁻¹. This implies that the multilayer assembly investigated complies with the National Building Code of Canada, which establishes a minimum effective thermal resistance of 3.08 m² K W⁻¹ for above-ground opaque assemblies in buildings without a heat-recovery ventilator and located in a climate zone designated as 7A (e.g., Quebec City). The effective wall's R -value differs by around 6% from 5.25 m² K W⁻¹, the theoretical steady-state thermal

resistance calculated prior to construction based on material property data provided by suppliers. This deviation can be associated with hidden flaws in the envelope structure, minor maintenance work, workmanship quality, aging of material properties, inaccuracies in temperature measurements, among other factors present in the field. This small difference indicates the robustness of the heat flux estimation and shows that the present inverse approach is capable of accurately evaluating the effective thermal behavior of building walls under real operating conditions. Therefore, this study can be considered successful in providing an alternative methodology for the assessment of the dynamic field thermal performance of envelope assemblies, thus enabling the quasi-online monitoring of energy efficiency targets.

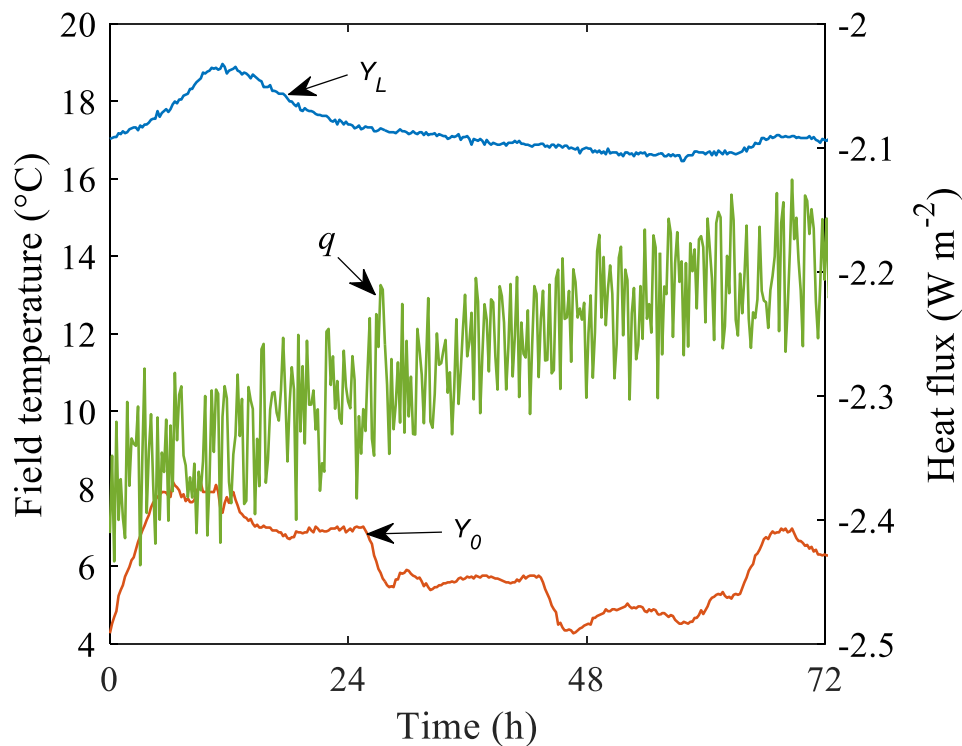


Figure 22. Data used to evaluate the effective in situ thermal resistance of the wall assembly.

It is important to mention that, as most of the methodologies currently available [120], the present approach determines the thermal performance of the assembly based on a single

detection region in which all the thermocouples are aligned along the cross-section. Therefore, it is primarily suitable for plane envelope walls with opaque layers that are perpendicular to the heat flux and do not have considerable thermal bridging and lateral heat transfer.

4.6 Summary

As natural resources have become more precious, the thermal behavior of buildings has become essential to maximize energy savings and has been addressed by strict regulations. Due to seasonal and daily variations in outdoor and indoor conditions, the dynamic heat flux transmitted by conduction through the building envelope is a key issue to support decision-making in thermal design and thus avoid undesirable heat losses and gains. This third case study described an inverse heat transfer analysis to obtain information on the annual transient heat flux exchanged by the indoor space of an occupied prefabricated detached house located in a temperate cold climate. A lightweight multilayer wall was monitored on site for one year, and the field temperature measurements were used in an inverse heat flux estimation procedure using the sequential function specification method. The internal wall surface was subject to an outward heat flux (i.e., heat loss) for most of the year. The peak heat loss was almost 5.5 W m^{-2} in winter and the peak heat gain was around 1.0 W m^{-2} in summer. In the heating period, a total amount of thermal energy due to heat conduction of around 18 kW h m^{-2} ($6.5 \times 10^7 \text{ J m}^{-2}$) left the interior environment. For the free cooling period, there was a total thermal gain of around 1 kW h m^{-2} ($3.5 \times 10^6 \text{ J m}^{-2}$). Based on the heat flux estimations, the in situ thermal resistance of the wall was determined at $4.96 \text{ m}^2 \text{ K W}^{-1}$, 6% lower than its theoretical value, but still in compliance with the Canadian building code.

5. General conclusions

This research work consisted of applying inverse analysis to the experimental investigation of the thermal and hygric properties and behavior of metallic and building materials. The findings and observations presented in this thesis helps to better understand the operational response of engineering components. Inverse problem solution allowed the simultaneous estimation of the temperature-dependent thermal properties of 304 stainless steel, as well as the simultaneous estimation of various hygrothermal properties of a multilayer lightweight wall. Additionally, the transient annual heat flux through a prefabricated wall assembly of an occupied house was determined. All these investigations were supported by numerical simulations carried out in COMSOL Multiphysics and experimentally measured data.

The main conclusions of this study are as follows:

- complementary transient experiments provided significant increase in the determinant of the information matrix, enabling enhanced Bayesian inversion.
- additional sensitive data allowed the simultaneous estimation of the four parameters describing the linearly temperature-dependent thermal conductivity and specific heat of 304 austenitic stainless steel.
- hygrothermal characterization based on one-year field measurements and subsequent model calibration enabled simulations to better assess the wall working behavior.
- in most cases, database properties overestimated the effective hygrothermal properties of the building envelope monitored.
- reference properties led to overestimating the annual thermal response of the wall assembly by about 30 % and the annual hygric response by about 24 %.

- the internal wall surface was subject to an outward heat flux (i.e., heat loss) for most of the year.
- the peak heat loss was almost 5.5 W m^{-2} in winter and the peak heat gain was around 1.0 W m^{-2} in summer.
- in the heating period, a total amount of thermal energy due to heat conduction of around 18 kW h m^{-2} left the interior environment.
- in the free cooling period, there was a total thermal gain of around 1 kW h m^{-2} .
- the in effective thermal resistance of the wall was determined at $4.96 \text{ m}^2 \text{ K W}^{-1}$, 6% lower than its theoretical value, but still in compliance with the Canadian building code.

Overall, this study provided theoretical and practical background on thermal and hygric characterization using experimental inverse approach. This can be useful for performing similar studies to feed materials database for in-depth knowledge of effective behavior of building materials and structures. Additionally, the thermal properties of metallic materials can be accurately estimated when standard techniques are not available.

6. Appendix

6.1 Publications

- Ramos N P, Antunes M M, and Lima e Silva S M M (2023). *A heat flux-corrected experimental inverse technique for simultaneously estimating the thermal properties of a metallic medium as functions of temperature*. **Experimental Heat Transfer**. DOI 10.1080/08916152.2023.2189328.
- Ramos N P, Antunes M M, Silva A A A P, and Lima e Silva S M M (2023). *Effects of tempering temperature on temperature-dependent thermal properties of 1045 steel*. **Journal of Materials Science** 58 1905–1924. DOI 10.1007/s10853-022-08137-0.
- Ramos N P, Antunes M M, and Lima e Silva S M M (2022). *Complementary transient thermal models and metaheuristics to simultaneously identify linearly temperature-dependent thermal properties of austenitic stainless steels*. **Physica Scripta** 97(11) 115006. DOI: 10.1088/1402-4896/ac99ac.
- Ramos N P, Antunes M M, Guimarães G, and Lima e Silva S M M (2022). *Simultaneous Bayesian estimation of the temperature-dependent thermal properties of a metal slab using a three-dimensional transient experimental approach*. **International Journal of Thermal Sciences** 179 107671. DOI: 10.1016/j.ijthermalsci.2022.107671.
- Ramos N P, Antunes M M, and Lima e Silva S M M (2021). *An experimental and straightforward approach to simultaneously estimate temperature-dependent thermophysical properties of metallic materials*. **International Journal of Thermal Sciences** 166 106960. DOI: 10.1016/j.ijthermalsci.2021.106960.

- Ramos N P, Carollo L F S, and Lima e Silva S M M (2020). *Contact resistance analysis applied to simultaneous estimation of thermal properties of metals*. **Measurement Science and Technology** 31(10) 105601. DOI 10.1088/1361-6501/ab8e6a.

6.2 Ongoing papers

- Ramos N P, Antunes M M, Abreu L A P, Faco H, and Lima e Silva S M M. Simultaneous estimation of effective temperature-dependent thermal properties of glass fiber-reinforced polymer for air-core reactor insulation via inverse approach.
- Ramos N P, Buenrostro L D, Lima e Silva S M M, and Gosselin L. Simultaneous estimation of hygrothermal properties of a prefabricated lightweight wall using one-year on-site measurements to solve inverse problems.
- Ramos N P, Buenrostro L D, Lima e Silva S M M, and Gosselin L. Inverse estimation of the annual heat flux through the internal surface of a multilayer wall in an occupied prefabricated house from field measurements.
- Ramos N P, Antunes M M, Silva A A A P, Guimarães G, and Lima e Silva S M M. Influence of quenching and tempering heat treatment on the heat flux to the workpiece in dry milling of AISI 1045 steel.

6.3 Thermal property measurements

- Measurement of the thermal conductivity of a skin cream using the hot-wire method for the company InoxNews.

- Measurement of the thermal conductivity of composite materials using the hot-plate method for the company General Electrics.

6.4 Sandwich PhD

From August 2022 to May 2023, PhD internship at the Thermal Energy Transfer laboratory at Université Laval, under the supervision of Professor Louis Gosselin. The research internship focused on applying inverse heat and moisture analysis to investigate the hygrothermal behavior of building walls and their materials.

7. References

- [1] J. Hadamard, *Lectures on Cauchy's Problem in Linear Partial Differential Equations*. Yale University Press, 1923.
- [2] O. M. Alifanov, *Inverse Heat Transfer Problems*. in International Series in Heat and Mass Transfer. Berlin, Heidelberg: Springer Berlin Heidelberg, 1994. doi: 10.1007/978-3-642-76436-3.
- [3] O. M. Alifanov, "Solution of an inverse problem of heat conduction by iteration methods," *Journal of Engineering Physics*, vol. 26, no. 4, pp. 471–476, Apr. 1974, doi: 10.1007/BF00827525.
- [4] K. A. Woodbury, Ed., *Inverse Engineering Handbook*. CRC Press, 2002. doi: 10.1201/9781420041613.
- [5] B. Czél, K. A. Woodbury, and G. Gróf, "Simultaneous estimation of temperature-dependent volumetric heat capacity and thermal conductivity functions via neural networks," *Int J Heat Mass Transf*, vol. 68, pp. 1–13, Jan. 2014, doi: 10.1016/j.ijheatmasstransfer.2013.09.010.
- [6] F. Pierron and S. Avril, "Experimental Mechanics - Inverse Problems in Experimental Solid Mechanics," in *Mechanical Engineering, Energy Systems and Sustainable Development -Volume V*, EOLSS Publications, 2009.
- [7] M. N. Özisik and H. R. B. Orlande, *Inverse Heat Transfer*. Routledge, 2018. doi: 10.1201/9780203749784.
- [8] J. L. J. Pereira, M. B. Francisco, C. A. Diniz, G. Antônio Oliver, S. S. Cunha, and G. F. Gomes, "Lichtenberg algorithm: A novel hybrid physics-based meta-heuristic for global optimization," *Expert Syst Appl*, vol. 170, p. 114522, May 2021, doi: 10.1016/j.eswa.2020.114522.
- [9] X. S. Yang, "Review of meta-heuristics and generalised evolutionary walk algorithm," *International Journal of Bio-Inspired Computation*, vol. 3, no. 2, p. 77, 2011, doi: 10.1504/IJBIC.2011.039907.
- [10] M. F. Tabassum *et al.*, "Optimal solution of engineering design problems through differential gradient evolution plus algorithm: a hybrid approach," *Phys Scr*, vol. 97, no. 1, p. 014002, Jan. 2022, doi: 10.1088/1402-4896/ac41ec.
- [11] G. C. V. Ramadas, E. M. G. P. Fernandes, A. M. V. Ramadas, A. M. A. C. Rocha, and M. F. P. Costa, "On Metaheuristics for Solving the Parameter Estimation Problem in Dynamic Systems: A Comparative Study," *Journal of Optimization*, vol. 2018, pp. 1–21, 2018, doi: 10.1155/2018/3213484.

- [12] Y. Jannot and A. Degiovanni, *Thermal Properties Measurement of Materials*. Wiley, 2018. doi: 10.1002/9781119475057.
- [13] L. Gosselin, M. Tye-Gingras, and F. Mathieu-Potvin, “Review of utilization of genetic algorithms in heat transfer problems,” *Int J Heat Mass Transf*, vol. 52, no. 9–10, pp. 2169–2188, Apr. 2009, doi: 10.1016/j.ijheatmasstransfer.2008.11.015.
- [14] J. P. Kaipio and C. Fox, “The Bayesian Framework for Inverse Problems in Heat Transfer,” *Heat Transfer Engineering*, vol. 32, no. 9, pp. 718–753, Aug. 2011, doi: 10.1080/01457632.2011.525137.
- [15] J. Berger, H. R. B. Orlande, N. Mendes, and S. Guernouti, “Bayesian inference for estimating thermal properties of a historic building wall,” *Build Environ*, vol. 106, pp. 327–339, Sep. 2016, doi: 10.1016/j.buildenv.2016.06.037.
- [16] N. Gnanasekaran and C. Balaji, “A Bayesian approach for the simultaneous estimation of surface heat transfer coefficient and thermal conductivity from steady state experiments on fins,” *Int J Heat Mass Transf*, vol. 54, no. 13–14, pp. 3060–3068, Jun. 2011, doi: 10.1016/j.ijheatmasstransfer.2011.01.028.
- [17] P. Pasquier and D. Marcotte, “Robust identification of volumetric heat capacity and analysis of thermal response tests by Bayesian inference with correlated residuals,” *Appl Energy*, vol. 261, p. 114394, Mar. 2020, doi: 10.1016/j.apenergy.2019.114394.
- [18] D. Lesnic, *Inverse Problems with Applications in Science and Engineering*. Boca Raton: Chapman and Hall/CRC, 2021. doi: 10.1201/9780429400629.
- [19] B. Lin, Y. Chen, and G. Zhang, “Technological progress and rebound effect in China’s nonferrous metals industry: An empirical study,” *Energy Policy*, vol. 109, pp. 520–529, Oct. 2017, doi: 10.1016/j.enpol.2017.07.031.
- [20] K. H. Lo, C. H. Shek, and J. K. L. Lai, “Recent developments in stainless steels,” *Materials Science and Engineering: R: Reports*, vol. 65, no. 4–6, pp. 39–104, May 2009, doi: 10.1016/j.mser.2009.03.001.
- [21] M. Naghizadeh and H. Mirzadeh, “Microstructural Evolutions During Reversion Annealing of Cold-Rolled AISI 316 Austenitic Stainless Steel,” *Metallurgical and Materials Transactions A*, vol. 49, no. 6, pp. 2248–2256, Jun. 2018, doi: 10.1007/s11661-018-4583-6.
- [22] N. P. Ramos, M. de Melo Antunes, A. A. A. P. da Silva, and S. M. M. de Lima e Silva, “Effects of tempering temperature on temperature-dependent thermal properties of 1045 steel,” *J Mater Sci*, vol. 58, no. 4, pp. 1905–1924, Jan. 2023, doi: 10.1007/s10853-022-08137-0.
- [23] J. Wilzer, F. Lüdtke, S. Weber, and W. Theisen, “The influence of heat treatment and resulting microstructures on the thermophysical properties of martensitic steels,” *J Mater Sci*, vol. 48, no. 24, pp. 8483–8492, Dec. 2013, doi: 10.1007/s10853-013-7665-2.

- [24] J. Valencia and P. N. Quested, “ASM Handbook, Casting - Thermophysical properties 15,” in *ASM Handbook - Casting*, ASM, 2008, pp. 468–481. doi: 10.1361/asmhba0005240.
- [25] R. G. Dourado da Silva, D. C. Ferreira, F. V. Avelar Dutra, and S. M. M. Lima e Silva, “Simultaneous real time estimation of heat flux and hot spot temperature in machining process using infrared camera,” *Case Studies in Thermal Engineering*, vol. 28, p. 101352, Dec. 2021, doi: 10.1016/j.csite.2021.101352.
- [26] W. Buck and S. Rudtsch, “Thermal properties - Measurement methods for materials properties,” in *Springer Handbook of Materials Measurement Methods*, H. Czichos, T. Saito, and L. Smith, Eds., Berlin, Heidelberg: Springer Berlin Heidelberg, 2006, pp. 399–428. doi: 10.1007/978-3-540-30300-8.
- [27] A. Martínez, M. Carmona, C. Cortés, and I. Arauzo, “Characterization of Thermophysical Properties of Phase Change Materials Using Unconventional Experimental Technologies,” *Energies (Basel)*, vol. 13, no. 18, p. 4687, Sep. 2020, doi: 10.3390/en13184687.
- [28] S. E. Gustafsson, E. Karawacki, and M. N. Khan, “Transient hot-strip method for simultaneously measuring thermal conductivity and thermal diffusivity of solids and fluids,” *J Phys D Appl Phys*, vol. 12, no. 9, pp. 1411–1421, Sep. 1979, doi: 10.1088/0022-3727/12/9/003.
- [29] W. J. Parker, R. J. Jenkins, C. P. Butler, and G. L. Abbott, “Flash Method of Determining Thermal Diffusivity, Heat Capacity, and Thermal Conductivity,” *J Appl Phys*, vol. 32, no. 9, pp. 1679–1684, Sep. 1961, doi: 10.1063/1.1728417.
- [30] B. Abad, D.-A. Borca-Tasciuc, and M. S. Martin-Gonzalez, “Non-contact methods for thermal properties measurement,” *Renewable and Sustainable Energy Reviews*, vol. 76, pp. 1348–1370, Sep. 2017, doi: 10.1016/j.rser.2017.03.027.
- [31] N. P. Ramos, L. F. dos Santos Carollo, and S. M. M. de Lima e Silva, “Contact resistance analysis applied to simultaneous estimation of thermal properties of metals,” *Meas Sci Technol*, vol. 31, no. 10, p. 105601, Oct. 2020, doi: 10.1088/1361-6501/ab8e6a.
- [32] Y. Jannot, V. Felix, and A. Degiovanni, “A centered hot plate method for measurement of thermal properties of thin insulating materials,” *Meas Sci Technol*, vol. 21, no. 3, p. 035106, Mar. 2010, doi: 10.1088/0957-0233/21/3/035106.
- [33] Y. Jannot, A. Degiovanni, and G. Payet, “Thermal conductivity measurement of insulating materials with a three layers device,” *Int J Heat Mass Transf*, vol. 52, no. 5–6, pp. 1105–1111, Feb. 2009, doi: 10.1016/j.ijheatmasstransfer.2008.09.017.
- [34] Y. Jannot, J. Meulemans, V. Schick, M. Capp, and I. Bargain, “A Comparative Fluxmetric (CFM) Method for Apparent Thermal Conductivity Measurement of

- Insulating Materials at High Temperature,” *Int J Thermophys*, vol. 41, no. 7, p. 94, Jul. 2020, doi: 10.1007/s10765-020-02676-x.
- [35] J. R. Ferreira-Oliveira, L. R. R. de Lucena, R. P. B. Dos Reis, C. J. de Araújo, and C. R. Bezerra-Filho, “Thermal diffusivity measurement of stainless-steel alloys through use of the Angstrom’s method,” *Experimental Heat Transfer*, vol. 35, no. 4, pp. 419–439, Jun. 2022, doi: 10.1080/08916152.2021.1887407.
- [36] Z. Barani *et al.*, “Thermal Properties of the Binary-Filler Hybrid Composites with Graphene and Copper Nanoparticles,” *Adv Funct Mater*, vol. 30, no. 8, Feb. 2020, doi: 10.1002/adfm.201904008.
- [37] T. R. Pavlov, D. Staicu, L. Vlahovic, R. J. M. Konings, P. Van Uffelen, and M. R. Wenman, “A new method for the characterization of temperature dependent thermo-physical properties,” *International Journal of Thermal Sciences*, vol. 124, pp. 98–109, Feb. 2018, doi: 10.1016/j.ijthermalsci.2017.10.008.
- [38] E. García, I. Amaya, and R. Correa, “Estimation of thermal properties of a solid sample during a microwave heating process,” *Appl Therm Eng*, vol. 129, pp. 587–595, Jan. 2018, doi: 10.1016/j.applthermaleng.2017.10.037.
- [39] F. Mohebbi, M. Sellier, and T. Rabczuk, “Estimation of linearly temperature-dependent thermal conductivity using an inverse analysis,” *International Journal of Thermal Sciences*, vol. 117, pp. 68–76, Jul. 2017, doi: 10.1016/j.ijthermalsci.2017.03.016.
- [40] B. Lamien *et al.*, “A Bayesian approach for the estimation of the thermal diffusivity of aerodynamically levitated solid metals at high temperatures,” *Int J Heat Mass Transf*, vol. 141, pp. 265–281, Oct. 2019, doi: 10.1016/j.ijheatmasstransfer.2019.06.054.
- [41] B. Sawaf, M. N. Ozisik, and Y. Jarny, “An inverse analysis to estimate linearly temperature dependent thermal conductivity components and heat capacity of an orthotropic medium,” *Int J Heat Mass Transf*, vol. 38, no. 16, pp. 3005–3010, Nov. 1995, doi: 10.1016/0017-9310(95)00044-A.
- [42] C.-H. Huang and Y. Jan-Yuan, “An inverse problem in simultaneously measuring temperature-dependent thermal conductivity and heat capacity,” *Int J Heat Mass Transf*, vol. 38, no. 18, pp. 3433–3441, Dec. 1995, doi: 10.1016/0017-9310(95)00059-I.
- [43] R. Fischer *et al.*, “The concept of Integrated Data Analysis of complementary experiments,” in *AIP Conference Proceedings*, AIP, 2007, pp. 195–202. doi: 10.1063/1.2821262.
- [44] R. L. McMasters, F. de Monte, and J. V. Beck, “Estimating Two Heat-Conduction Parameters From Two Complementary Transient Experiments,” *J Heat Transfer*, vol. 140, no. 7, Jul. 2018, doi: 10.1115/1.4038855.

- [45] Boyd and Little, “Complementary data fusion for limited-angle tomography,” in *Proceedings of IEEE Conference on Computer Vision and Pattern Recognition CVPR-94*, IEEE Comput. Soc. Press, 1994, pp. 288–294. doi: 10.1109/CVPR.1994.323842.
- [46] P. B. Weichman, D. R. Lun, M. H. Ritzwoller, and E. M. Lavelly, “Study of surface nuclear magnetic resonance inverse problems,” *J Appl Geophy*, vol. 50, no. 1–2, pp. 129–147, May 2002, doi: 10.1016/S0926-9851(02)00135-0.
- [47] J. J. Led and H. Gesmar, “The applicability of the magnetization-transfer NMR technique to determine chemical exchange rates in extreme cases. The importance of complementary experiments,” *Journal of Magnetic Resonance (1969)*, vol. 49, no. 3, pp. 444–463, Oct. 1982, doi: 10.1016/0022-2364(82)90257-8.
- [48] Y. Cao, F. Wang, Z. He, J. Yang, and Y. Cao, “Boosting Image Super-Resolution via Fusion of Complementary Information Captured by Multi-Modal Sensors,” *IEEE Sens J*, vol. 22, no. 4, pp. 3405–3416, Feb. 2022, doi: 10.1109/JSEN.2021.3139452.
- [49] H. N. Mehta, P. Benyathiar, D. K. Mishra, and M. Varney, “Complementary experiments for parameter estimation in heat transfer model,” *Food and Bioproducts Processing*, vol. 128, pp. 240–246, Jul. 2021, doi: 10.1016/j.fbp.2021.06.004.
- [50] P. Benyathiar, K. D. Dolan, and D. K. Mishra, “Optimal Design of Complementary Experiments for Parameter Estimation at Elevated Temperature of Food Processing,” *Foods*, vol. 11, no. 17, p. 2611, Aug. 2022, doi: 10.3390/foods11172611.
- [51] M. Bahrami, J. R. Culham, M. M. Yananovich, and G. E. Schneider, “Review of Thermal Joint Resistance Models for Nonconforming Rough Surfaces,” *Appl Mech Rev*, vol. 59, no. 1, pp. 1–12, Jan. 2006, doi: 10.1115/1.2110231.
- [52] C. V. Madhusudana, “Accuracy in thermal contact conductance experiments - the effect of heat losses to the surroundings,” *International Communications in Heat and Mass Transfer*, vol. 27, no. 6, pp. 877–891, Aug. 2000, doi: 10.1016/S0735-1933(00)00168-8.
- [53] M. G. Cooper, B. B. Mikic, and M. M. Yovanovich, “Thermal contact conductance,” *Int J Heat Mass Transf*, vol. 12, no. 3, pp. 279–300, Mar. 1969, doi: 10.1016/0017-9310(69)90011-8.
- [54] J. P. Kaipio and C. Fox, “The Bayesian Framework for Inverse Problems in Heat Transfer,” *Heat Transfer Engineering*, vol. 32, no. 9, pp. 718–753, Aug. 2011, doi: 10.1080/01457632.2011.525137.
- [55] C. A. A. Mota, H. R. B. Orlande, M. O. M. De Carvalho, V. Kolehmainen, and J. P. Kaipio, “Bayesian Estimation of Temperature-Dependent Thermophysical Properties and Transient Boundary Heat Flux,” *Heat Transfer Engineering*, vol. 31, no. 7, pp. 570–580, Jun. 2010, doi: 10.1080/01457630903425635.

- [56] J. Wang and N. Zabaras, “A Bayesian inference approach to the inverse heat conduction problem,” *Int J Heat Mass Transf*, vol. 47, no. 17–18, pp. 3927–3941, Aug. 2004, doi: 10.1016/j.ijheatmasstransfer.2004.02.028.
- [57] J. P. Kaipio and C. Fox, “The Bayesian Framework for Inverse Problems in Heat Transfer,” *Heat Transfer Engineering*, vol. 32, no. 9, pp. 718–753, Aug. 2011, doi: 10.1080/01457632.2011.525137.
- [58] N. P. Ramos, M. de Melo Antunes, G. Guimarães, and S. M. M. de Lima e Silva, “Simultaneous Bayesian estimation of the temperature-dependent thermal properties of a metal slab using a three-dimensional transient experimental approach,” *International Journal of Thermal Sciences*, vol. 179, p. 107671, Sep. 2022, doi: 10.1016/j.ijthermalsci.2022.107671.
- [59] D. S. Martínez, F. Illán, J. P. Solano, and A. Viedma, “Embedded thermocouple wall temperature measurement technique for scraped surface heat exchangers,” *Appl Therm Eng*, vol. 114, pp. 793–801, Mar. 2017, doi: 10.1016/j.applthermaleng.2016.12.039.
- [60] G. D’Alessandro, F. de Monte, and D. E. Amos, “Effect of Heat Source and Imperfect Contact on Simultaneous Estimation of Thermal Properties of High-Conductivity Materials,” *Math Probl Eng*, vol. 2019, pp. 1–15, Jun. 2019, doi: 10.1155/2019/5945413.
- [61] R. S. Graves, T. G. Kollie, D. L. McElroy, and K. E. Gilchrist, “The thermal conductivity of AISI 304L stainless steel,” *Int J Thermophys*, vol. 12, no. 2, pp. 409–415, Mar. 1991, doi: 10.1007/BF00500761.
- [62] S. J. Chang, Y. Kang, B. Y. Yun, S. Yang, and S. Kim, “Assessment of effect of climate change on hygrothermal performance of cross-laminated timber building envelope with modular construction,” *Case Studies in Thermal Engineering*, vol. 28, p. 101703, Dec. 2021, doi: 10.1016/j.csite.2021.101703.
- [63] M. Kamali and K. Hewage, “Development of performance criteria for sustainability evaluation of modular versus conventional construction methods,” *J Clean Prod*, vol. 142, pp. 3592–3606, Jan. 2017, doi: 10.1016/j.jclepro.2016.10.108.
- [64] M. Kamali and K. Hewage, “Life cycle performance of modular buildings: A critical review,” *Renewable and Sustainable Energy Reviews*, vol. 62, pp. 1171–1183, Sep. 2016, doi: 10.1016/j.rser.2016.05.031.
- [65] K. Orłowski, K. Shanaka, and P. Mendis, “Manufacturing, Modeling, Implementation and Evaluation of a Weatherproof Seal for Prefabricated Construction,” *Buildings*, vol. 8, no. 9, p. 120, Aug. 2018, doi: 10.3390/buildings8090120.
- [66] S. Van Linden and N. Van Den Bossche, “Watertightness performance of face-sealed versus drained window-wall interfaces,” *Build Environ*, vol. 196, p. 107824, Jun. 2021, doi: 10.1016/j.buildenv.2021.107824.

- [67] C. H. Lozinsky and M. F. Touchie, “Quantifying suite-level airtightness in newly constructed multi-unit residential buildings using guarded suite-level air leakage testing,” *Build Environ*, vol. 236, p. 110273, May 2023, doi: 10.1016/j.buildenv.2023.110273.
- [68] C. H. Lozinsky and M. F. Touchie, “Improving energy model calibration of multi-unit residential buildings through component air infiltration testing,” *Build Environ*, vol. 134, pp. 218–229, Apr. 2018, doi: 10.1016/j.buildenv.2018.02.040.
- [69] A. M. Tanyer, A. Tavukcuoglu, and M. Bekboliev, “Assessing the airtightness performance of container houses in relation to its effect on energy efficiency,” *Build Environ*, vol. 134, pp. 59–73, Apr. 2018, doi: 10.1016/j.buildenv.2018.02.026.
- [70] S. Panico, M. Larcher, V. Marincioni, A. Troi, C. Baglivo, and P. M. Congedo, “Identifying key parameters through a sensitivity analysis for realistic hygrothermal simulations at wall level supported by monitored data,” *Build Environ*, vol. 229, p. 109969, Feb. 2023, doi: 10.1016/j.buildenv.2022.109969.
- [71] M. Ruiz, V. Masson, M. Bonhomme, and S. Ginestet, “Numerical method for solving coupled heat and mass transfer through walls for future integration into an urban climate model,” *Build Environ*, vol. 231, p. 110028, Mar. 2023, doi: 10.1016/j.buildenv.2023.110028.
- [72] S. Panico, M. Larcher, D. Herrera Avellanosa, C. Baglivo, A. Troi, and P. Maria Congedo, “Hygrothermal simulation challenges: Assessing boundary condition choices in retrofitting historic European buildings,” *Energy Build*, vol. 297, p. 113464, Oct. 2023, doi: 10.1016/j.enbuild.2023.113464.
- [73] I. Vandemeulebroucke, S. Caluwaerts, and N. Van Den Bossche, “Decision framework to select moisture reference years for hygrothermal simulations,” *Build Environ*, vol. 218, p. 109080, Jun. 2022, doi: 10.1016/j.buildenv.2022.109080.
- [74] W. Dong, Y. Chen, Y. Bao, and A. Fang, “A validation of dynamic hygrothermal model with coupled heat and moisture transfer in porous building materials and envelopes,” *Journal of Building Engineering*, vol. 32, p. 101484, Nov. 2020, doi: 10.1016/j.job.2020.101484.
- [75] G. Tlajji, F. Pennec, S. Ouldboukhitine, M. Ibrahim, and P. Biwole, “Hygrothermal performance of multilayer straw walls in different climates,” *Constr Build Mater*, vol. 326, p. 126873, Apr. 2022, doi: 10.1016/j.conbuildmat.2022.126873.
- [76] Q. Zhan, Y. Xiao, F. Musso, and L. Zhang, “Assessing the hygrothermal performance of typical lightweight steel-framed wall assemblies in hot-humid climate regions by monitoring and numerical analysis,” *Build Environ*, vol. 188, p. 107512, Jan. 2021, doi: 10.1016/j.buildenv.2020.107512.

- [77] S. Rouchier, M. Rabouille, and P. Oberlé, “Calibration of simplified building energy models for parameter estimation and forecasting: Stochastic versus deterministic modelling,” *Build Environ*, vol. 134, pp. 181–190, Apr. 2018, doi: 10.1016/j.buildenv.2018.02.043.
- [78] M. Labat, M. Woloszyn, G. Garnier, and J. J. Roux, “Dynamic coupling between vapour and heat transfer in wall assemblies: Analysis of measurements achieved under real climate,” *Build Environ*, vol. 87, pp. 129–141, May 2015, doi: 10.1016/j.buildenv.2015.01.022.
- [79] H. Palani and A. Karatas, “Investigating the disparities between experimental and computational analyses of thermal performance in prefabricated wall panels,” *Appl Therm Eng*, vol. 236, p. 121568, Jan. 2024, doi: 10.1016/j.applthermaleng.2023.121568.
- [80] S. Yu, X. Liu, Y. Li, S. He, Y. Yao, and S. Sun, “Experimental and numerical simulation study on hygrothermal migration of damaged envelope walls during wind-driven rain,” *Build Environ*, vol. 243, p. 110653, Sep. 2023, doi: 10.1016/j.buildenv.2023.110653.
- [81] M. J. Sorgato, A. P. Melo, and R. Lamberts, “The effect of window opening ventilation control on residential building energy consumption,” *Energy Build*, vol. 133, pp. 1–13, Dec. 2016, doi: 10.1016/j.enbuild.2016.09.059.
- [82] C. Feng and H. Janssen, “Hygric properties of porous building materials (VII): Full-range benchmark characterizations of three materials,” *Build Environ*, vol. 195, p. 107727, May 2021, doi: 10.1016/j.buildenv.2021.107727.
- [83] U. Berardi and M. Naldi, “The impact of the temperature dependent thermal conductivity of insulating materials on the effective building envelope performance,” *Energy Build*, vol. 144, pp. 262–275, Jun. 2017, doi: 10.1016/j.enbuild.2017.03.052.
- [84] G. Giada, R. Caponetto, and F. Nocera, “Hygrothermal Properties of Raw Earth Materials: A Literature Review,” *Sustainability*, vol. 11, no. 19, p. 5342, Sep. 2019, doi: 10.3390/su11195342.
- [85] Y. Wang, C. Ma, Y. Liu, D. Wang, and J. Liu, “Effect of moisture migration and phase change on effective thermal conductivity of porous building materials,” *Int J Heat Mass Transf*, vol. 125, pp. 330–342, Oct. 2018, doi: 10.1016/j.ijheatmasstransfer.2018.04.062.
- [86] J. Piggot-Navarrete, P. Blanchet, M. R. Cabral, and C. Perez, “Investigating the impact of construction workmanship defects on the hygrothermal performance and airtightness of lightweight-structure wooden envelope systems,” *Build Environ*, vol. 243, p. 110705, Sep. 2023, doi: 10.1016/j.buildenv.2023.110705.
- [87] A. A. Alvarado-Alvarado, A. De Bock, T. Ysebaert, B. Belmans, and S. Denys, “Modeling the hygrothermal behavior of green walls in Comsol Multiphysics®: Validation against measurements in a climate chamber,” *Build Environ*, vol. 238, p. 110377, Jun. 2023, doi: 10.1016/j.buildenv.2023.110377.

- [88] R. Belloum, B. Agoudjil, N. Chennouf, and A. Boudenne, “Hygrothermal performance assessment of a bio-based building made with date palm concrete walls,” *Build Environ*, vol. 223, p. 109467, Sep. 2022, doi: 10.1016/j.buildenv.2022.109467.
- [89] T. Colinart, D. Lelievre, and P. Glouannec, “Experimental and numerical analysis of the transient hygrothermal behavior of multilayered hemp concrete wall,” *Energy Build*, vol. 112, pp. 1–11, Jan. 2016, doi: 10.1016/j.enbuild.2015.11.027.
- [90] D. Wu, M. Rahim, M. El Ganaoui, R. Djedjig, R. Bennacer, and B. Liu, “Experimental investigation on the hygrothermal behavior of a new multilayer building envelope integrating PCM with bio-based material,” *Build Environ*, vol. 201, p. 107995, Aug. 2021, doi: 10.1016/j.buildenv.2021.107995.
- [91] M. Sawadogo, F. Benmahiddine, A. Godin, M. Duquesne, R. Belarbi, and A. Hamami, “Development and hygrothermal performance analysis of a novel eco-friendly insulating wall under various climatic conditions,” *Build Environ*, vol. 245, p. 110841, Nov. 2023, doi: 10.1016/j.buildenv.2023.110841.
- [92] Q. Zhan, V. Pungercar, F. Musso, H. Ni, and Y. Xiao, “Hygrothermal investigation of lightweight steel-framed wall assemblies in hot-humid climates: Measurement and simulation validation,” *Journal of Building Engineering*, vol. 42, p. 103044, Oct. 2021, doi: 10.1016/j.job.2021.103044.
- [93] A. Sadłowska-Sałęga and J. Radoń, “Feasibility and limitation of calculative determination of hygrothermal conditions in historical buildings: Case study of st. Martin church in Wiśniowa,” *Build Environ*, vol. 186, p. 107361, Dec. 2020, doi: 10.1016/j.buildenv.2020.107361.
- [94] M. G. Gomes, A. M. Rodrigues, J. A. Bogas, and A. Freitas, “Thermophysical properties under different hygroscopic conditions of an innovative composite concrete pre-walls system,” *Constr Build Mater*, vol. 307, p. 124938, Nov. 2021, doi: 10.1016/j.conbuildmat.2021.124938.
- [95] M. Ibrahim, H. Sayegh, L. Bianco, and E. Wurtz, “Hygrothermal performance of novel internal and external super-insulating systems: In-situ experimental study and 1D/2D numerical modeling,” *Appl Therm Eng*, vol. 150, pp. 1306–1327, Mar. 2019, doi: 10.1016/j.applthermaleng.2019.01.054.
- [96] I. Costa-Carrapiço, B. Croxford, R. Raslan, and J. Neila González, “Hygrothermal calibration and validation of vernacular dwellings: A genetic algorithm-based optimisation methodology,” *Journal of Building Engineering*, vol. 55, p. 104717, Sep. 2022, doi: 10.1016/j.job.2022.104717.
- [97] J. Ren, Z. Zhao, J. Zhang, J. Wang, S. Guo, and J. Sun, “Study on the hygrothermal properties of a Chinese solar greenhouse with a straw block north wall,” *Energy Build*, vol. 193, pp. 127–138, Jun. 2019, doi: 10.1016/j.enbuild.2019.03.040.

- [98] K. A. Sabapathy and S. Gedupudi, “In situ thermal characterization of rice straw envelope of an outdoor test room,” *Journal of Building Engineering*, vol. 33, p. 101416, Jan. 2021, doi: 10.1016/j.jobe.2020.101416.
- [99] S. Rouchier, M. Woloszyn, Y. Kedowide, and T. Béjat, “Identification of the hygrothermal properties of a building envelope material by the covariance matrix adaptation evolution strategy,” *J Build Perform Simul*, vol. 9, no. 1, pp. 101–114, Jan. 2016, doi: 10.1080/19401493.2014.996608.
- [100] A. Jumabekova, J. Berger, A. Fouquier, and G. S. Dulikravich, “Searching an optimal experiment observation sequence to estimate the thermal properties of a multilayer wall under real climate conditions,” *Int J Heat Mass Transf*, vol. 155, p. 119810, Jul. 2020, doi: 10.1016/j.ijheatmasstransfer.2020.119810.
- [101] A. Al-Omari, X. Brunetaud, K. Beck, and M. Al-Mukhtar, “Coupled thermal–hygric characterisation of elastic behaviour for soft and porous limestone,” *Constr Build Mater*, vol. 62, pp. 28–37, Jul. 2014, doi: 10.1016/j.conbuildmat.2014.03.029.
- [102] J. Berger, D. Dutykh, and N. Mendes, “On the optimal experiment design for heat and moisture parameter estimation,” *Exp Therm Fluid Sci*, vol. 81, pp. 109–122, Feb. 2017, doi: 10.1016/j.expthermflusci.2016.10.008.
- [103] N. P. Ramos, M. de M. Antunes, and S. M. M. de Lima e Silva, “Complementary transient thermal models and metaheuristics to simultaneously identify linearly temperature-dependent thermal properties of austenitic stainless steels,” *Phys Scr*, vol. 97, no. 11, p. 115006, Nov. 2022, doi: 10.1088/1402-4896/ac99ac.
- [104] E. Julien, P. Blanchet, and L. Gosselin, “Case-Study: Fully Prefabricated Wood Wall Connection to Improve Building Envelope and On-Site Efficiency,” *Buildings*, vol. 12, no. 12, p. 2185, Dec. 2022, doi: 10.3390/buildings12122185.
- [105] P. Armand, J. C. Gilbert, and S. Jan-Jégou, “A Feasible BFGS Interior Point Algorithm for Solving Convex Minimization Problems,” *SIAM Journal on Optimization*, vol. 11, no. 1, pp. 199–222, Jan. 2000, doi: 10.1137/S1052623498344720.
- [106] M. Woloszyn and C. Rode, “Tools for performance simulation of heat, air and moisture conditions of whole buildings,” *Build Simul*, vol. 1, no. 1, pp. 5–24, Mar. 2008, doi: 10.1007/s12273-008-8106-z.
- [107] C. Balocco, G. Petrone, and G. Cammarata, “Numerical multi-physical approach for the assessment of coupled heat and moisture transfer combined with people movements in historical buildings,” *Build Simul*, vol. 7, no. 3, pp. 289–303, Jun. 2014, doi: 10.1007/s12273-013-0146-3.
- [108] M. Autengruber, M. Lukacevic, and J. Füssl, “Finite-element-based moisture transport model for wood including free water above the fiber saturation point,” *Int J Heat Mass Transf*, vol. 161, p. 120228, Nov. 2020, doi: 10.1016/j.ijheatmasstransfer.2020.120228.

- [109] N. P. Ramos, M. de M. Antunes, and S. M. M. de Lima e Silva, “Complementary transient thermal models and metaheuristics to simultaneously identify linearly temperature-dependent thermal properties of austenitic stainless steels,” *Phys Scr*, vol. 97, no. 11, p. 115006, Nov. 2022, doi: 10.1088/1402-4896/ac99ac.
- [110] C. Xu, S. Li, and K. Zou, “Study of heat and moisture transfer in internal and external wall insulation configurations,” *Journal of Building Engineering*, vol. 24, p. 100724, Jul. 2019, doi: 10.1016/j.jobe.2019.02.016.
- [111] H. J. Moon, S. H. Ryu, and J. T. Kim, “The effect of moisture transportation on energy efficiency and IAQ in residential buildings,” *Energy Build*, vol. 75, pp. 439–446, Jun. 2014, doi: 10.1016/j.enbuild.2014.02.039.
- [112] L. P. Thomas, B. M. Marino, and N. Muñoz, “Steady-state and time-dependent heat fluxes through building envelope walls: A quantitative analysis to determine their relative significance all year round,” *Journal of Building Engineering*, vol. 29, p. 101122, May 2020, doi: 10.1016/j.jobe.2019.101122.
- [113] Z. A. Al-Absi, M. I. M. Hafizal, and M. Ismail, “Experimental study on the thermal performance of PCM-based panels developed for exterior finishes of building walls,” *Journal of Building Engineering*, vol. 52, p. 104379, Jul. 2022, doi: 10.1016/j.jobe.2022.104379.
- [114] R. F. Rupp, N. G. Vásquez, and R. Lamberts, “A review of human thermal comfort in the built environment,” *Energy Build*, vol. 105, pp. 178–205, Oct. 2015, doi: 10.1016/j.enbuild.2015.07.047.
- [115] M. Nadarajan and V. Kirubakaran, “Simulation studies on small rural residential houses using sustainable building materials for thermal comfort – case comparison,” *Advances in Building Energy Research*, vol. 11, no. 2, pp. 193–207, Jul. 2017, doi: 10.1080/17512549.2016.1215260.
- [116] R. Caro and J. J. Sendra, “Are the dwellings of historic Mediterranean cities cold in winter? A field assessment on their indoor environment and energy performance,” *Energy Build*, vol. 230, p. 110567, Jan. 2021, doi: 10.1016/j.enbuild.2020.110567.
- [117] X. Jin, X. Zhang, Y. Cao, and G. Wang, “Thermal performance evaluation of the wall using heat flux time lag and decrement factor,” *Energy Build*, vol. 47, pp. 369–374, Apr. 2012, doi: 10.1016/j.enbuild.2011.12.010.
- [118] I. Danielski and M. Fröling, “Diagnosis of Buildings’ Thermal Performance - A Quantitative Method Using Thermography Under Non-steady State Heat Flow,” *Energy Procedia*, vol. 83, pp. 320–329, Dec. 2015, doi: 10.1016/j.egypro.2015.12.186.
- [119] J. Berger and B. Kadoch, “Estimation of the thermal properties of an historic building wall by combining modal identification method and optimal experiment design,” *Build Environ*, vol. 185, p. 107065, Nov. 2020, doi: 10.1016/j.buildenv.2020.107065.

- [120] Y. Yang, Z. Chen, T. Vogt Wu, A. Sempey, and J.-C. Batsale, “In situ methodology for thermal performance evaluation of building wall: A review,” *International Journal of Thermal Sciences*, vol. 181, p. 107687, Nov. 2022, doi: 10.1016/j.ijthermalsci.2022.107687.
- [121] S. Cai, B. Zhang, and L. Cremaschi, “Review of moisture behavior and thermal performance of polystyrene insulation in building applications,” *Build Environ*, vol. 123, pp. 50–65, Oct. 2017, doi: 10.1016/j.buildenv.2017.06.034.
- [122] J. Alencastro, A. Fuertes, and P. de Wilde, “The relationship between quality defects and the thermal performance of buildings,” *Renewable and Sustainable Energy Reviews*, vol. 81, pp. 883–894, Jan. 2018, doi: 10.1016/j.rser.2017.08.029.
- [123] T. Theodosiou, K. Tsikaloudaki, K. Kontoleon, and C. Giarma, “Assessing the accuracy of predictive thermal bridge heat flow methodologies,” *Renewable and Sustainable Energy Reviews*, vol. 136, p. 110437, Feb. 2021, doi: 10.1016/j.rser.2020.110437.
- [124] B. Mobaraki, F. J. Castilla Pascual, F. Lozano-Galant, J. A. Lozano-Galant, and R. Porras Soriano, “In situ U-value measurement of building envelopes through continuous low-cost monitoring,” *Case Studies in Thermal Engineering*, vol. 43, p. 102778, Mar. 2023, doi: 10.1016/j.csite.2023.102778.
- [125] L. Yang, Y. Qiao, Y. Liu, X. Zhang, C. Zhang, and J. Liu, “A kind of PCMs-based lightweight wallboards: Artificial controlled condition experiments and thermal design method investigation,” *Build Environ*, vol. 144, pp. 194–207, Oct. 2018, doi: 10.1016/j.buildenv.2018.08.020.
- [126] P. T. Tsilingiris, “Wall heat loss from intermittently conditioned spaces—The dynamic influence of structural and operational parameters,” *Energy Build*, vol. 38, no. 8, pp. 1022–1031, Aug. 2006, doi: 10.1016/j.enbuild.2005.11.012.
- [127] T. Pilet and T. Rakha, “Modeling of transient conduction in building envelope assemblies: A review,” *Sci Technol Built Environ*, vol. 28, no. 6, pp. 706–716, Jul. 2022, doi: 10.1080/23744731.2022.2068315.
- [128] N. Bishara, G. Pernigotto, A. Prada, M. Baratieri, and A. Gasparella, “Experimental determination of the building envelope’s dynamic thermal characteristics in consideration of hygrothermal modelling – Assessment of methods and sources of uncertainty,” *Energy Build*, vol. 236, p. 110798, Apr. 2021, doi: 10.1016/j.enbuild.2021.110798.
- [129] N. C. Balaji, M. Mani, and B. V. Venkatarama Reddy, “Dynamic thermal performance of conventional and alternative building wall envelopes,” *Journal of Building Engineering*, vol. 21, pp. 373–395, Jan. 2019, doi: 10.1016/j.job.2018.11.002.

- [130] Z. Fang and Y. Chen, “Applicability of the transfer function method and periodic response factors method in coincident design weather data generation,” *Energy Build*, vol. 250, p. 111254, Nov. 2021, doi: 10.1016/j.enbuild.2021.111254.
- [131] F. Tariku and F. Hemmati, “RC-Network based thermal bridge calculation method for transient heat transfer analysis of multidimensional building envelope details: A frequency response analysis-based method,” *Energy Build*, vol. 300, p. 113648, Dec. 2023, doi: 10.1016/j.enbuild.2023.113648.
- [132] S. Zhou, F. Bai, G. Razaqpur, and B. Wang, “Effect of key parameters on the transient thermal performance of a building envelope with Trombe wall containing phase change material,” *Energy Build*, vol. 284, p. 112879, Apr. 2023, doi: 10.1016/j.enbuild.2023.112879.
- [133] S. Zhang, L. Yang, B. Suonam, H. Dong, and Y. Liu, “Method for dynamic thermal insulation design revealing almost real heat transfer characteristics of building envelopes in different Chinese regions,” *Energy Build*, vol. 274, p. 112419, Nov. 2022, doi: 10.1016/j.enbuild.2022.112419.
- [134] R. G. Martinez, A. Riverola, and D. Chemisana, “Disaggregation process for dynamic multidimensional heat flux in building simulation,” *Energy Build*, vol. 148, pp. 298–310, Aug. 2017, doi: 10.1016/j.enbuild.2017.05.029.
- [135] D. Mazzeo, G. Oliveti, and N. Arcuri, “A Method for Thermal Dimensioning and for Energy Behavior Evaluation of a Building Envelope PCM Layer by Using the Characteristic Days,” *Energies (Basel)*, vol. 10, no. 5, p. 659, May 2017, doi: 10.3390/en10050659.
- [136] P. K. S. Rathore, S. K. Shukla, and N. K. Gupta, “Yearly analysis of peak temperature, thermal amplitude, time lag and decrement factor of a building envelope in tropical climate,” *Journal of Building Engineering*, vol. 31, p. 101459, Sep. 2020, doi: 10.1016/j.jobbe.2020.101459.
- [137] G. Vox, I. Blanco, F. Convertino, and E. Schettini, “Heat transfer reduction in building envelope with green façade system: A year-round balance in Mediterranean climate conditions,” *Energy Build*, vol. 274, p. 112439, Nov. 2022, doi: 10.1016/j.enbuild.2022.112439.
- [138] S. Rouchier, “Solving inverse problems in building physics: An overview of guidelines for a careful and optimal use of data,” *Energy Build*, vol. 166, pp. 178–195, May 2018, doi: 10.1016/j.enbuild.2018.02.009.
- [139] Q. Zhou and F. Xue, “Pushing the boundaries of modular-integrated construction: A symmetric skeleton grammar-based multi-objective optimization of passive design for energy savings and daylight autonomy,” *Energy Build*, vol. 296, p. 113417, Oct. 2023, doi: 10.1016/j.enbuild.2023.113417.

- [140] H. Palani and A. Karatas, “Investigating the disparities between experimental and computational analyses of thermal performance in prefabricated wall panels,” *Appl Therm Eng*, vol. 236, p. 121568, Jan. 2024, doi: 10.1016/j.applthermaleng.2023.121568.
- [141] D. Hong, G. Li, L. Wei, and Z. Yi, “An improved sequential function specification coupled with Broyden combined method for determination of transient temperature field of the steel billet,” *Int J Heat Mass Transf*, vol. 186, p. 122489, May 2022, doi: 10.1016/j.ijheatmasstransfer.2021.122489.
- [142] S. Sun, Z. Chang, Y. Ji, G. Wang, and L. Wei, “Inverse Estimation of Transient Heat Flux Using Sequential Function Specification Method,” *Heat Transfer Engineering*, pp. 1–11, Mar. 2023, doi: 10.1080/01457632.2023.2185488.
- [143] Y. Wang, N. Wang, and Q. Ren, “Predicting surface heat flux on complex systems via Conv-LSTM,” *Case Studies in Thermal Engineering*, vol. 33, p. 101927, May 2022, doi: 10.1016/j.csite.2022.101927.
- [144] F. Wang, P. Zhang, Y. Wang, C. Sun, and X. Xia, “Real-time identification of severe heat loads over external interface of lightweight thermal protection system,” *Thermal Science and Engineering Progress*, vol. 37, p. 101583, Jan. 2023, doi: 10.1016/j.tsep.2022.101583.
- [145] K. A. Woodbury, H. Najafi, F. Monte, and J. V. Beck, *Inverse Heat Conduction*. Wiley, 2023. doi: 10.1002/9781119840220.
- [146] K. A. Woodbury and S. K. Thakur, “Redundant data and future times in the inverse heat conduction problem,” *Inverse Problems in Engineering*, vol. 2, no. 4, pp. 319–333, Jul. 1996, doi: 10.1080/174159796088027610.
- [147] K. A. Woodbury and J. V. Beck, “Estimation metrics and optimal regularization in a Tikhonov digital filter for the inverse heat conduction problem,” *Int J Heat Mass Transf*, vol. 62, pp. 31–39, Jul. 2013, doi: 10.1016/j.ijheatmasstransfer.2013.02.052.
- [148] W. J. Minkowycz, E. M. Sparrow, and J. Y. Murthy, Eds., *Handbook of Numerical Heat Transfer*. Wiley, 2000. doi: 10.1002/9780470172599.
- [149] B. Blackwell and J. V. Beck, “A technique for uncertainty analysis for inverse heat conduction problems,” *Int J Heat Mass Transf*, vol. 53, no. 4, pp. 753–759, Jan. 2010, doi: 10.1016/j.ijheatmasstransfer.2009.10.014.